STUDY OF CHANGE IN ORIENTATION OF ADVENTITIAL COLLAGEN IN CEREBRAL BLOOD VESSELS DUTRING AND POST-AXIAL OVERSTRETCH

by

Abhidnya Vijaykumar Patharkar

A thesis submitted to the faculty of
The University of Utah
in partial fulfillment of the requirements for the degree of

Master of Science

Department of Mechanical Engineering

The University of Utah

May 2018

The University of Utah Graduate School

STATEMENT OF THESIS APPROVAL

The thesis of **Abhidnya Vijaykumar Patharkar**

has been approved by the following supervisory committee members:

Kenneth L. Monson	, Chair	**10/19/2017** Date Approved
Brittany Coats	, Member	**10/19/2017** Date Approved
Ashley Spear	, Member	**10/19/2017** Date Approved

and by **Timothy Ameel** , Chair/Dean of

the Department/College/School of **Mechanical Engineering**

and by David B. Kieda, Dean of The Graduate School.

ABSTRACT

Cerebral blood vessels are critical to maintaining the health of the brain. The function of these vessels gets disrupted during traumatic brain injury (TBI). Even when cerebral vessels do not bleed or rupture during TBI, they may be subjected to excessive deformation beyond their physiological or in-vivo (IV) length. This alters their mechanical properties.

The earlier investigation by Bell reported softening of the cerebral blood vessels, when stretched beyond their IV length, beginning at an overstretch level of 1.2. The recent investigation in our lab using Collagen Hybridizing Peptide (CHP) to detect collagen damage reported that collagen fibers begin to rupture when the vessels are stretched axially to approximately 1.3 times their IV length. It can thus be predicted that rearrangements in the microstructure of the vessels might be responsible for softening below this threshold, rather than ruptures or breaking of the fibers. The earlier investigation using CHP also found that the fibers oriented in the direction of loading tend to get damaged with overstretch.

Given that collagen plays a significant role in the mechanical properties of blood vessels at large deformations, we hypothesized that changes in collagen orientation were the microstructural mechanism responsible for the sub-rupture softening observed. Based on the previous work, we expected to see axial fibers in the adventitia become less uniform in their orientation following axial overstretch. Medial fibers are not expected to have a

significant change in their orientation since they are circumferentially oriented. We investigated these questions using sheep middle cerebral arteries (MCAs).

We tested three MCAs from three different ewes, using a horizontal tester previously developed in our lab. Collagen fibers were imaged using nonlinear optical microscopy (NLOM). The captured data were then processed using Orientation J, Fibril Tool, and Line Tool and was finally analyzed statistically to test the hypothesis.

It was found that collagen retains its mean orientation post-overstretch. Based on image processing tools used here, it was found that axially oriented, adventitial fibers did not become more disorganized, as hypothesized, post-overstretch. We need advanced methods of data acquisition and image processing to determine if there is any subtle change in collagen orientation, which could not be detected in this investigation. To the best of our knowledge, this is the first study investigating the effect of mild axial overstretch on collagen orientation in cerebral arteries.

TABLE OF CONTENTS

CHAPTER 1

INTRODUCTION

In the United States, in 2009, there were an estimated 2.4 million cases of traumatic brain injury (TBI) [1]. Annual estimates of death due to TBI and stroke are 53,000 [2] and 130,000 [3], respectively, with corresponding treatment costs of 76.5 [1] and 36.5 [3] billion dollars. TBI often results in cerebral hemorrhage. Blood vessel damage is the cause of this hemorrhage, but in cases where there is no rupture or bleeding of the blood vessels, they may still get damaged at sub-failure levels. Such damage may lead to stroke [4-6] or other significant pathological conditions such as cerebral blood flow (CBF) alterations, autoregulation impairments, subarachnoid hemorrhage (SAH), vasospasm, blood-brain barrier (BBB) disruption, and edema formation [7].

Cerebral blood vessels are mainly composed of three layers: intima, media, and adventitia. Intima is a single layer of endothelial cells lining the arterial wall. The media consists of a network of bundles of collagen fibrils, elastin, and smooth muscle cells. The adventitia consists mainly of fibroblasts and fibrocytes, histological ground-matrix, and collagen fibers organized in thick bundles [8]. The collagen fibers in the media are circumferentially oriented whereas those from the adventitia are axially oriented [8]. The collagen fiber is made up of fibrils, which are wound together in the form of a triple helix. The stress-strain response of a single collagen fiber is shown in Fig. 1.1

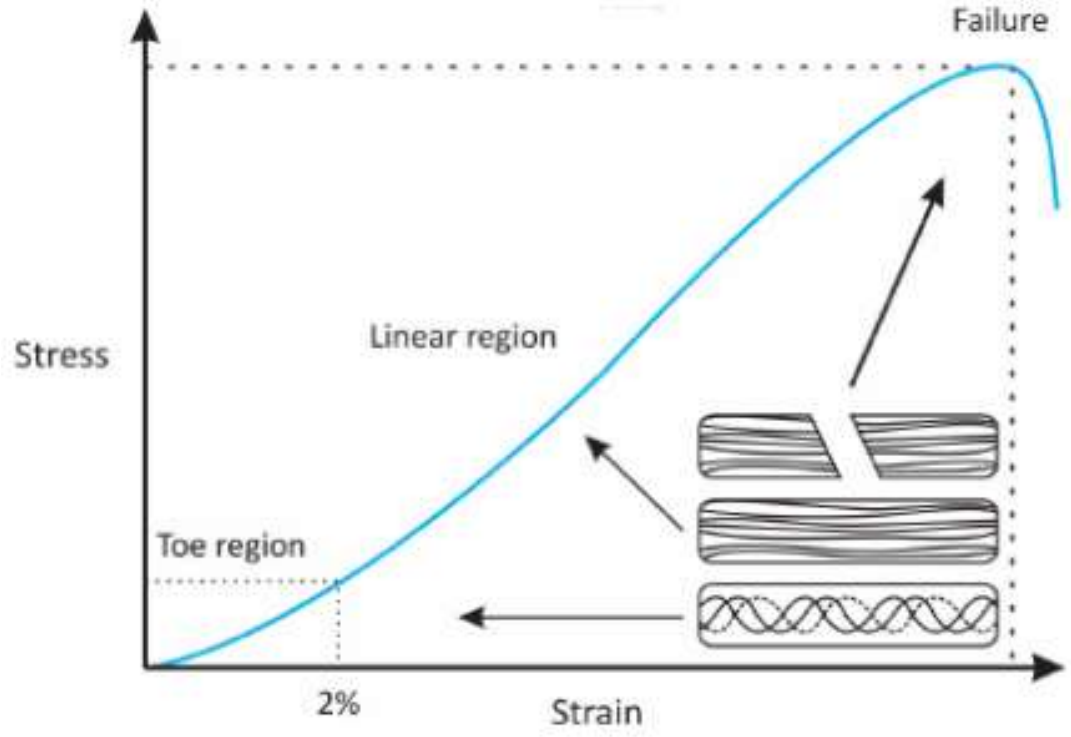

Fig. 1.1 Stress-strain response of a collagen.
(Redrawn from 'The Physiology of Sports Injuries and Repair Processes'; http://dx.doi.org/10.5772/54234)

Collagen fibers demonstrate crimp banding among their fibrils [9]. A toe region in the stress-strain response of the collagen fiber is associated with straightening of the fiber. (Crimp gets released as the fiber straightens.)

Bell [10] characterized the softening phenomenon in cerebral arteries at various levels of overstretch that may be experienced during TBI. While the detailed loading conditions they experience are yet undefined, the vessels are expected to align themselves with deformations imposed on the surrounding brain tissue, as fibers embedded in a matrix. Therefore, alterations of cerebral artery mechanical properties resulting from a large range of axial overstretch values were explored. Bell [10] found that even mild levels of overstretching (1.2 * in-vivo stretch) altered vessel response and that the magnitude of

the imposed changes increased with the extent of overstretch. More specifically, post-overstretch response exhibited softening such that stress values at a given level of strain were lower after overstretch than their corresponding values before overstretch. The observed softening also resulted in increased nonlinearity of the stress-strain curve, with toe region slope decreasing and large deformation slope increasing [10] as shown in Fig. 1.2. Bell [10] did not observe a change in the values of ultimate stress and ultimate strain post mild overstretch. A large overstretch would straighten the collagen fibers. If the vessel sample is further stretched where few of the fibers begin to fail, it is obvious that there would be a reduction in the stress that it bears, corresponding to the same strain, post-overstretch. Since the vessel samples are not subjected to a large overstretch and still bear less stress, Bell [10] predicted that this is primarily due to rearrangement of microstructural components rather than ruptures in the fibrous components. The Lab of Head Injury and Vessel Biomechanics at The University of Utah recently utilized Collagen Hybridizing Peptide (CHP) developed by the Yu group at the University of Utah to demonstrate molecular-level unfolding of collagen with axial overstretch. It was found that overstretch of approximately 1.3 produces damage among fibers aligned with the direction of loading.

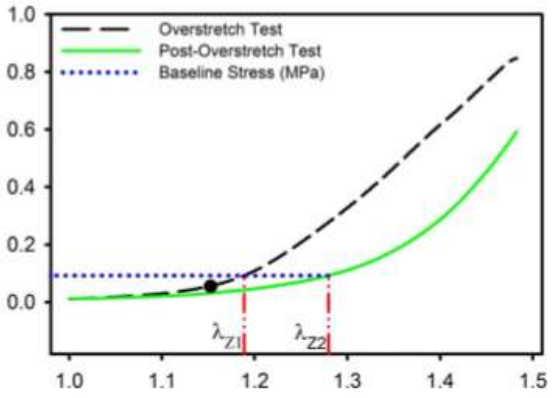

Fig. 1.2 Arterial softening shown by Bell et al.,(2015)

This damage increases with overstretch severity was another finding from the same study. Furthermore, mechanical properties of the artery are mainly governed by elastin and collagen fibers [11]. It has been reported that elastin is not responsible for softening of the arteries [12]. The change in collagen orientation with an increase in the number of preconditioning cycles and following sub-failure loading has been reported in other biological tissues such as a ligament tissue ([13]-[15]) (the findings of these results are summarized in the Background chapter). If we take into consideration all the above findings, we can relate the softening behavior of cerebral blood vessels to the change in collagen orientation. The form of loading in Bell's investigation is axial. A recent finding from the lab that used CHP to quantify damage to collagen fibers post-overstretch indicates that the axially oriented adventitial fibers might be more affected than circumferentially oriented medial fibers. Thus, there should be more disorganization in axially oriented adventitial fibers, i.e., more fibers are expected to have reoriented themselves away from the axial direction. Since there is an increase in softening response and amount of collagen damage depending on the severity of overstretch, this disorganization is expected to become likewise severe.

When the histogram (Gaussian distribution) of the orientations is plotted for the adventitial and medial fibers corresponding to the in-vivo configuration, we see peaks centered on 0˚ and 90˚, respectively. The collagen fibers forming the adventitia are symmetrically organized (in a double helical structure) [8] and hence, post-overstretch, the histogram for adventitia should still show the mean at 0˚, with a possible reduction in the peak value corresponding to the mean and increase in its standard deviation, indicating more disorganized fibers. During overstretch, the histogram for adventitia should show the

mean at 0˚, with an increase in peak value corresponding to the mean, and a decrease in its standard deviation. The histogram for the media is not expected to change dramatically, since the fibers are not assumed to play a key role in carrying the axial load.

We thus hypothesized that axially oriented adventitial collagen fibers would become less uniform in orientation following overstretch. This disorganization was expected to increase monotonically with an amount of overstretch. The medial circumferential fibers were not expected to show any significant change in orientation post-overstretch. On an individual fiber level, adventitial fibers were expected to become more circumferential post-overstretch, whereas medial fibers were expected to maintain their orientation.

As stated earlier, mainly elastin and collagen fibers govern mechanical properties. Chen [4] studied the orientation of collagen fibers in the adventitia of a coronary artery (explained in the Background chapter) in a circumferentially overstretched configuration and observed changes in their orientation, i.e., the fibers inclined more in the circumferential direction with the increase in the circumferential overstretch. Thus, we also expected the adventitial fibers to be more organized and to incline in the axial direction (0˚) in our case, i.e., in an axially overstretched configuration. Again, the inclination was expected to increase in severity with overstretch. The medial fibers might change their orientation as well to become more axially inclined.

The previous investigation [10] in the Lab of Head Injury and Vessel Biomechanics studied mechanical properties of cerebral blood vessels post-overstretch. Another recent investigation studied molecular level collagen damage post-overstretch using Collagen Hybridizing Peptide (CHP). CHP could only help visualize the damaged collagen. Our

hypothesis predicted change in collagen orientation with or without any damage to collagen. Since we had never before implemented any imaging technique in the lab that could visualize collagen to study the change in collagen orientation during and post-overstretch, we had to discover an appropriate imaging technique and develop an experimental method that could incorporate this technique to give the accurate results. We also carried out validation and verification of the newly developed experimental technique to check the accuracy of these results. This being our very first attempt to study the microstructural mechanism, we could not account for all the factors affecting the results. We thus decided to treat this as a pilot study. For the future scope, we will work on overcoming the limitations of the newly developed experimental technique to improve the accuracy of the technique itself and hence also the results.

CHAPTER 2

BACKGROUND

2.1 Prior work

As stated earlier, researchers have observed a change in orientation of collagen post- and during overstretch in other biological soft tissues. Details of their work are mentioned as follows.

Quinn [13] studied collagen fiber alignment in a rat facet capsular ligament. Soft tissues get loaded due to various different pathophysiological phenomena that do not produce visible damage or failure of these tissues. These tissues still get damaged structurally, which is indicated by the reduction in their tangent stiffness during loading. In order to know if there is any correlation between this sub-failure damage and collagen fiber realignment, research was conducted using quantitative polarized light microscopy (QPLM).

The Instron tensile testing machine was outfitted with quantitative polarized light imaging system. The tissue was loaded into tension with the Instron machine and quantitative polarized light imaging was used to acquire pixel-wise collagen fiber alignment maps with transmission of polarized light through the tissue. These maps were generated from every 20 images, which corresponded to 180˚ rotation of the polarizer. The vector correlation technique was then employed to detect anomalous fiber alignement.

From every alignment map acquired, correlation measurements were obtained from the maps preceding and following it. For each pixel, a vector correlation value was determined by comparing the data between alignment maps in a 5 x 5 pixel window centered at a particular pixel. The vector correlation measured the mean orientation for the fibers as well as the strength of alignment in mean direction. Vector correlation maps were produced for each fiber alignment map throughout the applied loading based on these pixel by pixel correlation calculations. The pixels having signal-to-noise ratio less than 2 were eliminated from the correlation calculations. This investigation found that the fiber kinematics within a ligament can significantly deviate from their normal alignment before the gross failure occurs and that the anomalous collagen fiber realignment can occur without visible changes on the tissue's surface. The QPLI system can be effectively used to detect subtle changes in collagen fiber alignment. The method was validated by correlating the mechanical response of the sample with the corresponding anomalous fiber realignment, e.g., first anomalous fiber realignment was observed with the first yield detection. This system was later used for further investigation on the similar topics as mentioned below.

Miller [14] used the technique verified by Quinn [13] to measure the collagen fiber realignment during mechanical testing of a mature mouse supraspinatus tendon. The study hypothesized that collagen fiber realignment and uncrimping are two main mechanisms responsible for the structural response of a tendon to the loading. In order to test the hypothesis, the tensile testing machine and QPLM system were used. The tendons were preconditioned for a different number of cycles to study the effect of preconditioning on collagen fiber realignment. After the preconditioning, the tendons were stretched axially and finally pulled to failure. The investigation showed that the collagen fiber realignment

was observed during preconditioning as well as axial stretching of the tendon at all the studied locations though the change in the number of preconditioning cycles did not affect the results as far as the collagen realignment is concerned.

Quinn [16] did a similar study in ligament to find out if collagen fiber realignment is associated with the changes in mechanical response observed during preconditioning. The investigation found that collagen fiber realignment along with viscoelasticity of the soft tissue contributes to these changes.

Miller [15] (another study by the same group) used the technique verified by Quinn [13] to measure the effect of preconditioning and stress relaxation on local collagen fiber realignment of a rat supraspinatus tendon. The study followed a series of steps as mentioned below.

The sample was preloaded to a nominal load of 0.01 N. It was then preconditioned between 0.1 and 0.5 N for 10 cycles. After the sample was brought back to the lower load of 0.1 N, it was kept on a hold for 300 s. The sample was then stretched to 0.42 mm at a rate of 0.35 mm/s. It was allowed to reach the equilibrium load for 600 s (stress relaxation). It was then brought back to zero displacement at a rate of 0.35 mm/s. The collagen fiber orientation graphs were collected throughout the testing. They were later used to plot the histograms. The histograms are as shown in the Fig. 2.1.

As it can be observed from the histograms, preconditioning affects collagen fiber organization. The stress relaxation does not have an effect on collagen fiber organization. This information provides a basis to support our hypothesis. The first thing to be recognized from this review is to find a method to image collagen in the cerebral blood vessel samples and then develop a suitable image processing technique to detect the collagen fiber angle.

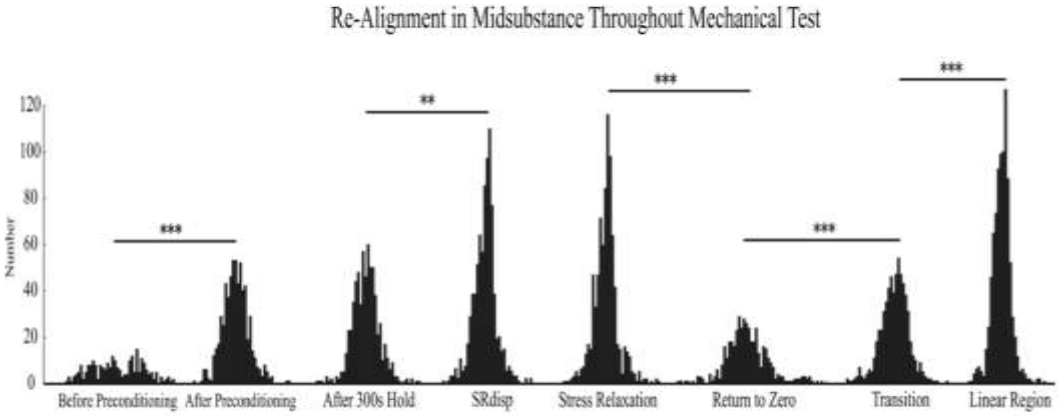

Fig. 2.1 Histograms for collagen fiber organization throughout the mechanical testing. (Redrawn from [15])

2.2 Overview of microscopy techniques

We did a literature survey to determine the most commonly used microscopy techniques to image collagen and also to pick up the one that best fits our purpose of imaging a fresh, live, uncut, cylindrical vessel sample. The techniques can be listed as follows: light microscopy, polarized light microscopy, electron microscopy, confocal microscopy, and simple harmonic generation with two-photon excited fluorescence. The average thickness of adult sheep middle cerebral artery is approximately 130 μm and hence, a technique was required that can image tissue with this large thickness. Cerebral blood vessels have a different collagen orientation in different layers [8]. Adventitial fibers are primarily longitudinal in their orientation whereas medial fibers are mainly circumferentially oriented. We needed to monitor orientation changes in each layer of the tissue separately, which makes it necessary to have a depth-resolved imaging technique. Based on the literature survey and experience of the senior lab members in imaging of the sheep middle cerebral artery, we have analyzed effectiveness of each of the

above-mentioned imaging techniques to fulfill our requirements. The description of each of these techniques is as follows:

- Light microscopy (LM): This type of microscopy is effective in imaging collagen for tissues with thickness in the range of 5-10 μm. Li [17] did a quantitative analysis of human umbilical vein (HUV) collagen. Masson's trichrome stain was used to stain the microstructural components of the blood vessel. The tissue was frozen and then fixed before it was stained. After the tissue was stained, it was sectioned into 5 μm thick slices and was imaged under a light microscope to visualize collagen. Canham [18] studied human coronary arteries at distended pressure. Arteries were dissected from the hearts after an autopsy. Arteries were fixed in formalin, embedded in paraffin, and sectioned into 7 μm thick slices. The slices were then stained with different stains (trichrome, hematoxylin, and eosin etc.). These slices were then visualized under the light microscope for visualizing collagen, elastin, and smooth muscle cells. It is evident from the observations that tissue needs to be stained for visualizing collagen under the light microscope. Staining the tissue primarily requires fixation and sectioning of the tissue into smaller sections. The technique does not satisfy the requirements for imaging collagen in our experiment and hence was omitted.
- Polarized light microscopy (PLM): This type of microscopy is effective in imaging collagen for tissues with the thickness approximately in the range of 5-10 μm. Quinn [13] used a quantitative polarized light microscopy to quantify collagen in a rat facet capsular ligament. This microscopy gives an average orientation for the entire depth of the tissue. It does not provide us with an average orientation for a single layer (intima, media or adventitia) of the tissue unless the layers are separated and imaged independently. Finlay

[19] also used PLM for imaging 3-dimensional organization of collagen of the human brain arteries. The arteries were fixed and sectioned having a thickness of approximately 5 to 7 μm. They were then stained with picrosirius red for imaging. This highlights the fact that the PLM is not very effective in determining the average collagen orientation in every single layer of the tissue separately. It is primarily effective for tissue with lesser thickness (lesser than that we have in sheep middle cerebral arteries) and needs staining. Staining needs the tissue samples to be fixed. It cannot thus be used to image collagen in case of our experiment.

- Electron microscopy (EM): This type of microscopy is effective in imaging collagen for tissues with the thickness approximately in the range of 4-8 μm. Orberg [20] used SEM to study collagen fibers in the intestine. Rat intestines were used for this purpose. The samples from rat intestines were fixed, coated with a gold-palladium alloy, and scanned under the electron microscope. The largest fiber diameter observed under a microscope is reported to be 4 μm. Geer [21] used tissue samples from human aorta. The aorta was sliced into thin ribbons. It was then hydrated, fixed, sectioned, and stained with lead citrate or lead hydroxide. Sections were examined and photographed under the electron microscope. This type of microscopy again requires fixation and hence cannot be used for visualizing collagen in our experiment.
- Confocal microscopy (CM): This type of microscopy can image a tissue with a wide range of thickness (approximately 100 μm). The tissue is typically stained with different types of markers that mark collagen. After the tissue is stained, a suitable confocal laser is used corresponding to the excitation and emission wavelength of the marker to visualize collagen under a confocal microscope. Rezakhaniha [22] studied collagen

waviness and orientation of the adventitia of common carotid arteries. The common carotid arteries from rabbits were excised. CNA35-OG488 was used to mark collagen in these arteries. The arteries were incubated overnight in a 2 μM solution of CNA35-OG488 in PBS. Some of the arteries were cut open while the rest of them were kept intact and imaged under a confocal microscope to visualize collagen fibers labeled with the fluorescent marker. The average thickness of the adventitia was 0.13 mm or 130 μm. The thickness of the arteries imaged was approximately 100 μm. The Lab of Head Injury and Vessel Biomechanics has used the collagen type-1 antibody to stain the type-1 collagen in the sheep middle cerebral arteries. This microscopy allows live imaging of the fresh, intact, and cylindrical vessel sample. It was thus decided to explore this method for imaging the vessel sample in our experiment.

- Second harmonic generation with two-photon excited fluorescence: This type of microscopy is effective in imaging collagen for tissues with thickness as large as 300 μm. Wicker [23] studied normal basilar artery structure. Basilar arteries were harvested from male rabbits. They were then divided into two equal segments and mounted onto custom glass cannulae approximately 300 μm in diameter. The arteries were then placed under a nonlinear optical microscope to visualize collagen. Nonlinear optical microscopy (NLOM) can image collagen when it is fresh and intact. As it can be noticed from description and preparation of the vessel sample for various types of microscopy, confocal microscopy, and nonlinear optical microscopy (second harmonic generation with two-photon excited fluorescence) are the best-suited techniques to image collagen in blood vessels. We thus decided to explore these two techniques. In case of cerebral blood vessels, adventitia has primarily type-1 collagen whereas media has primarily type-3 collagen [8]. In order to

visualize collagen under a confocal microscope, we thus needed to use antibody stains for both collagen type-1 and type-3.

2.3 Investigated microscopy techniques

2.3.1 Confocal microscopy with collagen antibody staining

Collagen antibody staining is an antibody-based method to detect a specific protein (collagen) in a tissue sample. An antibody (Ab), also known as an immunoglobulin (Ig), is a large, Y-shaped protein produced mainly by plasma cells that are used by the immune system to neutralize pathogens such as bacteria and viruses [24].

The antibody staining protocol primarily used 2 reagents. They are the primary antibody and the secondary antibody. The primary antibody binds to a target antigen. The secondary antibody is especially efficient in immunolabeling. The secondary antibody binds to the primary antibody, which is directly bound to the target antigen. It helps to increase sensitivity and signal amplification while imaging [25]. The reagents used for the purpose of antibody staining are mentioned in Table 2.1. Donkey block was used to prevent any nonspecific binding. The vessel sample was obtained from Lamb Intensive Care Unit (LICU) at the University of Utah. All procedures met requirements established by the Institutional Animal Care and Use Committee at the University of Utah. The animal was Columbia-Rambouillet ewe. The ewe was euthanized via an overdose of Beuthanasia (MWI Veterinary Supply, Boise, ID, USA). The head was taken off within an hour of death. The brain was then removed from the skull within 1 more hour. The brain was placed in a container filled with phosphate buffered saline solution (PBS; KCl 27, KH_2PO_4 18, NaCl 1370, Na_2HPO_4 100, $CaCl_2.2H_20$ 10, $MgCl_2.6H_20$ 5; concentrations in

Table 2.1 Table specifying details of collagen antibodies.

No	Type of antibody		Primary	Secondary
1	Collagen type-1		Anti-Collagen I antibody (ab34710) [Source: abcam.com][26	Donkey Anti-Rabbit IgG H&L (Alexa Fluor® 555) (ab150074) [Source: abcam.com].
2	Collagen type-3		Goat anti-type III collagen-BIOT [Source: Southern Biotech]	Donkey anti-goat IgG(H+L), rat/mouse SP ads-FITC [Source: SouthernBiotech].

mM) for transport back to the lab. In the lab, MCAs were dissected from the brain. The MCAs were stored in a refrigerator until testing. A part of either of the MCAs that was straight was used for the purpose of testing. The following protocol was implemented for antibody staining of the cerebral blood vessel sample. The round cerebral blood vessel was cut open by making a cut along the length of the vessel. The primary antibody was diluted with a block (Concentration 1:150). The vessel sample was incubated with the primary antibody for 12 hours. The vessel sample was washed thrice with PBS for 2 hours each. The secondary antibody was also diluted with the block (Concentration 1:150). The vessel sample was incubated in the secondary antibody for 12 hours. The vessel sample was washed thrice with PBS for 2 hours each. The vessel sample was mounted on the slide with Fluoromount-G^{TM} with the adventitia on the top. It was then covered using a coverslip and imaged under a confocal microscope. The settings used for the confocal microscopy are as follows. Samples were imaged at 10x (512 x 512 pixels) using a laser scanning confocal microscope (Fluoview 1000, Olympus). Serial slices were taken in 5 μm increments, producing a z-stack through the entire wall. The secondary antibody signal was excited with the 488 nm Argon gas laser. The collagen antibody staining worked only for the type-1 collagen molecule as shown in Fig. 2.2 and not for type-3 collagen. The reasons that might have been responsible for type-3 collagen antibody to not work are listed as follows: The cerebral blood vessels are extremely small in size as compared to the other biological tissues. The amount of media, or type-3 collagen, might thus be too small for the primary antibody to bind to them. The primary antibody molecules are large in size, which makes their penetration inside the media difficult or the media of cerebral blood vessels does not have type-3 collagen. The possibility that cerebral blood vessels might not have type-3

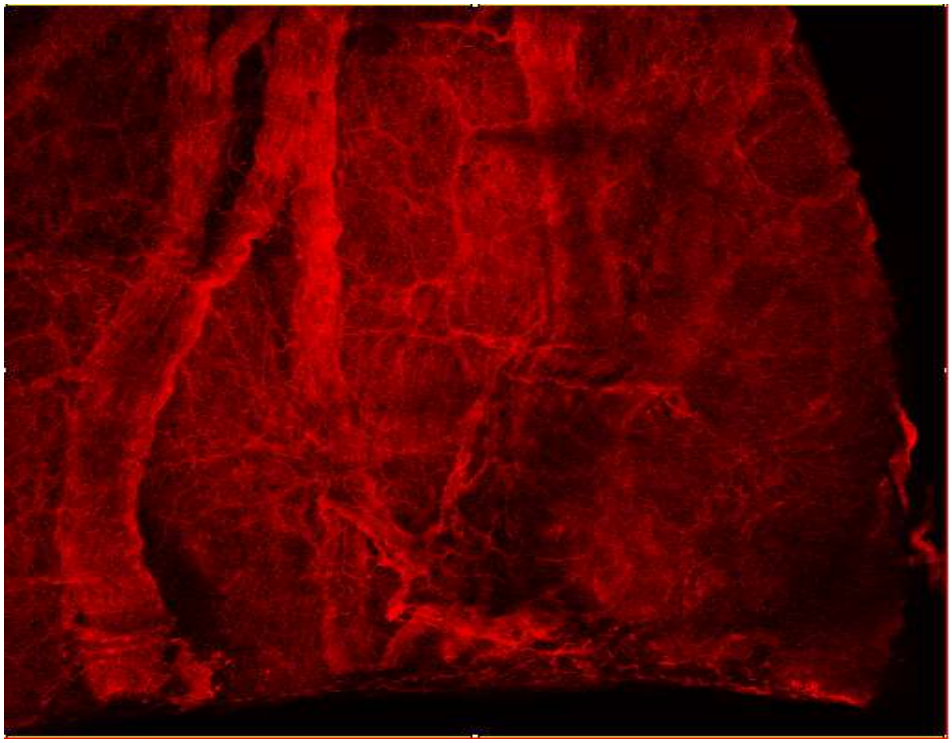

Fig 2.2 Cerebral blood vessel sample stained with type-1 collagen antibody and imaged under a confocal microscope.

collagen was eliminated by staining the blood vessel sample with Picro Sirius Red (PSR) staining. A PSR-stained vessel sample shows yellow-orange birefringence for type-1 and green birefringence for type-3 collagen fibers [26]. The tissue was fixed in formalin and embedded in paraffin wax. It was then sectioned (5 µm), and sections were stained using PSR. The stained sections of the tissue were then imaged under an optical polarized light microscope. The images showed both yellow-orange birefringence and green birefringence, which are indicative of type-1 and type-3 collagen fibers, respectively, as shown in Fig. 2.3. The rest of the possibilities for type-3 antibody to not work, could not be tested due to stain unavailability. Since type-3 antibody did not work this method was eliminated from use in the experiment. We thus decided to explore other imaging technique, i.e., the second harmonic generation using two-photon excited fluorescence.

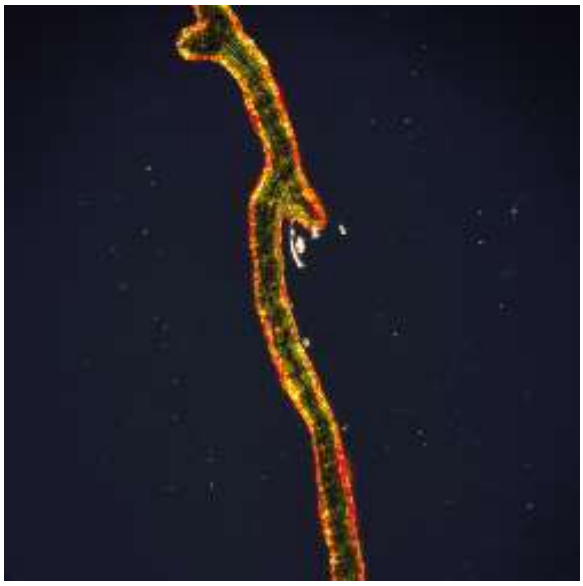

Fig. 2.3 Cerebral blood vessel sample stained with PSR and imaged under an optical polarized light microscope.

2.3.2 Second harmonic generation imaging using 2-P excitation

The collagen molecule is non-centrosymmetric. This property is used to image collagen with a second harmonic generation using two-photon excitation [29]. A photon is used to excite an electron. When an electron is excited to a different energy state than its original energy state, it retains its excited state for some duration of time and then leaves that state to come to a ground state by emission of a photon of a less energy. The photon having less energy has a higher wavelength. This is the reason why the photon that is used to excite the electron has a lower wavelength than the photon that gets emitted. This is why the excitation wavelength is less than that of the emission wavelength [30]. In the case of 2-P microscopy, the electron is excited by 2 photons of half the required energy. The electron, after being in this state for a definite period of time, returns to its ground state by emission of a photon of less energy, but the emission wavelength, in this case, is less than that of the excitation wavelength because of use of 2 photons. The principle of the second

harmonic generation can be explained as follows: As electromagnetic radiation propagates through the matter, its electric field exerts forces on the sample's internal charge distribution. The consequent redistribution of charge generates an additional field component, referred to as electric polarization, which has both linear and nonlinear components. The nonlinear components become significant only at very high light intensities. Their effect is to generate overtones, or harmonics, at exact multiples of the original frequency. As far as the second harmonic is concerned, this generation happens only if the molecule's electrical properties are different in each direction so the ability is peculiar to molecules which are non-centrosymmetric [30].

Ultima Intra Vital multiphoton microscope (MPM) (Bruker Corporation) was used for the purpose of SHG imaging using 2P excitation. The settings used for imaging are as follows. Image size-512 x 512; Dwell time- 8-10 us; Magnification- 1 x; 2P laser power-6-8% (attenuation mode); 2P laser frequency- 800 nm; Transmitted signal- Sub Blue PMT 500-900; z-step- 5 µm.

Sample acquisition is the same as that for the antibody staining. Tissue does not require any specific preparation for NLOM. The vessel sample was cut open and placed with the adventitia on top. It was mounted using Fluoromount-G^{TM} and covered with a coverslip. Both type-1 (adventitial) and type-3 (medial) collagen were imaged successfully as shown in Fig. 2.4, Fig. 2.5, Fig. 2.6, Fig. 2.7, Fig. 2.8, and Fig. 2.9 using NLOM. The method was thus finalized to be used for imaging in the final experiment.

It was observed during one of the trial experiments that the clarity or visibility of collagen is a function of the age of the sheep from which the vessel is extracted. Adventitial collagen from newborn lambs was not visible. It was visible, but with lesser clarity than in

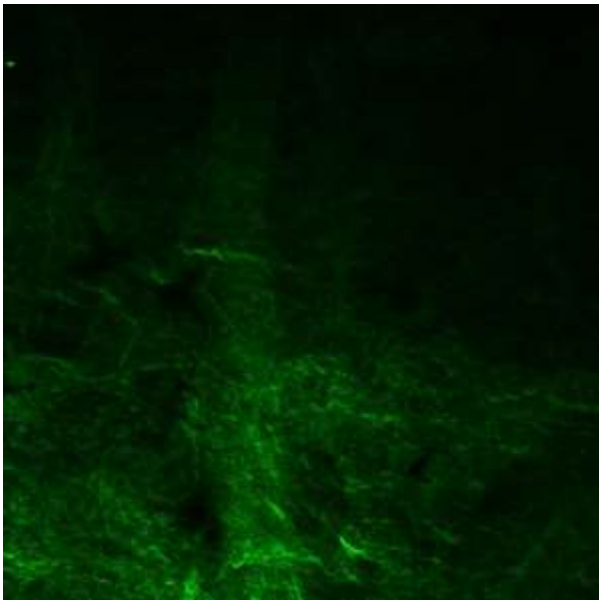

Fig. 2.4 NLOM image of an adventitia of a baby sheep

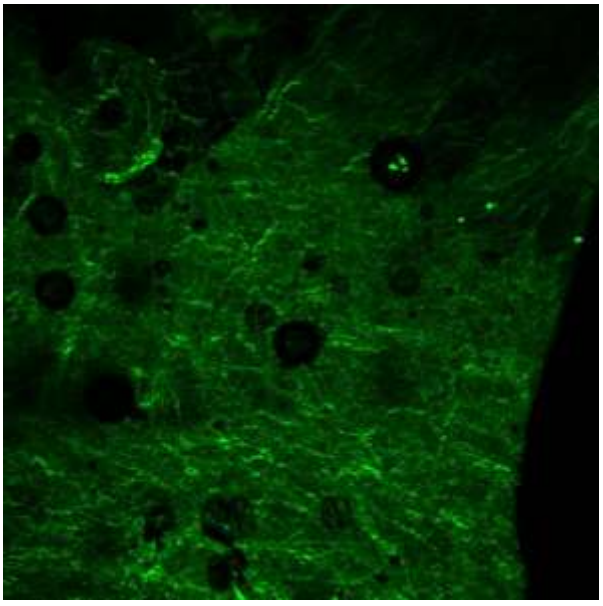

Fig. 2.5 NLOM image of an adventitia of a juvenile sheep

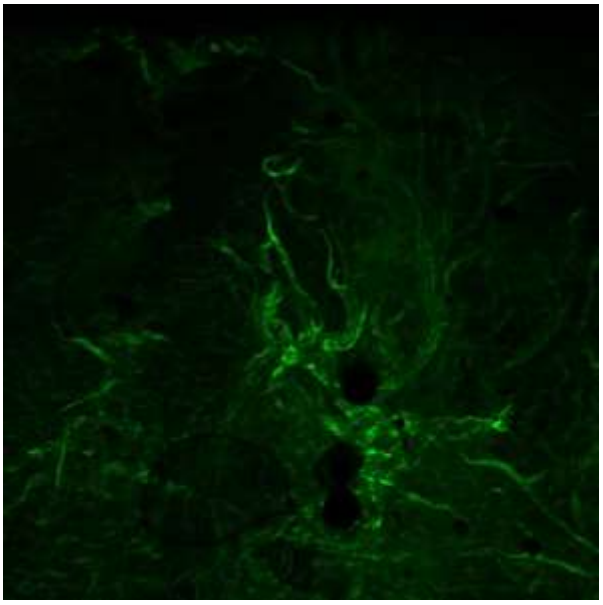

Fig. 2.6 NLOM image of an adventitia of a ewe

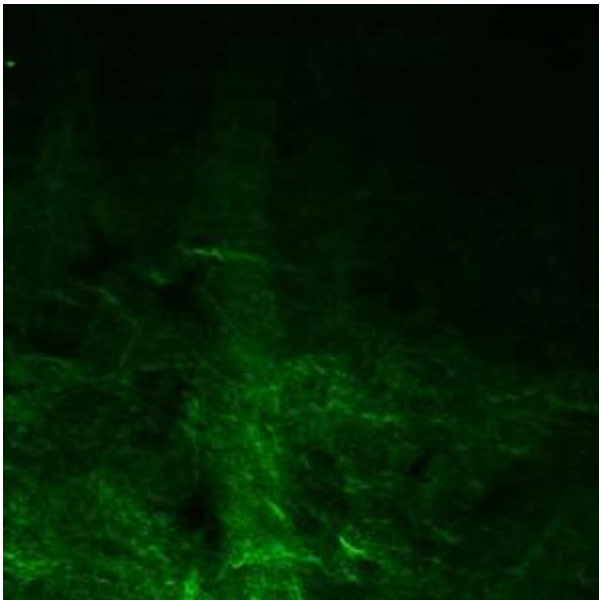

Fig. 2.7 NLOM image of a media of a baby sheep

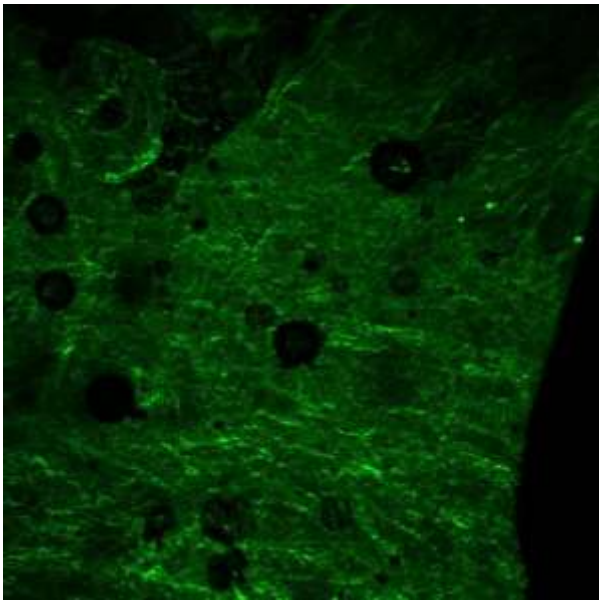

Fig. 2.8 NLOM image of a media of a juvenile sheep

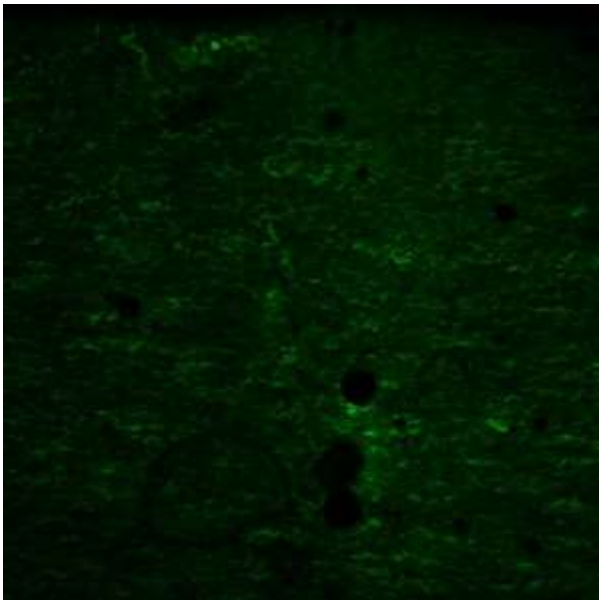

Fig. 2.9 NLOM image of a media of a ewe

adults, in juveniles. In the case of vessel samples from adult sheep, collagen is clearly visible. It was thus preferred to use adults for the purpose of the entire experiment. We have listed below a set of images for adventitial collagen captured from cerebral blood vessels of a baby, juvenile, and adult sheep.

2.4 Literature survey specifying use of NLOM for imaging and quantification of collagen

As mentioned earlier, for the study to be thorough and insightful, we need to verify the ability of the imaging technique (NLOM here) that we plan to use. We did a literature survey to check the ability of this method to image collagen for the effective quantification.

Zoumi [27] studied coronary artery microstructure using second-harmonic and two-photon fluorescence microscopy. The experiment used rabbit aortas and pig coronary arteries. Two mm-thick cross-section rings were sectioned from the vessel. Some of the rings were kept fresh and imaged while others were fixed in 4% formalin. The arteries were excited with an average wavelength of 800 nm. Different bandpass filters were used to collect SHG, TPF, and combined SHG and TPF data. After the arteries were imaged with SHG/TPF set-up, they were stained with hematoxylin and eosin (for the aorta) and toluidine blue O (for the coronary arteries). The stained sections were then imaged with Olympus BH-2 upright optical microscope. The wall thickness and the luminal diameter were measured with the optical microscope so as to validate the results from MPM. In order to correlate the images of the microstructure with the stress state of the vessel wall, the vessel was examined under four different stress and strain conditions. The conditions were as follows: 1. Zero-stress state; 2. No load (zero- transmural pressure); 3. 30-mm Hg

distension; 4. 180-mm Hg distension. Collagen fibers showed a decrease in the average fiber thickness and the average width of collagen fibers in the distended state when compared to zero-stress or no-load state. The fibers were thinner towards the lumen and become thicker towards the outer wall. From all the observations, it was concluded that multiphoton microscopy is a highly sensitive and promising technique to study the microstructural properties of the blood vessel wall.

Watson [28] studied collagen fiber angle distribution in mouse models of atherosclerosis. The aortas were harvested from the mice who were fed a high-fat Western diet and on a regular Chow diet. The thoracic aorta and abdominal aorta samples were collected from them. These samples were flattened to a slide. The collagen images of the sample were obtained with TPEF-SHG microscopy. The average orientation of collagen fibers was calculated. It was found that the collagen fibers in mice maintained on Chow diet were aligned at an average angle of 63˚ whereas those maintained on high-fat Western diet were aligned at an average orientation of 20 ˚. The mice fed with high-fat Western diet seem to have their collagen fibers reoriented in a circumferential direction. Mice on high-fat Western diet are prone to develop aneurysms. This apparent shift in absolute angle coincides with the development of extensive aortic atherosclerosis, suggesting the atherosclerotic factors contribute to collagen fiber angle orientation.

Chen [4] studied some of the microstructural properties of elastin and collagen fibrils from coronary adventitia. For studying collagen properties, it was needed to image the collagen. The multiphoton microscopy (MPM) was used for that purpose. The coronary arteries were dissected from the hearts of healthy pigs. The arteries were inverted so as to expose intima and media. These layers were then peeled off carefully to expose adventitia.

The adventitia was then mounted on a mechanical tester and stretched axially so as to achieve a stretch ratio of 1.3. The adventitia was imaged with MPM in this state. The adventitia was then pressurized to different luminal pressures so as to obtain circumferential stretch ratio of 1.2, 1.4, 1.6, and 1.8. The images were captured from the adventitia at all of these stretch levels.

Fluorescent microspheres were used to track the scan area and deformation of individual fibers. The necessary image processing was done manually as well as using MATLAB to determine the orientation angle of collagen fibers. A histogram of orientations was plotted individually for each layer of the adventitia for all the configurations. The histogram or the bell-shaped curve obtained for different fiber orientations was represented by an exponential function. The parameters included in the exponential function were determined. It was observed that with an increase in the circumferential overstretch, the fiber orientation angle decreased and became oriented more in the circumferential direction. The parameters representing the exponential curve showed a trend as well. Fig. 2.10 shows the variation of the orientation angle with the circumferential stretch ratio. This shows that the orientation of collagen fibers changes when the sample is overstretched circumferentially. It is reasonable to expect that similar thing would happen when the sample is overstretched axially since the microstructural properties in both the directions are governed by elastin and collagen fibrils forming the vessel wall.

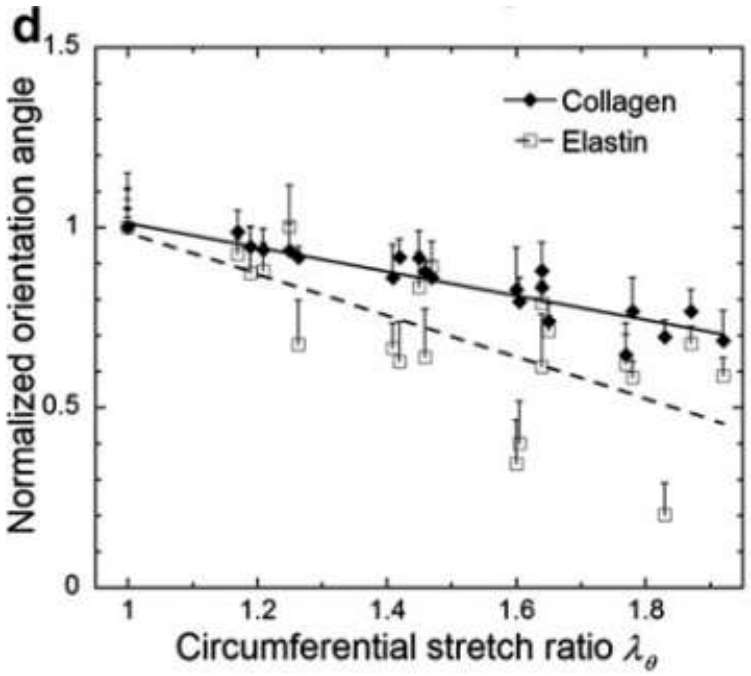

Fig. 2.10 Graph of normalized orientation angle plotted against circumferential stretch ratio. (Redrawn from Chen [4])

CHAPTER 3

METHODS

3.1 Sample acquisition and preparation

A total of three middle cerebral artery (MCA) sections were dissected from 3 adult sheep. Two of the sheep were obtained from the Lamb Intensive Care Unit (LICU) at the University of Utah. All procedures met requirements established by the Institutional Animal Care and Use Committee at the University of Utah. The animals were Columbia-Rambouillet ewes. These ewes were euthanized via an overdose of Beuthanasia (MWI Veterinary Supply, Boise, ID, USA). The third one was obtained from K Bar Livestock, LLC. It was first sedated with propofol (5-10 mg/kg IV), then euthanized with Beuthanasia D (1 mL/4.5 kg IV). The head was taken off within an hour of death. The brain was then removed from the skull within 1 more hour. The brain was placed in a container filled with phosphate buffered saline solution (PBS; KCl 27, KH_2PO_4 18, NaCl 1370, Na_2HPO_4 100, $CaCl_2.2H_20$ 10, $MgCl_2.6H_20$ 5; concentrations in mM) for transport back to the lab. In the lab, MCAs were dissected from the brain. The MCAs were stored in a refrigerator until testing. A part of either of the MCAs, which is straight, was used for the purpose of testing. The side branches were ligated with individual fibrils from unwound 6-0 silk suture. This enabled the vessel sample to hold the pressure during the experiment. Vessel samples were secured to stainless steel needles with suture, and cyanoacrylate glue,

and tested within 48 hours of death ([31]-[33]).

3.2 Experimental apparatus

The horizontal tester developed in the Lab of Head Injury and Vessel Biomechanics [34] was used for the purpose of testing the vessel sample. The tester provides the facility for axial testing of the cerebral blood vessel samples. A wide range of vessel samples (having approximate lengths between 2 mm and 12 mm) can be tested with this set-up. Different sizes of the needles on which the vessel samples are mounted accommodate for different lengths and diameters of the vessel sample. Moving parts on the tester set-up can also accommodate for testing of the vessel samples with greater lengths. The vessel sample is placed on the needles that match with its inner diameter. The needles are made up of different size stainless steel hypodermic tubing to accommodate different vessel diameters. As mentioned in [34], the tester consists of a PBS bath. The bath included a glass window in its base for light. The set-up had two needles mounted on it. One of the needles (proximal needle) was attached to a voice coil actuator (MGV52-25-1.0, Akribis, Singapore) with a low-friction sled. A digital encoder having a resolution of 1.0 μm was used to measure the displacement of this needle. This needle was free to slide horizontally on the sled track, thus overstretching the vessel sample in an axial direction. The other needle was kept fixed in its position during the entire duration of the experiment. This needle (distal needle) was connected to an X-Y stage (MS-125-XY, Newport, Irvine, CA) that allowed fine adjustment for aligning this needle with the proximal needle. This ensured that the vessel sample was on the same plane. A digital video camera (PL-A641, Pixelink, Ottawa, Canada) mounted to the light microscope (Ziess 2000 C, Carl Zeiss Microscopy,

Thornwood, NY) was used to record vessel deformations during preconditioning. The vessel sample was perfused with a PBS syringe attached to the computer-controlled linear actuator (DA0.25-AB-HT17075-4-P, Ultra Motion, Cutchogue, NY) during preconditioning and from a hanging, open syringe during overstretching. The fluid path passed through the proximal needle, mounted MCA, and the distal needle, to a closed valve that prevented the flow. The inline pressure transducers (26PCDFM6G, Honeywell, Golden Valley, MN) were located both proximal and distal to the mounted vessel sample. They were placed equidistant from the vessel sample and the average between these two transducers was taken to be the pressure inside the vessel sample, or the luminal pressure. A custom LABVIEW program (National Instruments, Austin, TX) provided the test control and data and video acquisition during preconditioning.

3.3 Testing protocol

The vessel sample was mounted on needles. It was kept immersed in the PBS bath for the entire duration of the experiment. After the vessel sample was mounted, it was preconditioned by oscillating the luminal pressure (6.7–13.3 kPa; 50–100 mm of Hg) for five cycles while the length was held constant. Preconditioning tests were repeated at gradually increasing lengths until the in-vivo length was identified [35].

Following the preconditioning, the tester was detached from the voice coil actuator and the digital encoder to carry it to the microscopy core (Fluorescence Microscopy Core Facility, a part of the Health Sciences Cores at the University of Utah) for further testing on the vessel sample. A small assembly, as shown in Fig. 3.1, was mounted on the tester next to the fixture on which the proximal needle was placed (proximal needle fixture) for providing accurate displacements to the vessel sample during the testing. The assembly

Fig. 3.1 Micrometer screw gauge and ball bearing assembly to give precise motion to the needle.

consisted of a micrometer screw gauge (Eisco Labs Micrometer Screw Gauge, Nickel Plated Brass - Range 0-25x0.01 mm), a ball bearing (6.3 x 12 x 3 mm; deep groove ball bearing), and an acrylic block (23.8 x 23.4 x 5.55 mm) with a hole (diameter- 6.3 mm) drilled at the center. The ball bearing was fixed inside the hole in the acrylic block by gluing the bearing's outer race to the inner surface of the hole. The ball bearing was press-fitted onto the micrometer screw gauge shaft such that the inner race of the bearing could rotate with it. One of the side surfaces of the acrylic block was fixed to the proximal needle fixture. The assembly provided a linear motion to the block and the fixture with the rotation of the micrometer screw gauge shaft. The set screws were used to keep the proximal needle in position in order to prevent sliding on the track during transport of the tester to the microscopy core.

The vessel sample was photobleached at some spots. The microscope software (Prairi View Imaging) provides the facility of photobleaching. This facility is available in

the microscope software (T Series details - Cycle type-PA; Repetitions- 10; Period- 3.41621 seconds; Iterations-1; 2P Laser- 100%). Four spots were created to form a diamond-shaped region or a single spot was created at the center of the field of view (FOV). They were made in order to make sure that the same region was imaged at all times during the testing.

For testing, the following protocol was implemented. The Ultima Intra Vital Multiphoton Microscope (MPM) (Bruker Corporation) was used to image collagen in the cerebral blood vessels. The microscope was used in two-photon (2P) mode. The vessel sample was pressurized to 13.3 kPa using an open syringe of PBS, mounted at the required height and using the same flow path as during preconditioning. The experiment was carried out at a quasi-static rate, so the pressure would not change unless there was a leakage through the vessel sample wall. The vessel sample was first detected using the autofluorescence of elastin. The vessel sample was first imaged at its in-vivo length. The z-stack was captured in the in-vivo position with a step of 5 µm at first. The overstretch values for $\lambda_z \approx 1.1$, 1.2, 1.3, and 1.4 (λ_z corresponds to 1 for in-vivo length) were calculated from the corresponding in-vivo lengths of the vessel samples. The overstretch values were selected in this range since this investigation is motivated by the earlier investigation by Bell [10], including changes occurring in the mechanical properties of the blood vessel samples post mild axial overstretch, who studied overstretch at these levels. Also, collagen damage analysis utilizing "collagen hybridizing peptide (CHP)" was done in this range. The set screws were loosened and the vessel sample was overstretched, first to get λ_z equal to $1.1 * \lambda_{IV.}$ The vessel sample was held in the overstretched position for approximately 2 minutes for capturing a z-stack in this position since we wanted to analyze the change in

collagen fiber angle, if any, in the overstretched configuration. The vessel sample was then returned to its in-vivo length. The average time period to bring the vessel sample back to its in-vivo length post-overstretch varied from 30 seconds to 20 minutes. Sometimes, the vessel sample would not be on the same plane post-overstretch. In order to better image the vessel sample, the microscope settings and the vessel sample position had to be readjusted. This was the main reason responsible for this delay. After the vessel sample was returned to its in-vivo length, it was again fixed with set screws, thus preventing its movement. The needle position was used as a reference to determine if the vessel sample was returned to its in-vivo configuration.

In order to determine whether viscoelasticity might affect the fiber angle, we captured the z-stack of the vessel sample immediately after it was brought back to its in-vivo length and then waited for approximately 15 minutes before again capturing the z-stack without changing any settings.

3.4 Data analysis

3.4.1 Image processing

Various z-stacks obtained at in-vivo position, before and after the vessel sample was overstretched to different stretch levels, were analyzed in order to test the hypothesis. The procedure followed for the analysis is mentioned as follows: The z-stacks were cropped so as to include the region either enclosing the photobleached spots or in between the photobleached spots, in order to be confident about quantifying the same region before and after the overstretch. For the data with a single photobleached spot, the images were cropped so as to have this photobleached spot at the center. The z-stacks had to be

reoriented sometimes since the vessel sample wall was not exactly horizontal. The reorientation was done in order to have the vessel sample wall in a horizontal position. Otherwise, the calculated orientation for collagen fibers might give inappropriate values.

A single adventitial image was picked from each of the configurations that were showing similar features. The image was picked from the top surface of the vessel sample so as to avoid any error in the orientation measurement arising from the collagen data captured through side walls of the vessel sample. After the image was selected, it was analyzed with different techniques. First, a set of 2 or 3 fibers were selected in each image corresponding to each configuration.

Configuration necessarily refers to a state of the vessel sample in which the data were captured. We had 9 different configurations for the first 2 experiments corresponding to in-vivo, overstretch-1, overstretch-2, overstretch-3, overstretch-4, in-vivo post-overstretch-1, in-vivo post-overstretch-2, in-vivo post-overstretch-3, and in-vivo post-overstretch-4 whereas for the last experiment, the data in the overstretched configurations could not be captured due to problems with the microscope stage, which restricted motion of the objective lens, leaving us with only 5 datasets.

A single line was drawn on each of the fibers manually while the image was pulled in ImageJ. The orientation of this line drawn on the fiber was measured and was referred to as a fiber orientation for that particular fiber. This was a preliminary analysis done to know if the orientation of the collagen fiber was showing any trend with overstretch. This was done to help us understand if the images provide quality data for quantification of the fiber orientation. After the preliminary analysis using the hand-drawn line, the image was divided into different regions of interest. A region of interest was selected in such a way

that fibers in a particular region have an identical orientation. Fibril Tool (ImageJ plugin) was used to quantify average orientation for every single region of interest.

The image was then analyzed using Orientation J Distribution, which assigns weights to every single orientation based on a number of fibers oriented in that direction and their intensity. Mean fiber angle and standard deviation for each image were calculated as explained later in this chapter.

In order to see if viscoelasticity affects the results, a montage of the z-stacks that were captured immediately after the vessel sample was brought back to its in-vivo length and after a certain period of time (as mentioned earlier) were formed. These montage images were subtracted from each other in order to see if the resulting images showed any significant features indicating viscoelastic recovery.

3.4.2 Statistical analysis

The data obtained from processing the images with Orientation J Distribution gave a set of the angles from '-90°' to '+90°' and weights assigned to those angles. The weights were treated as frequencies. The mean and the standard deviation were calculated using the following formulae:

$$\text{Mean} = \Sigma (f_i * x_i) / \Sigma f_i \qquad [X] \qquad (1)$$

$$\text{Variance} = \Sigma f_i * (x_i - X)^2 / \Sigma f_i \qquad [\text{Var}] \qquad (2)$$

$$\text{Standard Deviation} = (\text{Var})^{0.5} \qquad [\text{SD}] \qquad (3)$$

where f_i = frequency of i^{th} orientation; x_i = i^{th} orientation.

After the mean and the standard deviation were calculated for each image

separately, two-tailed t-tests were carried out for comparing the in-vivo data with the in-vivo post-overstretch data and the data corresponding to the overstretched configuration. The groups are not considered statistically different if $p >= 0.05$.

The data were then divided among different ranges near the mean orientation. The ranges were selected such that the mean orientation was lying approximately at the center of these bin ranges and thus, plotting the data from these ranges would help determine any subtle change in the mean orientation. The area under the curve for each of these ranges was calculated for each stack and the results were plotted on a single graph.

CHAPTER 4

METHODS EVALUATION

This was the first experiment in the lab that was conducted outside the lab space. After preconditioning, we had to carry the tester to the microscopy core for imaging during the rest of the experimental procedure. This type of transportation of the vessel sample, in a pressurized state where the pressure is considerably below in-vivo pressure, was a whole new experimental technique that we employed in the lab. Also, we had never successfully used 2P microscopy before to image collagen fibers in the cerebral blood vessels. We had to quantify the orientation of collagen fibers before, after, and during overstretch in order to verify our hypothesis. Based on this requirement, we decided to make use of Image-J modules: Line Tool, Fibril Tool, and Orientation J Distribution, to quantify the collagen fiber orientation. We had not previously tested the validity of these tools to determine the orientation of collagen fibers. We thus found it essential to verify and validate the ability of all these techniques and procedures to meet their intended purpose. We thus carried out validation and verification of every step of an experimental protocol.

4.1 Experimental testing for validation of preconditioning protocol

As mentioned above, we had to carry out preconditioning of the vessel sample to determine its in-vivo length. The entire set-up for carrying out preconditioning was

available only in the lab space. We thus preconditioned the vessel sample in the lab space, after which we restricted any fluid to enter and exit the vessel sample and removed the pressure column. We then used set screws on the tester to keep the vessel sample intact in its length during its travel to the microscopy core. After this, we detached the tester and carried it to the microscopy core. This led to a significant time gap (approximately an hour) between the preconditioning of the vessel sample and its imaging at the microscopy core. Earlier experiments carried out in the lab did preconditioning and mechanical testing in succession without having a time gap of more than 5 minutes. Also, the pressure was always maintained equal to the in-vivo pressure after preconditioning. We thus wanted to verify the effect of transportation time and procedure, if any, on the mechanical response of the vessel sample indicating changes in the mechanical structure of its fibers since the mechanical response of the vessel sample is governed by elastin and collagen fibers [11]. We carried out this study as mentioned below.

The vessel sample acquisition and preparation is as mentioned in section 3.1. It is known to us that after the preconditioning, the stress-strain (or force-displacement) curve obtained for tensile testing of the biological tissue sample shows a repetitive nature and corresponding stress-strain (force, displacement) values between two fixed strains. We decided to base our study on this fact. We decided to carry out tensile axial testing from the buckled state to the in-vivo state. Earlier investigation [10] has reported that the vessel sample, if stretched beyond its physiological length, gets softened and its mechanical properties get altered as well. This made us restrict our testing in the range of buckled length and in-vivo length since testing beyond in-vivo length would not show us repetitive stress-strain curves after the preconditioning. The first step was thus to determine the in-

vivo length of the vessel sample.

In order to know the in-vivo length of the vessel sample, we followed our regular experimental preconditioning protocol. Once the in-vivo length was determined and the corresponding voice coil position was noted, the vessel sample was brought back to its buckled state and the luminal pressure was made zero. The vessel sample was kept at this pressure for approximately 3 hours such that it no more remained preconditioned. It is important to note here that the voice coil position corresponding to the buckled state and the in-vivo state of the vessel sample were both noted and since the tester was not detached or the software recording the data was not restarted during the experiment, the voice coil positions could be used throughout the testing to produce repetitive loading of the vessel sample in the same range.

The vessel sample was then stretched axially from the buckled state to the in-vivo state at zero luminal pressure. Force and displacement values were obtained for this testing (denoted by zero load test-1). The vessel sample was then preconditioned (as is done in the actual experiment) and again the axial stretching from buckled to in-vivo state was carried out (denoted by zero load test-2). Force and displacement values were again acquired for this testing. In order to replicate the experimental conditions, the vessel sample was kept stationary at in-vivo length and in-vivo pressure for approximately 2 hours (the vessel sample is carried out to the microscopy core in a pressurized state and fixed at its in-vivo length.) Similar axial tensile testing and data acquisition as before were done after this waiting period (denoted by zero load test-3). Although we transport the vessel sample from lab to the core in a pressurized state, it is not maintained at in-vivo pressure since it is not possible to maintain a fluid column during the transport to raise the luminal pressure to the

in-vivo pressure. We took this into consideration and after the earlier testing, we reduced the luminal pressure in the vessel sample to zero. We then again kept the vessel sample stationary for 1 more hour to replicate the experimental conditions during the transport and carried out similar testing and data acquisition at the end of it (denoted by zero load test-4).

We plotted force-displacement curves with the acquired data and compared them together to know if the vessel sample remained preconditioned during the transport. We could claim the vessel sample remained preconditioned if the force-displacement curves plotted through the data obtained from zero load test-2, zero load test-3, and zero load test-4 match well. It is expected to see a considerable difference between the data obtained from zero load test-1 and zero load test-2 since they represent before and after preconditioning states, respectively. We filtered the force data collected from the experiment and plotted it against the voice coil position.

It can be observed from the graphs as shown in Fig. 4.1 that the force-displacement curve before preconditioning is steeper than that of the force-displacement curve after preconditioning. It can also be observed that almost 50% of the preconditioning is lost at the end of 2 hours when the vessel sample was maintained at the in-vivo pressure, whereas almost 80% of the preconditioning is lost at the end of 1 more hour when the vessel sample was maintained at zero luminal pressure.

4.2 Verification for quantification of collagen orientation

As stated above, we were capturing collagen images for the first time with the use of 2P microscopy. Before we could use these data for any quantification, we wanted to verify

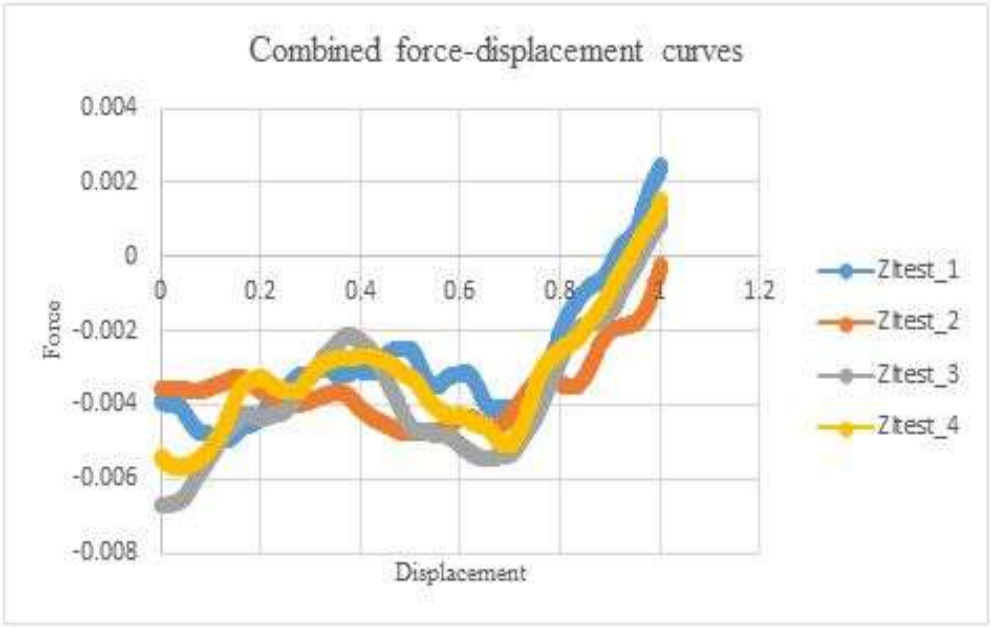

Fig. 4.1 Combined force-displacement curves plotted for 4 tests (Zltest_1, Zltest_2,Zltest_3,Zltest_4) (Zltest_1= Before preconditioning; Zltest_2=Immediately after preconditioning; Zltest_3= Two hours after preconditioning; Zltest_4= Three hours after preconditioning)

the quality of these data. We thus compared 2P images for collagen obtained in our experiment with the images obtained using the same technique by other research groups.

The comparison was done visually since there is no other basis for comparison as different types of blood vessels have been imaged by other research groups. The detailed description of the literature to which we referred to verify the quality of our data is mentioned in the following text. We made sure to refer 2P images for collagen only for those studies where the data were used for quantification of collagen orientation.

The images (refer to Fig. 4.2) in this study were obtained from the aorta of mice fed with a Chow diet (left) and Western diet (right). The images were processed to obtain the mean fiber orientation. It was found in the study that the mean collagen fiber angle for mice on

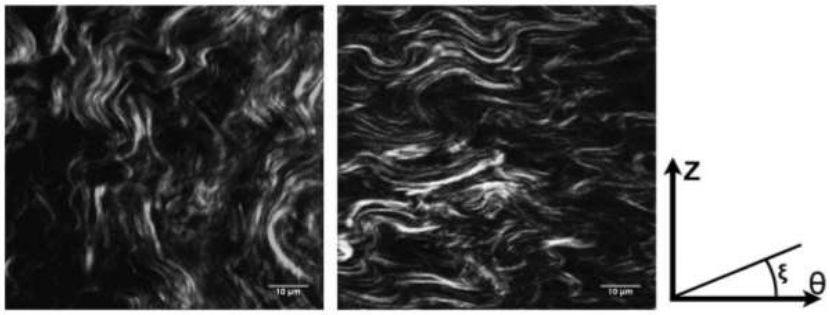

Fig. 4.2 2-P images of the aorta of mice.
Source: Comparison of Aortic Collagen Fiber Angle Distribution in Mouse Models of Atherosclerosis using Second-Harmonic Generation (SHG) Microscopy [28].

a Chow diet was approximately equal to 63˚ whereas the mean collagen fiber angle for mice on Western diet was approximately equal to 20˚.

The images (refer to Fig. 4.3) in this study were obtained from the normal basilar arteries (cerebral arteries) of rabbits. The cerebral arteries were pressurized to different luminal pressures (pressures mentioned on the left of the images) and then the data were captured from the vessel samples. These images were then processed to get the average angle of collagen from each of the layers of the sample (adventitia, media) separately.

Other images (refer to Fig. 4.4) in this study were obtained from the carotid arteries of the pig. The images are collected from both the media and the adventitia of the carotid arteries. They were later processed with the mechanism developed at their lab to quantify collagen orientation.

We also show an image for adventitial collagen (refer to Fig. 4.5) from our experiment.

It can be observed that the images collected from literature are comparable in quality with the data obtained in our experiments. The images of collagen collected from the literature have been used to quantify collagen orientation. The main goal of our

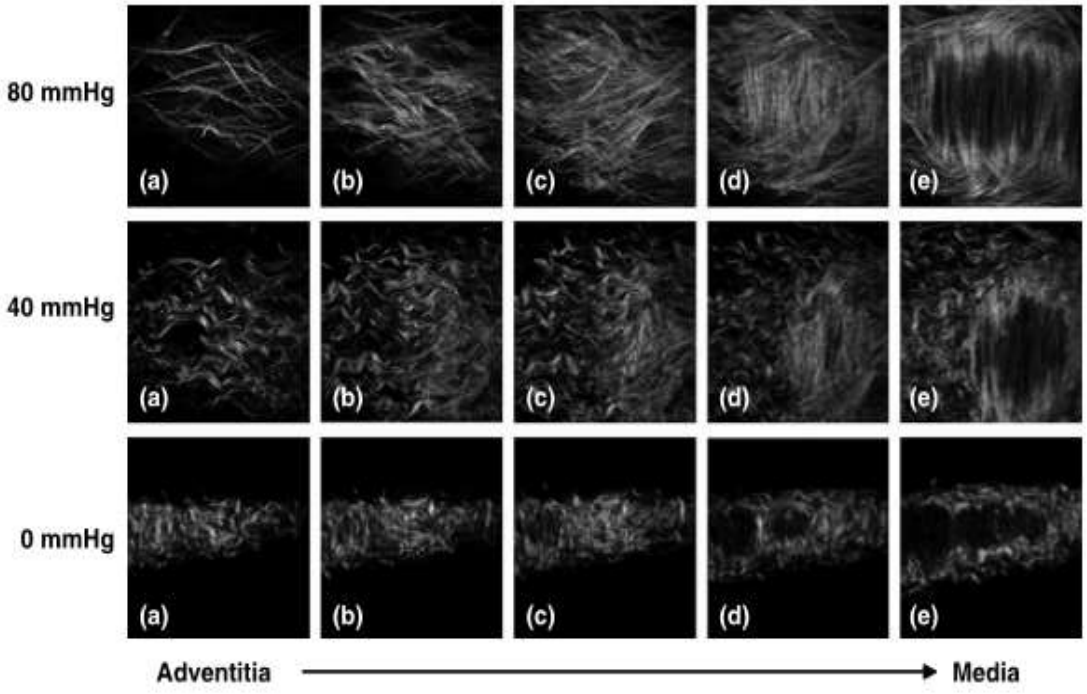

Fig. 4.3 2-P images of the normal basilar artery of rabbits.
Source: Normal basilar artery structure and biaxial mechanical behavior [23].

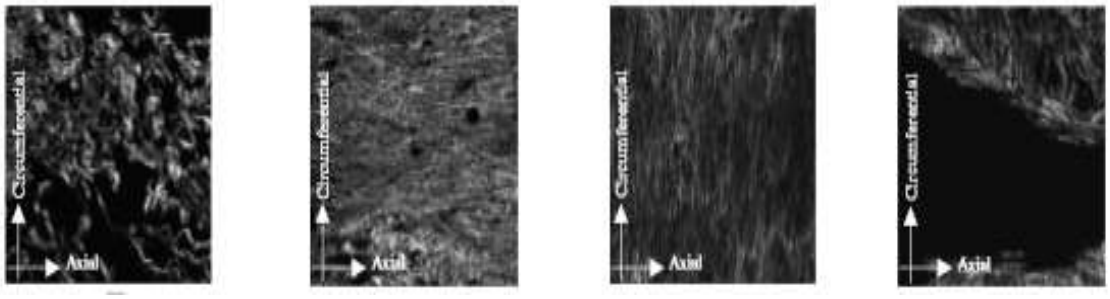

Fig. 4.4 2-P images of the carotid artery of pigs.
Source: A comparative analysis of the collagen architecture in the carotid artery: Second harmonic generation versus diffusion tensor imaging [37].

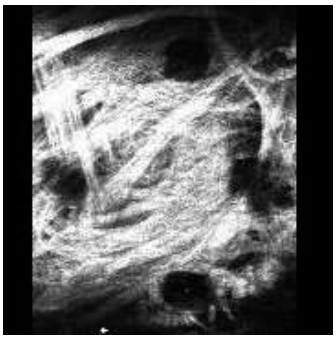

Fig. 4.5 2-P image of a middle cerebral artery of a sheep [Scale: 1.62 um/pixel; size: 512 x 512].

experiment being the quantification of collagen fiber orientation, the quality of the data obtained must be able to fulfill our purpose. We also obtained a histogram of orientations for our adventitial image using Orientation J Distribution. The histogram shows a peak around 0˚. We thus concluded that the images for our experiments provide quality data.

4.3 Validation of image processing techniques

For quantification of collagen orientation, we have primarily used three techniques: manual quantification using Line Tool, quantification using Fibril Tool, and quantification with Orientation J Distribution.

4.3.1 Orientation quantification by Line Tool

Manual quantification method was verified by asking two different volunteers to quantify the collagen fiber orientation in the same images following the same procedure for quantification and matching the values as well as the trend observed in orientation values during and post-overstretch with the results that we obtained. We plotted graphs for all the experiments and each of the observers. The graphs matched really well. The manual

quantification method using Line Tool can thus be considered as a trustworthy method for quantification of collagen orientation.

4.3.2 Orientation quantification by Fibril Tool

For verification of Fibril Tool as a tool for quantification of the fiber orientation, we drew a polygon around the fiber to represent a region of interest. It was made sure that the polygon drawn here surrounds the line drawn for manual quantification so as to ensure quantification of the same region around the fiber. Fibril Tool was then used to quantify the average orientation for the polygon. This orientation was then compared with the orientation obtained manually to quantify the error. We then varied the brightness and contrast of the image in order to see the effect of intensity on the orientation quantification. We analyzed the image shown in the Fig. 4.6.

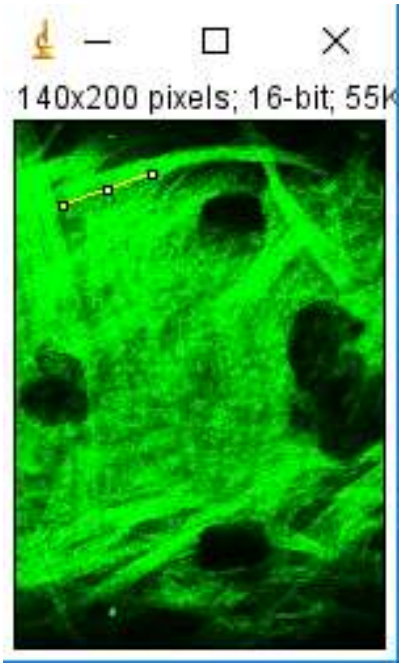

Fig. 4.6 Adventitial image with a line drawn on the fiber for manual quantification [Scale: 1.62 um/pixel; size: 512 x 512].

Fig. 4.6 shows the image with a line drawn manually on one of the fibers for quantification of the orientation. Fig. 4.7 shows the polygon drawn around the fiber, which acts as a region of interest to quantify the orientation with Fibril Tool. Fig. 4.8 shows the image with the reduced intensity. The placement of the polygon has been kept the same for understanding the effect of intensity on image processing. Fig. 4.9 shows the image with increased contrast to understand the effect of contrast. Table 4.1 lists the case and corresponding orientation of the collagen fiber. As it can be observed from Table 4.1, the value corresponding to the orientation for a particular region of interest or an image varies with the brightness and contrast of the image. It is also very different from the value that was quantified by manually drawing the line on the fiber. If we have to compare orientation of fibers in different images, using Fibril Tool, we have to make sure that the brightness and contrast of the images are the same.

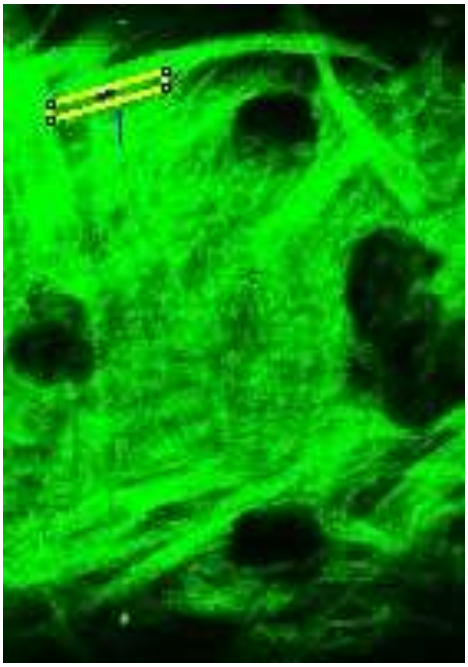

Fig. 4.7 Adventitial image with a polygon drawn around the fiber for quantification with Fibril Tool [Scale: 1.62 um/pixel; size: 512 x 512].

Fig. 4.8 Adventitial image with reduced brightness with a polygon drawn around the fiber for quantification with Fibril Tool [Scale: 1.62 um/pixel; size: 512 x 512].

Fig. 4.9 Adventitial image with increased contrast with a polygon drawn around the fiber for quantification with Fibril Tool [Scale: 1.62 um/pixel; size: 512 x 512].

Table 4.1 Table for quantification of collagen fiber orientation using Fibril Tool.

No	Case	Orientation
1	Image with a line drawn on fiber for quantification of orientation	19.44
2	Image with polygon drawn for quantification with Fibril Tool	36.8
3	Image with decreased brightness with polygon drawn for quantification with Fibril Tool	35.97
4	Image with increased contrast with polygon drawn for quantification with Fibril Tool	38.57

4.3.3 Orientation quantification by Orientation J Distribution

We knew that Orientation J Distribution quantifies the orientation based on the number of fibers oriented in a particular direction as well as the intensity of the fibers. In order to determine the effect of each of them individually, we drew a certain pattern of lines in paint (orientation of these lines were known to us). We added and subtracted the lines in the original pattern of these lines. We then varied the intensity of these added lines so as to check the effect of the intensity. As it can be observed from Fig. 4.10 (a), the black lines were drawn at an orientation of 0˚, 15˚, 30˚, 45˚, 60˚, and 75˚. The orientation graph was obtained with Orientation J Distribution for this image. As it can be observed from Fig. 4.10 (b), the graph shows peaks at these angles with the largest peak corresponding to 45˚, indicating the largest black line. When a black line corresponding to an angle of 60 ˚ was replaced with a gray line as shown in Fig. 4.11 (a), the corresponding peak disappeared as shown in Fig. 4.11 (b). When a set of gray lines was drawn in between the black lines as shown in Fig. 4.12 (a), we expected to see peaks corresponding to the orientation of

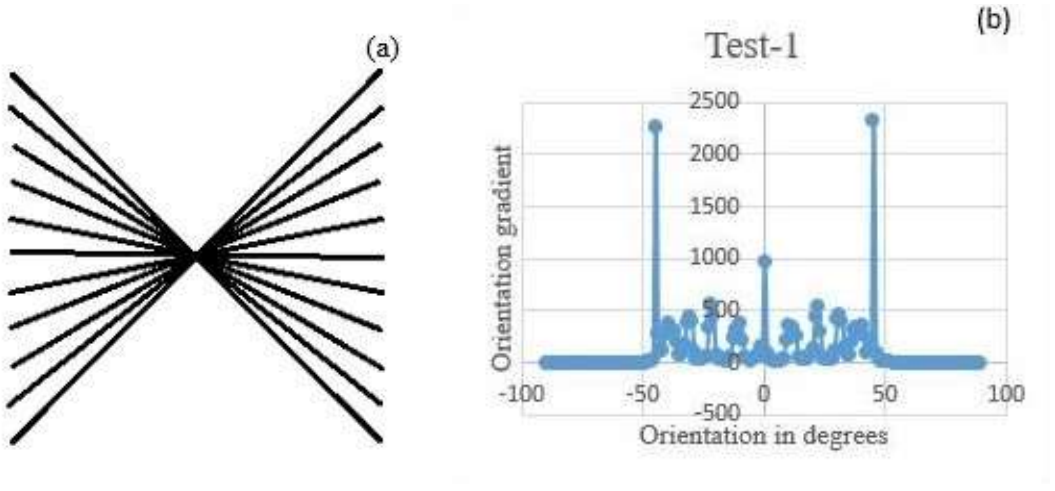

Fig. 4.10 Orientation J Distribution graphs - 1 (a) A set of black lines corresponding to 0˚, 15˚, 30˚, 45˚, 60˚ and 75˚; (b) Orientation graphs obtained for (a).

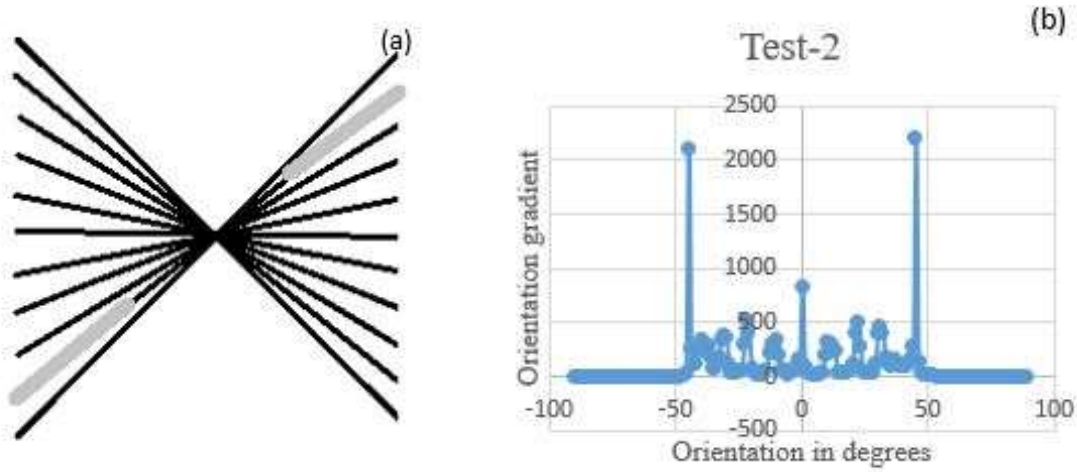

Fig. 4.11 Orientation J Distribution graphs - 2 (a) A set of black lines with a gray line corresponding to 60˚; (b) Orientation graphs obtained for (a)

these gray lines. As it can be observed from the orientation graph shown in Fig. 4.12 (b), we did not observe any peak corresponding to any of these gray lines. This tells us that the results obtained through Orientation J Distribution are governed by the difference in intensity of the lines here or features in general. When these gray lines were replaced with the brown lines as shown in Fig. 4.13 (a) having comparable intensity with the black lines, we again did not see peaks corresponding to these lines but a single peak was observed at around 45˚ as shown in Fig. 4.13 (b). This clearly shows us the inability of the tool to quantify the orientation distribution if there are many features in the images having very different intensities. The images of collagen captured for our experiment consisted of many features within the same image having different intensities. It is thus more likely that the orientation graphs for our images do not represent the orientation distribution accurately.

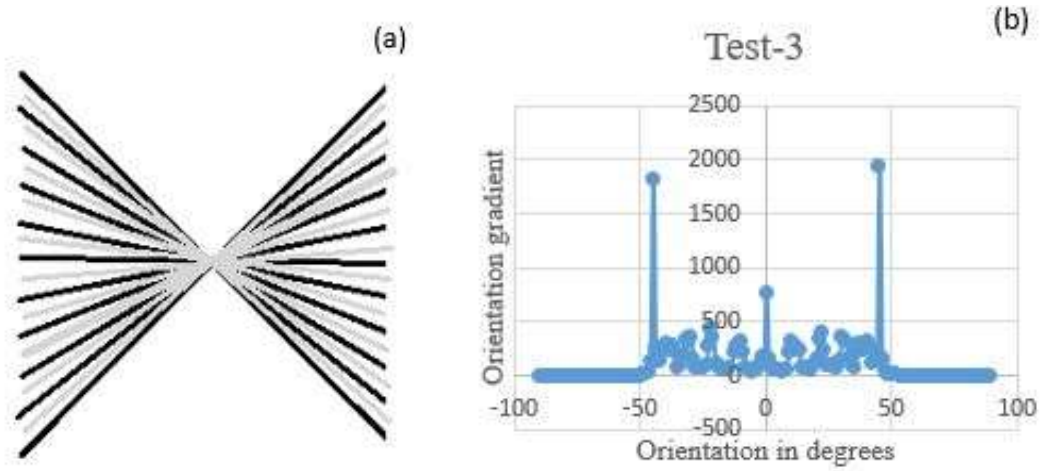

Fig. 4.12 Orientation J Distribution graphs - 3 (a) A set of black lines with a set of gray lines drawn in the middle of black lines; (b) Orientation graph obtained for (a).

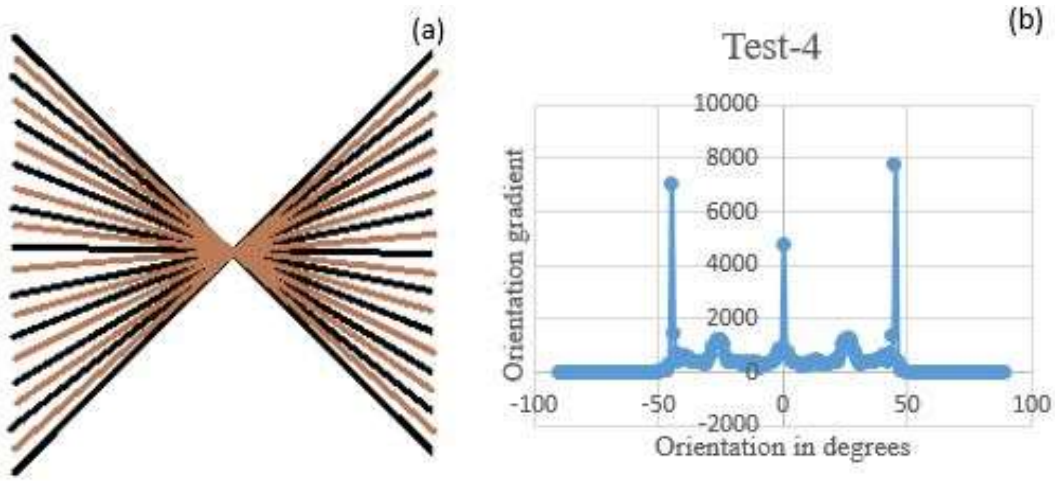

Fig. 4.13 Orientation J Distribution graphs - 4 (a) A set of black lines with a set of brown lines drawn in the middle; (b) Orientation graph obtained for (a).

4.4 Analysis to check the effect of photobleaching on the vessel sample

We used photobleached spots to make sure that we were quantifying the same region before and after overstretching the vessel sample. These photobleached spots were created on the vessel surface by exposing a particular spot on the surface of the vessel sample to a two-photon laser with extremely high laser power for a small duration of time (approximately 2 to 3 minutes). It was thus needed to check if this exposure of the vessel sample surface to a laser is responsible for any change in the mechanical properties of the vessel sample or if it makes any effect on quantification of the orientation. We did a literature survey in order to know the effect of photobleaching on the mechanical properties of the biological tissue. For knowing its effect on the image processing, we created black spots at various locations together and also one by one in the images (to replicate photobleached spots) using ImageJ, and then used Orientation J Distribution to quantify the orientation in the original and modified images (images with photobleached spots). We found out mean and standard deviation for the datasets obtained with Orientation J Distribution and compared them together in order to know if the datasets are the same. We considered the dataset corresponding to the image with no photobleached spot as a reference and calculated average cumulative error for all the other configurations.

We referred to Jayyosi [36] to verify the effect of photobleaching on mechanical properties of the biological tissue. They studied the effect of photobleaching on the mechanical properties of a human liver capsule. They carried out stress and strain measurements for a human liver capsule undergoing uniaxial tensile testing. Human liver capsules were removed from a liver of a postmortem human subject. The capsule was cut into dog-bone-shaped samples as shown in Fig. 4.14 using a die cutter, giving a 45 mm

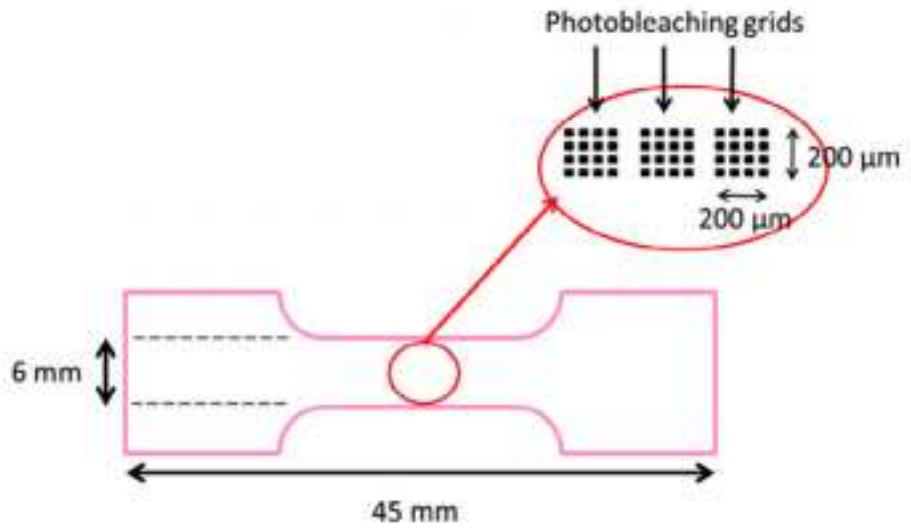

Fig. 4.14 Figure showing the geometry of the sample used to study photobleaching. (Redrawn from [36])

length and a 6 mm section. A 2P microscope was used to produce a grid of various rectangular photobleached spots as shown in Fig. 4.15. The exposure time and the laser power were varied so as to study the effect of differences in them. A specimen was subjected to a uniaxial tensile testing and the corresponding stress-strain values were measured. The vessel sample was then photobleached with various rectangular spots. The same uniaxial tensile testing was then repeated and corresponding stress-strain values were calculated again. It was reported that the mechanical properties of the sample remained unaffected and hence, it was concluded that photobleaching does not affect the mechanical properties of the biological tissue. It just destroys the autofluorescence of the biological tissue in the photobleached region.

In order to verify if photobleaching affects the image processing results, we used Orientation J Distribution. (We could use Orientation J Distribution here since we used the same same image with little modification for replicating photobleaching.) The topmost

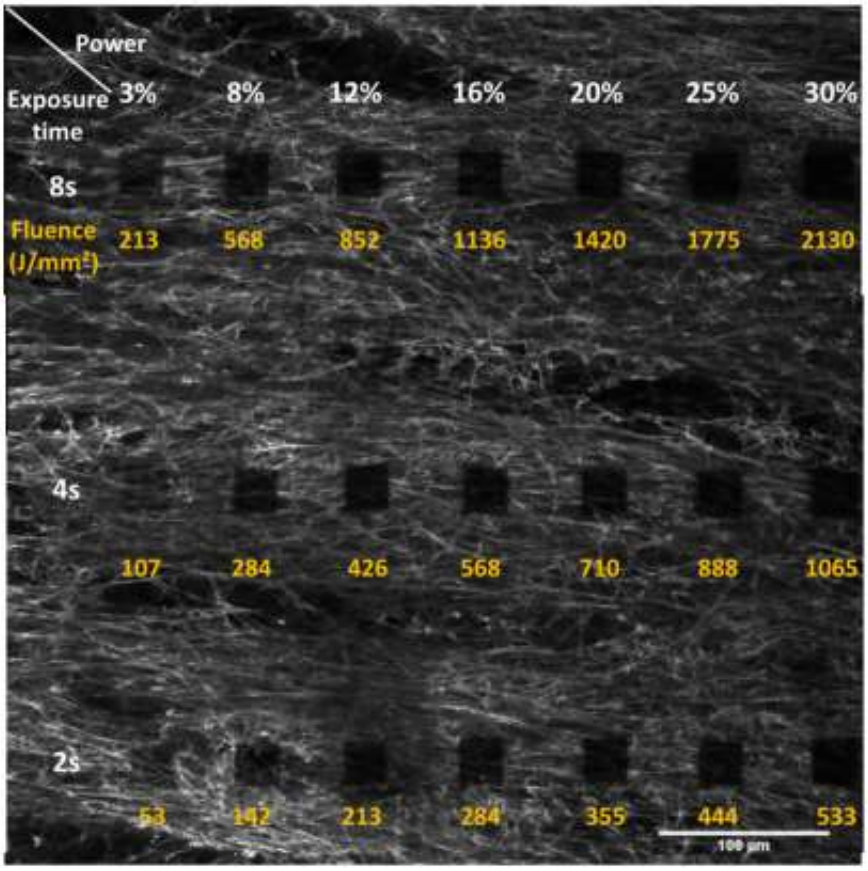

Fig. 4.15 Biological tissue sample with various rectangular photobleached spots produced using different laser power and exposure time of 2P laser. (Redrawn from [36])

image from the adventitia was chosen from the experiment-1. Various spots in the image were chosen and filled as if they are photobleached as shown in the following Fig. 4.16 (a), Fig. 4.17 (a), Fig. 4.18 (a), Fig. 4.19 (a), Fig. 4.20 (a), Fig. 4.21 (a), and Fig. 4.22 (a).

The orientation graphs were obtained using Orientation J Distribution for different images as shown in Fig. 4.16 (b), Fig. 4.17 (b), Fig. 4.18 (b), Fig. 4.19 (b), Fig. 4.20 (b), Fig. 4.21 (b), and Fig. 4.22 (b). All of the images were processed with Orientation J Distribution. The graphs are shown next to the images. It can be observed from the graphs that irrespective of which portion of the image is filled, the graph still retains the trend and shows peak around the same orientation.

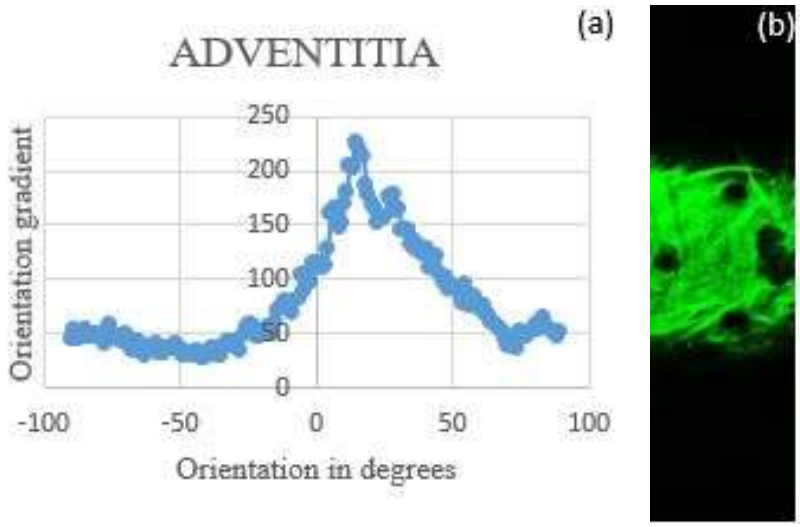

Fig. 4.16 Adventitial orientation graph and image set 1 (a) Orientation graph for the adventitial image shown in (b); (b) Top adventitial image [Scale: 1.62 um/pixel; size: 512 x 512].

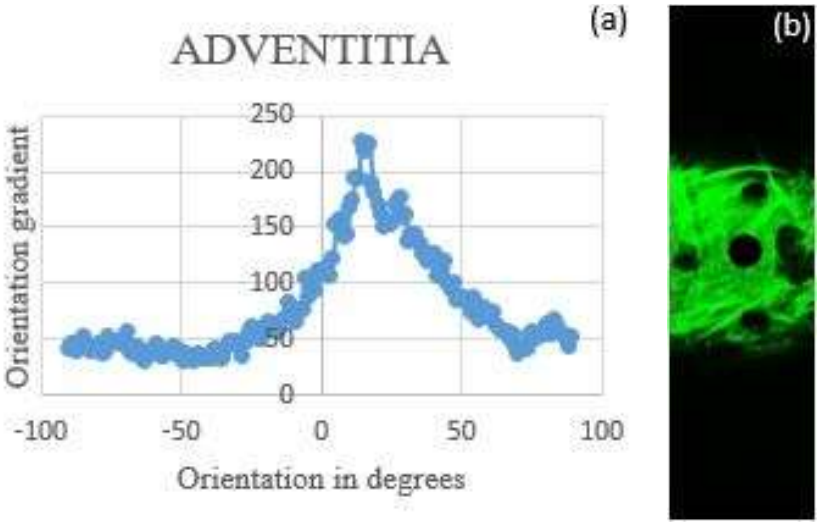

Fig. 4.17 Adventitial orientation graph and image set 2 (a) Orientation graph for the adventitial image shown in (b); (b) Top adventitial image with photobleached spot created at the center of the image using ImageJ [Scale: 1.62 um/pixel; size: 512 x 512].

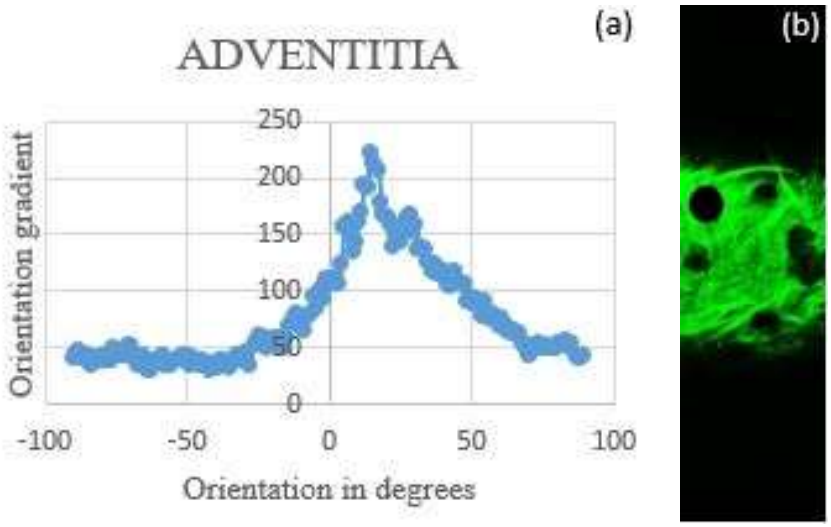

Fig. 4.18 Adventitial orientation graph and image set 3 (a) Orientation graph for the adventitial image shown in (b); (b) Top adventitial image with photobleached spot created at the top left of the image using ImageJ [Scale: 1.62 um/pixel; size: 512 x 512].

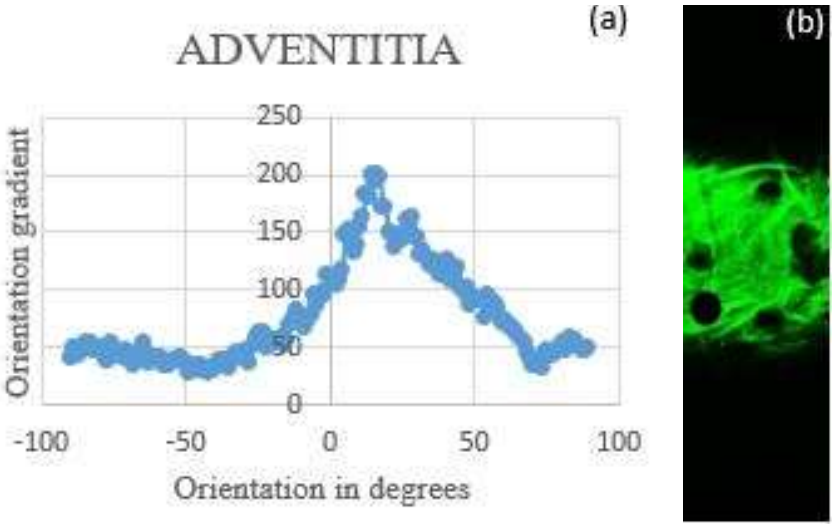

Fig. 4.19 Adventitial orientation graph and image set 4 (a) Orientation graph for the adventitial image shown in (b); (b) Top adventitial image with photobleached spot created at the bottom left of the image using ImageJ [Scale: 1.62 um/pixel; size: 512 x 512].

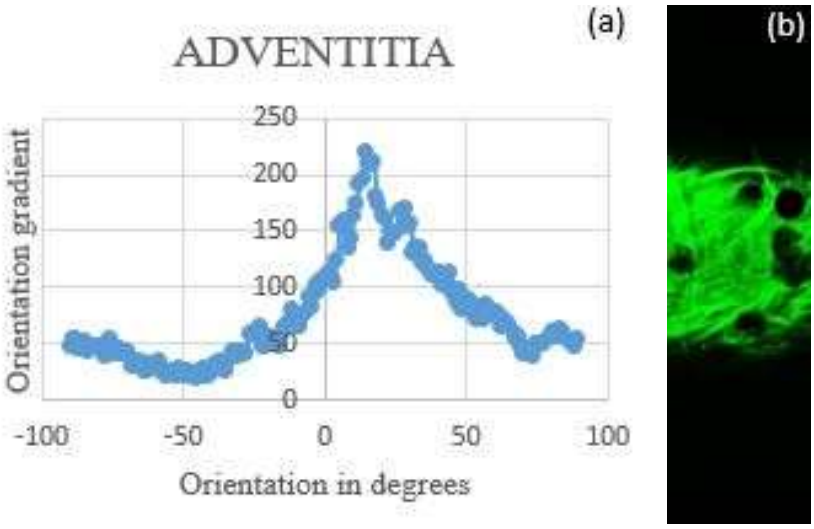

Fig. 4.20 Adventitial orientation graph and image set 5 (a) Orientation graph for the adventitial image shown in (b); (b) Top adventitial image with photobleached spot created at the top right of the image using ImageJ [Scale: 1.62 um/pixel; size: 512 x 512].

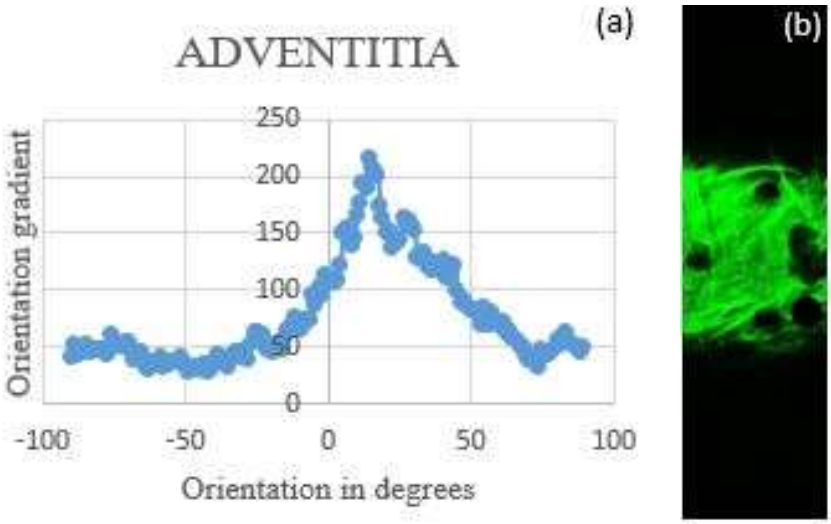

Fig. 4.21 Adventitial orientation graph and image set 6 (a) Orientation graph for the adventitial image shown in (b); (b) Top adventitial image with photobleached spot created at the bottom right of the image using ImageJ [Scale: 1.62 um/pixel; size: 512 x 512].

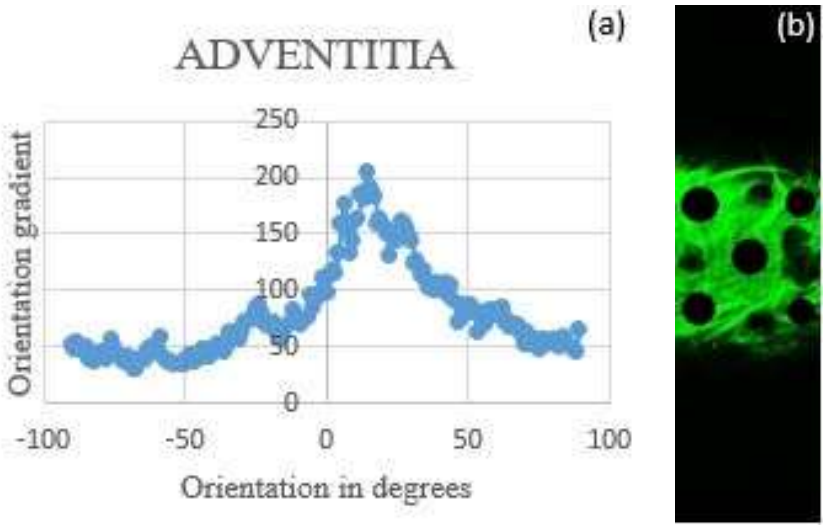

Fig. 4.22 Adventitial orientation graph and image set 7 (a) Orientation graph for the adventitial image shown in (b); (b) Top adventitial image with photobleached spots created in the image using ImageJ [Scale: 1.62 um/pixel; size: 512 x 512.

In order to verify this conclusion numerically, we found out the mean and standard deviation for the data. Table 4.2 for all the cases is shown. It can be observed from the table that the mean and the standard deviation are almost equal for each and every case. We also compared the values near the mean orientation obtained from the orientation graphs. We found the percentage difference by comparing the values for an image when some portion is filled as if it is photobleached to the values for an image that is not filled.

Case 1- This shows an adventitial image for in-vivo configuration for experiment-1 (refer to Fig. 4.16 (b)). The orientation graph was obtained for this image using Orientation J Distribution (refer to Fig. 4.16 (a)). This case was used as a reference for comparison using an average cumulative error.

Case 2- A black spot was created (replicating a photobleached spot) at the center of the original image, i.e., chosen for analysis using Image J (refer to Fig. 4.17 (b)). The

Table 4.2 Mean and standard deviation calculated for different datasets corresponding to different cases.

Case Number	Mean	Standard Deviation
Case – 1	11	42.35
Case – 2	11	42.28
Case – 3	11	42.17
Case – 4	10	43.00
Case – 5	12	42.23
Case – 6	10	42.94
Case – 7	9	43.19

orientation graph was obtained for this image using Orientation J Distribution (refer to Fig. 4.17 (a)).

Case 3- A black spot was created (replicating a photobleached spot) on the top left corner of the original image, i.e., chosen for analysis using Image J (refer to Fig. 4.18 (b)). The orientation graph was obtained for this image using Orientation J Distribution (refer to Fig. 4.18 (a))

Case 4- A black spot was created (replicating a photobleached spot) on the bottom left corner of the original image, i.e., chosen for analysis using Image J (refer to Fig. 4.19 (b)). The orientation graph was obtained for this image using Orientation J Distribution (refer to Fig. 4.19 (a)).

Case 5- A black spot was created (replicating a photobleached spot) on the top right corner of the original image, i.e., chosen for analysis using Image J (refer to Fig. 4.20 (b)). The orientation graph was obtained for this image using Orientation J Distribution (refer to Fig. 4.20 (a)).

Case 6- A black spot was created (replicating a photobleached spot) on the bottom right corner of the original image, i.e., chosen for analysis using Image J (refer to Fig. 4.21 (b)). The orientation graph was obtained for this image using Orientation J Distribution (refer to Fig. 4.21 (a)).

Case 7- Black spots were created (replicating photobleached spots) at all the spots mentioned in all the previous cases combined together, in the original image, i.e., chosen for analysis using Image J (refer to Fig. 4.22 (b)). The orientation graph was obtained for this image using Orientation J Distribution (refer to Fig. 4.22 (a)).

Table 4.3 lists values of average cumulative errors calculated for datasets acquired with Orientation J Distribution. If we observe the table, the average cumulative errors range from '-1.32' to '-4.52'. We can thus say that the average cumulative errors are close to '0', which clearly indicates lack of bias. (Average cumulative error close to '0' indicates lack of bias.) We can thus say that these datasets are not statistically different and hence claim that photobleaching does not affect the results.

Table 4.3 Table representing average cumulative error for two datasets being compared.

No	Datasets being compared	Average cumulative error
1	Case 1 and 2	-1.32
2	Case 1 and 3	-2.52
3	Case 1 and 3	-3.44
4	Case 1 and 3	-4.52
5	Case 1 and 3	-3.78
6	Case 1 and 3	-1.19

CHAPTER 5

RESULTS – PILOT STUDY

Three MCAs from three different adult ewes were successfully tested. The in-vivo lengths of the vessel samples were determined from preconditioning, at 4.2, 5.3, and 4.8 mm, respectively. We expected collagen fibers to become more organized and oriented towards the axial direction when the vessel sample was axially overstretched. We observed from the collected experimental data (the adventitial images for all the vessel samples) that this expectation held true. The adventitial images from experiment-2 were found to be the most evident among all the experiments, due to the high autofluorescence of collagen fibers, as shown in Fig. 5.1.

Fig. 5.1 shows the adventitial images corresponding to in-vivo and overstretched configurations of the vessel sample from experiment-2. The images show that the same fibers were more organized and oriented towards the axial direction when the vessel sample was overstretched than when it was in its in-vivo configuration. To further confirm this fact, we quantified the orientation of a single fiber (here indicated by a yellow line drawn on a fiber using data from experiment-2) from the images and observed significant changes in fiber angle when compared with in-vivo and overstretched (overstretch=1.4 in-vivo) configurations (shown later).

For the in-vivo post-overstretch-2 and in-vivo post-overstretch-4 configurations,

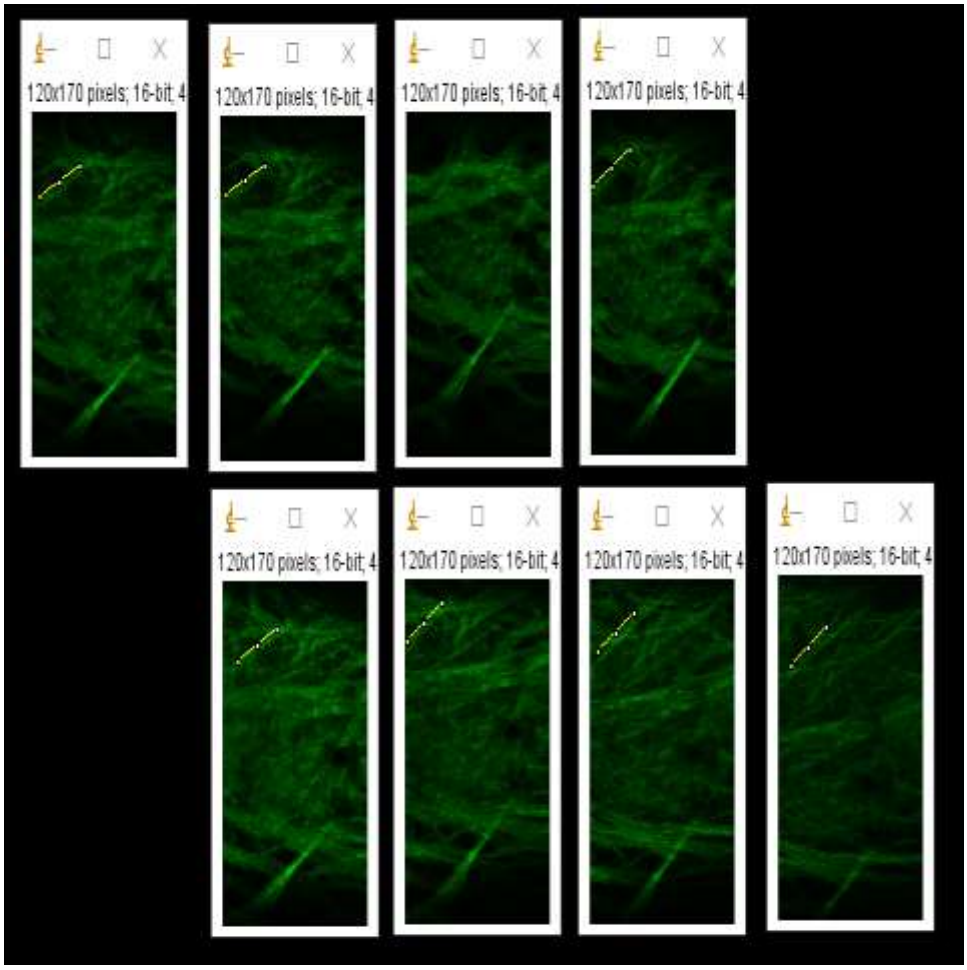

Fig. 5.1 Adventitial images from experiment-2 for different configurations [The top row consists of adventitial images from in-vivo configurations in the sequence as follows: in-vivo; in-vivo post-overstretch-1; in-vivo post-overstretch-2; in-vivo post-overstretch-3 shown from left to right whereas the bottom row consists of adventitial images from overstretched configurations in the sequence as follows: overstretch-1; overstretch-2; overstretch-3; and overstretch-4] [Scale: 1.62 um/pixel; size: 512 x 512].

fiber required for the quantification was not visible, so we could not quantify these configurations. We observed a noise in the images for the in-vivo post-overstretch configurations. This can be attributed to the softening of the blood vessel samples. Although we did not collect a force data signal to support the fact that the vessel sample was softened for this level of overstretch, we have observed in earlier experiments carried out in the lab that the blood vessels get softened when undergoing an axial overstretch, starting approximately from an overstretch level of 1.2 [10]. This results in fibers getting shifted off the focal plane of an objective lens, causing noise induction in the signal.

We wanted to quantify both the adventitial and the medial fibers, but the image processing methods that we used required images to show the fibers distinctly for the purpose of the quantification. The medial fibers were not distinct and hence could not be quantified. Fig. 5.2 shows an image of medial fibers outlined by a yellow border. As can be seen from this figure, the medial fibers are neither distinct nor do they have any identifiable features, and thus cannot be used for comparing the collagen orientation before and after overstretching. We thus used only the adventitial images for testing our hypothesis.

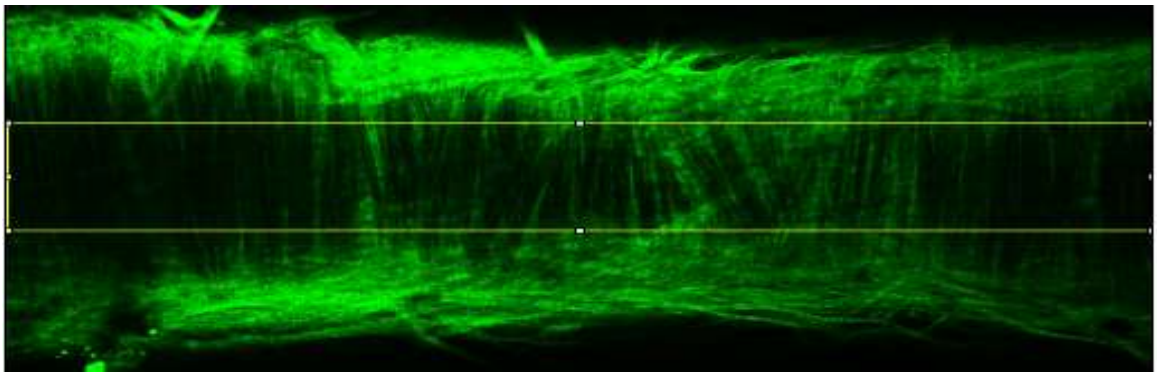

Fig. 5.2 Image from experiment-1 in which media is marked by a yellow border [Scale: 1.62 um/pixel; size: 512 x 512]

5.1 Experiment-1 results

5.1.1 Single fiber analysis

5.1.1.1 Fiber-1 analysis

To test our hypothesis, we did a preliminary analysis of the images involving a manual quantification of the orientation. Fig. 5.3 shows the first fiber (marked with a yellow line) from experiment-1 whose orientation was quantified manually using Line Tool in Image J. The figure shows that the orientation of this fiber in all in-vivo post-overstretch configurations was similar to that of its orientation in in-vivo configuration. It can also be observed that the orientation of this fiber for overstretched configurations decreased with increase in the severity of overstretch. Table 5.1 shows the orientation of fiber-1 for the in-vivo and overstretched configurations quantified by all three observers (Observers were chosen randomly). We observed a certain trend in the collagen orientation with overstretching. For a better understanding of this observed trend, we represented the variation in fiber orientation for different configurations using a percentage difference calculated with reference to the in-vivo configuration. The calculated percentage difference clearly showed that the fiber orientation decreased with increase in the severity of overstretch, indicated by increase in negative percentage value or decrease in positive percentage value. The trend observed here seems to have few exceptions where the fiber orientation has been reported to increase with severity of overstretch. This might be because of the fact that a line drawn on the fiber for manual quantification of the fiber orientation is based on a personal judgment, and not done with the help of any software program. We thus decided to observe the trend instead of independent values. We expected that the trend would give us a correct idea of the mechanism behind this. We note here

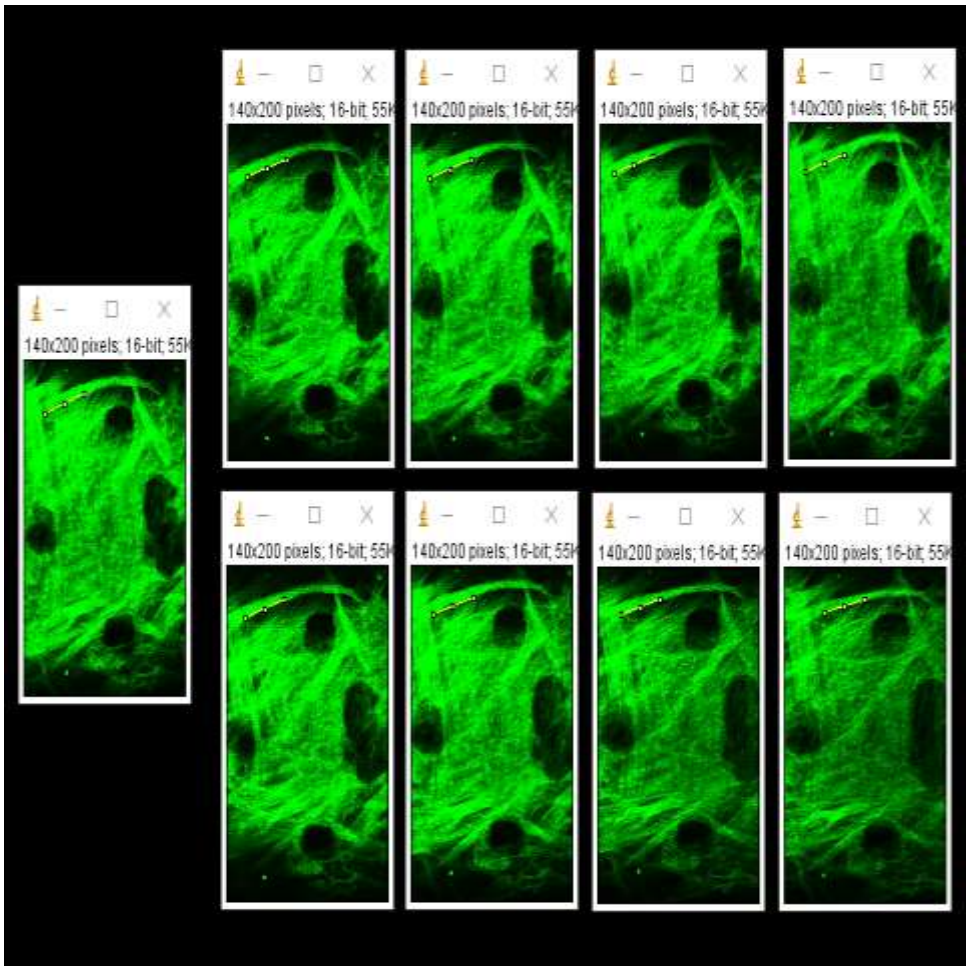

Fig. 5.3 Single fiber analysis for fiber-1 picked up from adventitial images from experiment-1- in-vivo configuration (single image on the left); in-vivo post-overstretch-1 (top row; first from left); in-vivo post-overstretch-2 (top row; second from left); in-vivo post-overstretch-3 (top row; third from left); in-vivo post-overstretch-4 (top row; forth from left); overstretch-1 (bottom row; first from left); overstretch-2 (bottom row; second from left); overstretch-3 (bottom row; third from left); overstretch-4 (bottom row; forth from left) [Scale: 1.62 um/pixel; size: 512 x 512].

Table 5.1 Single fiber analysis results for fiber-1 picked up from adventitial images for in-vivo and all overstretched configurations from experiment-1.

	Fiber angle (1)	Percentage difference with respect to in-vivo configuration	Fiber angle (2)	Percentage difference with respect to in-vivo configuration	Fiber angle (3)	Percentage difference with respect to in-vivo configuration
in-vivo	19.026	-	21.371	-	19.44	-
Overstretch-1	21.448	12.73	20.556	-3.81	17.928	-7.77
Overstretch-2	17.241	-9.38	17.819	-16.62	15.945	-17.97
Overstretch-3	19.026	0	17.103	-19.97	14.826	-23.73
Overstretch-4	15.422	-18.94	14.036	-34.32	12.875	-33.77

that the collagen orientation decreased when the vessel sample was overstretched and its severity increased with increase in the amount of overstretch.

Table 5.2 shows the orientation of fiber-1 for the in-vivo and in-vivo post-overstretch configurations quantified by all three observers. We did not really observe a significant change in collagen orientation for these configurations for the in-vivo post-overstretch-2 configuration onwards. For a better understanding of this fact, we have represented the variation in fiber orientation for different in-vivo post-overstretch configurations using a percentage difference calculated with reference to the in-vivo configuration. There was a significant difference in the fiber orientation corresponding to the in-vivo and in-vivo post-overstretch-1 configurations. We reported earlier in the Methods Evaluation chapter that some amount of preconditioning, was lost during transport. This fact can be associated with the observation stated here. Preconditioning restructures fiber organization. This reorganization of fibers, which takes place during preconditioning, was lost during transport, which is indicated by a loss of preconditioning. When a vessel sample is overstretched for the first time after being transported to the microscopy core, fibers must be reorganized as if the vessel sample was preconditioned. This must result in significant differences in the collagen orientation in its in-vivo configuration when compared with its orientation in the in-vivo post-overstretch-1 configuration. The fiber orientation does not show much variation for in-vivo post-overstretch-2 configuration onwards, which is easier to understand from the calculated percentage difference for fiber-1. The fact that the collagen orientation did not change again shows that there are few exceptions where the fiber orientation has been reported to increase or decrease inconsistently post-overstretch. This again might be because of the

Table 5.2 Single fiber analysis results for fiber-1 picked up from adventitial images for in-vivo and all in-vivo post-overstretch configurations from experiment-1.

	Fiber angle (1)	Percentage difference with respect to in-vivo	Fiber angle (2)	Percentage difference with respect to in-vivo	Fiber angle (3)	Percentage difference with respect to in-vivo
in-vivo	19.026	-	21.371	-	19.44	-
in-vivo post-overstretch-1	23.199	21.93	21.371	0	16.39	-15.68
in-vivo post-overstretch-2	20.772	9.17	18.435	-13.73	16.991	-12.59
in-vivo post-overstretch-3	25.71	35.13	21.371	0	16.39	-15.68
in-vivo post-overstretch-4	23.199	21.93	18.435	-13.73	16.39	-15.68

fact that a line drawn on the fiber for a manual quantification is based on personal judgment and not with the help of any software program. We thus decided to consider the observed trend over independent values.

We thus report that there was no change in the collagen orientation post-overstretch. In order to better represent the data, we plotted the graphs, with the orientation values represented on the y-axis and corresponding configurations for which they were reported on the x-axis.

Fig. 5.4 shows a graph of orientations for fiber-1 for all three observers corresponding to the in-vivo and overstretched configurations. A line joining points on the graph has a negative slope. This indicates reorganization of the fibers towards the axial direction and that the fibers became more organized and inclined towards the axial direction as overstretch became severe.

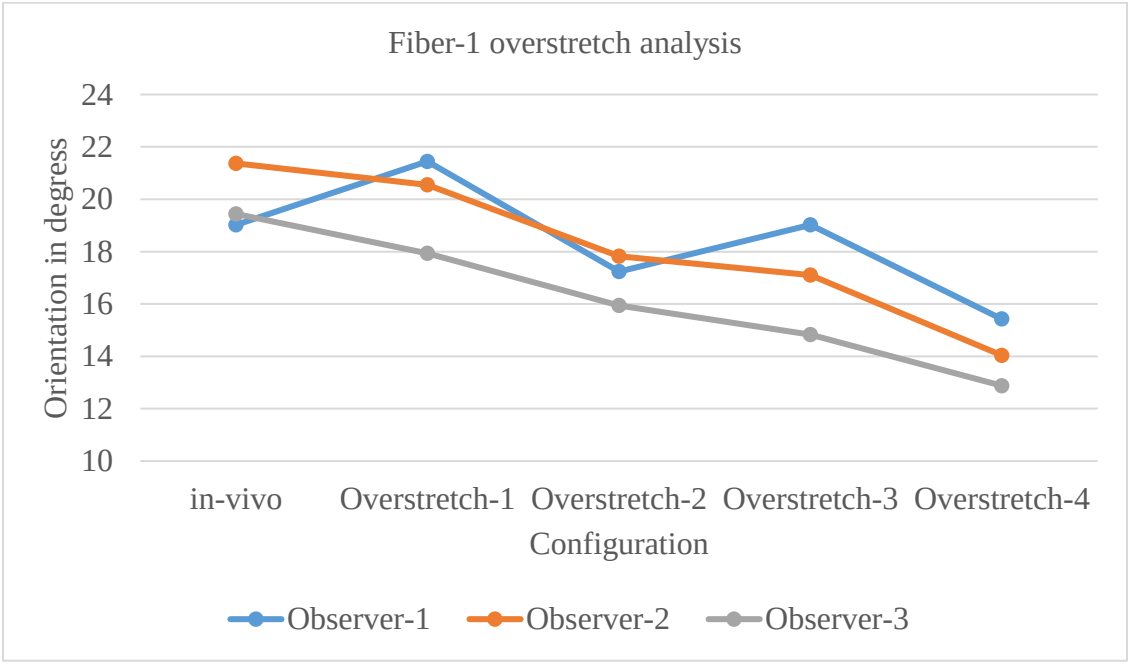

Fig. 5.4 Graph of the orientation of fiber-1 for experiment-1 against overstretched configuration for which it is reported.

Fig. 5.5 shows a graph of orientations for fiber-1 for all three observers corresponding to the in-vivo and in-vivo post-overstretch configurations. A line joining points on the graph remains almost parallel to the x-axis. The x-axis represents the configuration whereas y-axis represents the collagen orientation in degrees. A graph parallel to the x-axis necessarily represents no change in the collagen orientation with a change in the amount of overstretch. This indicates that collagen retained its orientation post-overstretch.

5.1.1.2 Fiber-2 analysis

Fig. 5.6 shows the second fiber (marked with a yellow line) from experiment-1 whose orientation was quantified manually using Line Tool in Image J. We have done

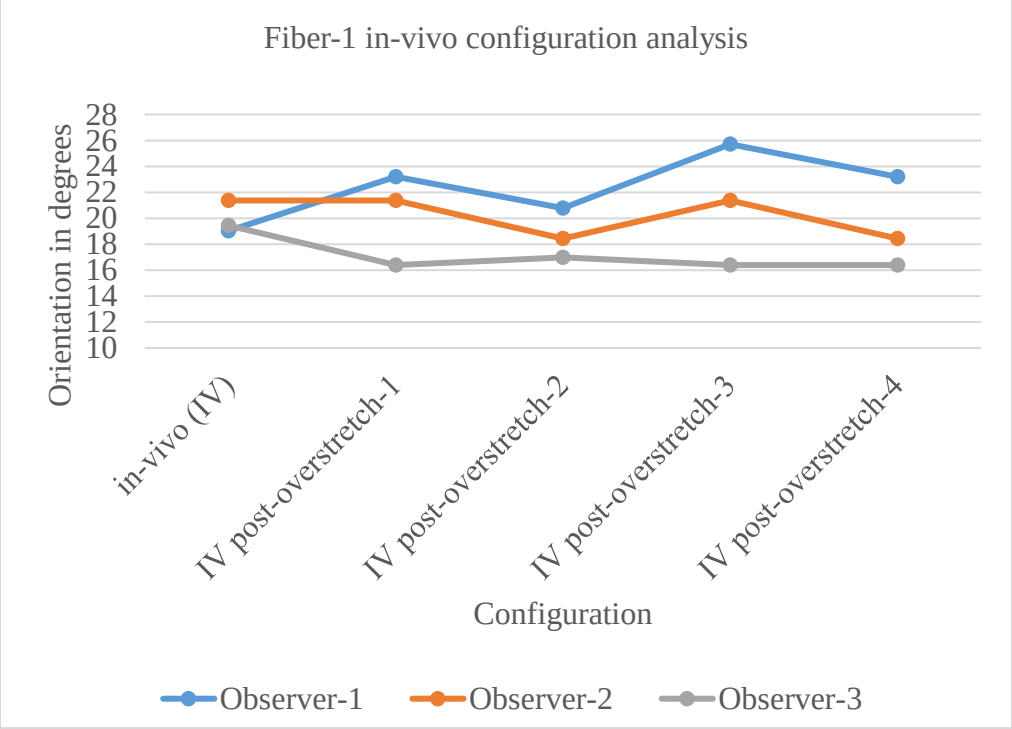

Fig. 5.5 Graph of the orientation of fiber-1 for experiment-1 against in-vivo configuration for which it is reported.

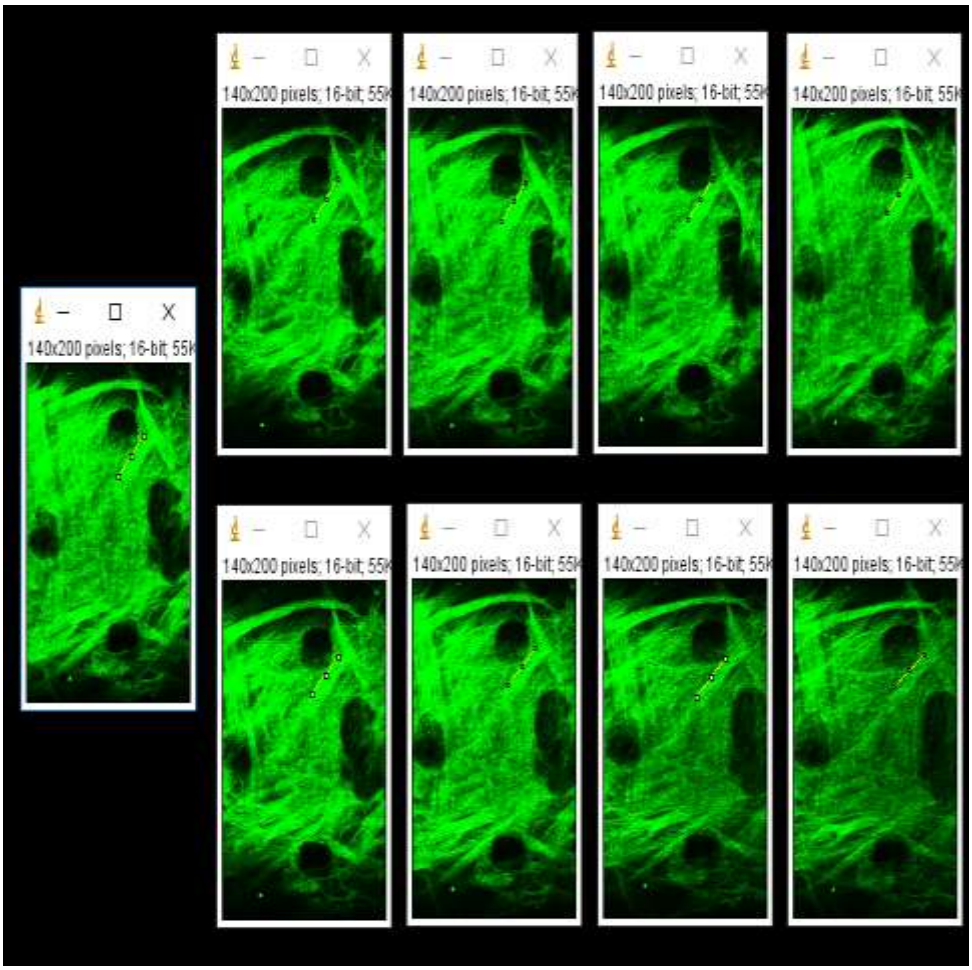

Fig. 5.6 Single fiber analysis for fiber-2 picked up from adventitial images from experiment-1- in-vivo configuration (single image on the left); in-vivo post-overstretch-1 (top row; first from left); in-vivo post-overstretch-2 (top row; second from left); in-vivo post-overstretch-3 (top row; third from left); in-vivo post-overstretch-4 (top row; forth from left); overstretch-1 (bottom row; first from left); overstretch-2 (bottom row; second from left); overstretch-3 (bottom row; third from left); overstretch-4 (bottom row; forth from left) [Scale: 1.62 um/pixel; size: 512 x 512].

the same analysis for fiber-2 and fiber-3 as that for fiber-1. A similar trend in the collagen orientation change can be observed for fiber-2 for different overstretched and in-vivo post-overstretch configurations as that of fiber-1, with the increase in the severity of overstretch.

Table 5.3 shows the orientation of fiber-2 for the in-vivo and overstretched configurations quantified by all three observers. It can be understood from the calculated percentage difference for the orientation of fiber-2 for all the configurations with respect to the in-vivo configuration that the fiber orientation decreased with increase in the severity of overstretch, as indicated by the increase in a negative percentage value or decrease in a positive percentage value. A personal judgment when marking the fiber is again responsible for the few values reported for the orientation that suggest a deviation from the observed trend. It can thus be reported from the observed trend that the collagen orientation decreased when the vessel sample was overstretched and its severity increased with increase in the amount of overstretch. Table 5.4 shows the orientation of fiber-2 for experiment-1 quantified by all three observers. The calculated percentage difference for the orientation of fiber-2 for all in-vivo post-overstretch configurations with respect to the in-vivo configuration shows that there is a significant difference in a fiber orientation between the in-vivo and in-vivo post-overstretch-1 configurations. As stated earlier, a loss of preconditioning can again be responsible for this difference. The fiber orientation does not show a lot of variation for the in-vivo post-overstretch-2 configuration onwards. A personal judgement when marking the fiber is again responsible for those few values reported for the orientation suggesting a deviation from the observed trend. It can thus be reported from the observed trend that that there was no change in the collagen orientation post-overstretch. In order to better observe the trend, we plotted the graphs with

Table 5.3 Single fiber analysis results for fiber-2 for all 3 observers picked up from adventitial images for in-vivo and overstretched configurations for experiment-1.

	Fiber angle (1)	Percentage difference with respect to in-vivo	Fiber angle (2)	Percentage difference with respect to in-vivo	Fiber angle (3)	Percentage difference with respect to in-vivo
in-vivo	53.13	-	45	-	50.194	-
Overstretch-1	45	-15.30	43.668	-2.96	43.727	-12.88
Overstretch-2	43.668	-17.81	40.426	-10.16	43.727	-12.88
Overstretch-3	43.668	-17.81	40.426	-10.16	42.397	-15.53
Overstretch-4	36.87	-30.60	37.185	-17.36	36.158	-27.96

Table 5.4 Single fiber analysis results for fiber-2 for all 3 observers picked up from adventitial images for in-vivo and in-vivo post-overstretch configurations for experiment-1.

	Fiber angle (1)	Percentage difference with respect to in-vivo	Fiber angle (2)	Percentage difference with respect to in-vivo	Fiber angle (3)	Percentage difference with respect to in-vivo
in-vivo	53.13	-	45	-	50.194	-
in-vivo post-overstretch-1	46.332	-12.80	45	0	48.814	-2.75
in-vivo post-overstretch-2	48.991	-7.79	43.877	-2.49	47.603	-5.16
in-vivo post-overstretch-3	45	-15.30	45	0	48.814	-2.75
in-vivo post-overstretch-4	45	-15.30	45	0	47.603	-5.16

orientation values represented on the y-axis against the corresponding configurations for which they were reported on the x-axis. Fig. 5.7 shows a graph of orientations for fiber-2 for all three observers corresponding to the in-vivo and overstretched configurations. The line joining points on the graph has a negative slope. This indicates reorganization of the fibers towards the axial direction and that the fibers became more organized and inclined towards the axial direction as overstretch became severe. Fig. 5.8 shows a graph of orientations for fiber-2 for all three observers corresponding to the in-vivo and in-vivo post-overstretch configurations. A line joining points on the graph remains almost parallel to the x-axis. A graph parallel to the x-axis necessarily represents no change in the collagen orientation with change in the amount of overstretch. This indicates that collagen retained its orientation post-overstretch.

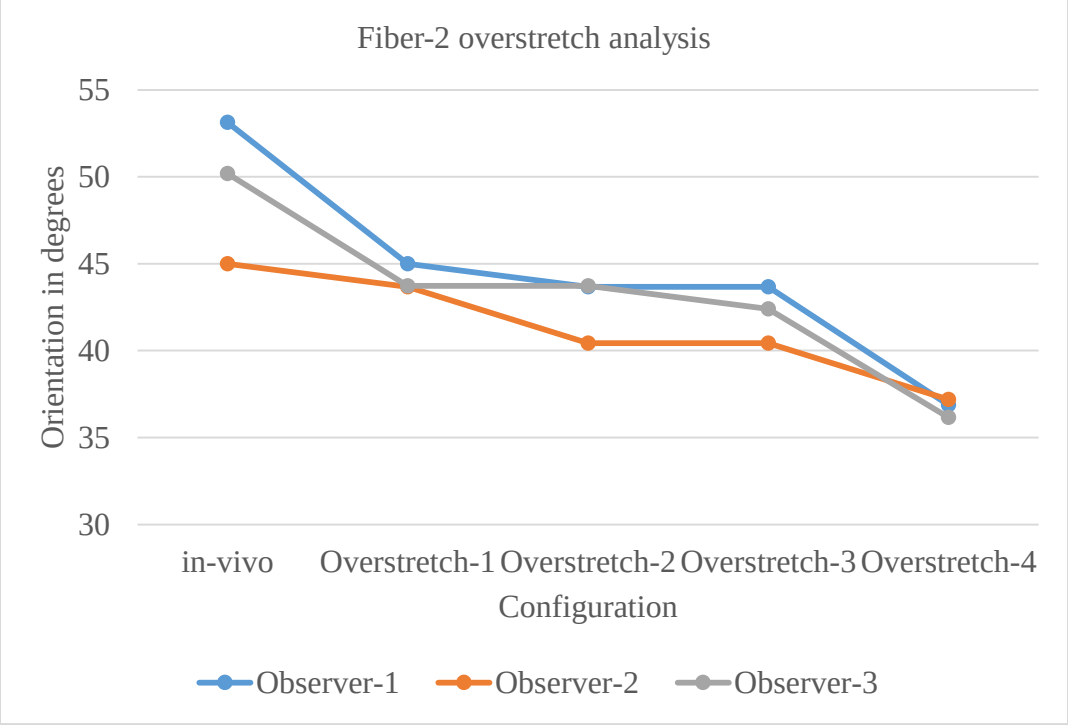

Fig. 5.7 Graph of the orientation of fiber-2 for experiment-1 against overstretched configuration for which it is reported.

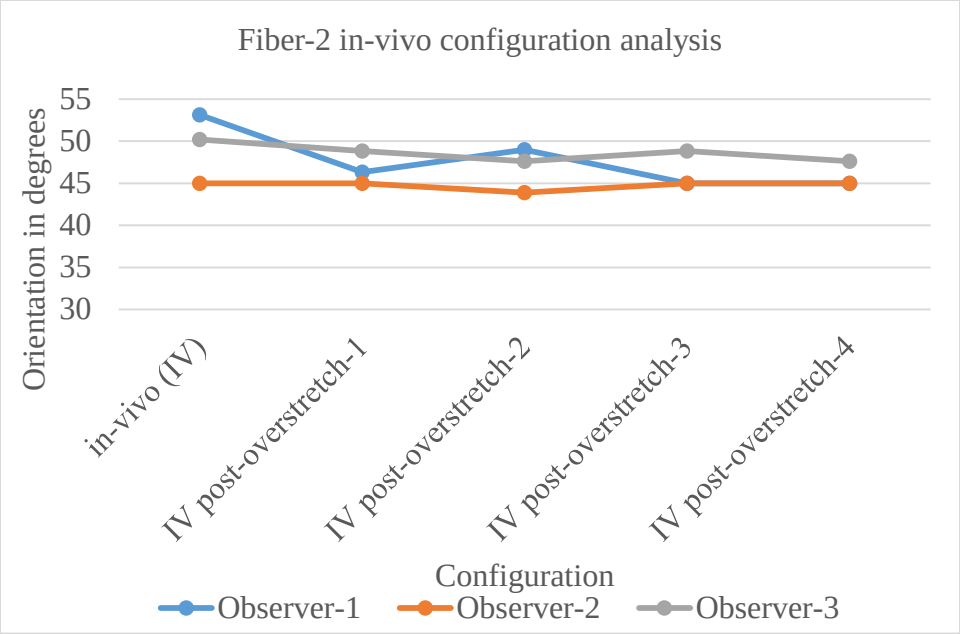

Fig. 5.8 Graph of the orientation of fiber-2 for experiment-1 against in-vivo configuration for which it is reported.

5.1.1.3 Fiber-3 analysis

Fig. 5.9 shows the third fiber (marked with a yellow line) from experiment-1 whose orientation was quantified manually using Line Tool in Image J. A similar trend in the collagen orientation change can be observed for fiber-3 for different overstretched and in-vivo post-overstretch configurations to that of fiber-1, with the increase in the severity of overstretch. Table 5.5 shows the orientation of fiber-3 for the in-vivo and overstretched configurations quantified by all three observers. It can be understood from the calculated percentage difference for the orientation of fiber-3 for all the configurations with respect to the in-vivo configuration that the fiber orientation decreased with increase in the severity of overstretch, as indicated by the increase in negative percentage value or decrease in positive percentage value. A personal judgment when marking the fiber is again responsible for the few values reported for orientation that

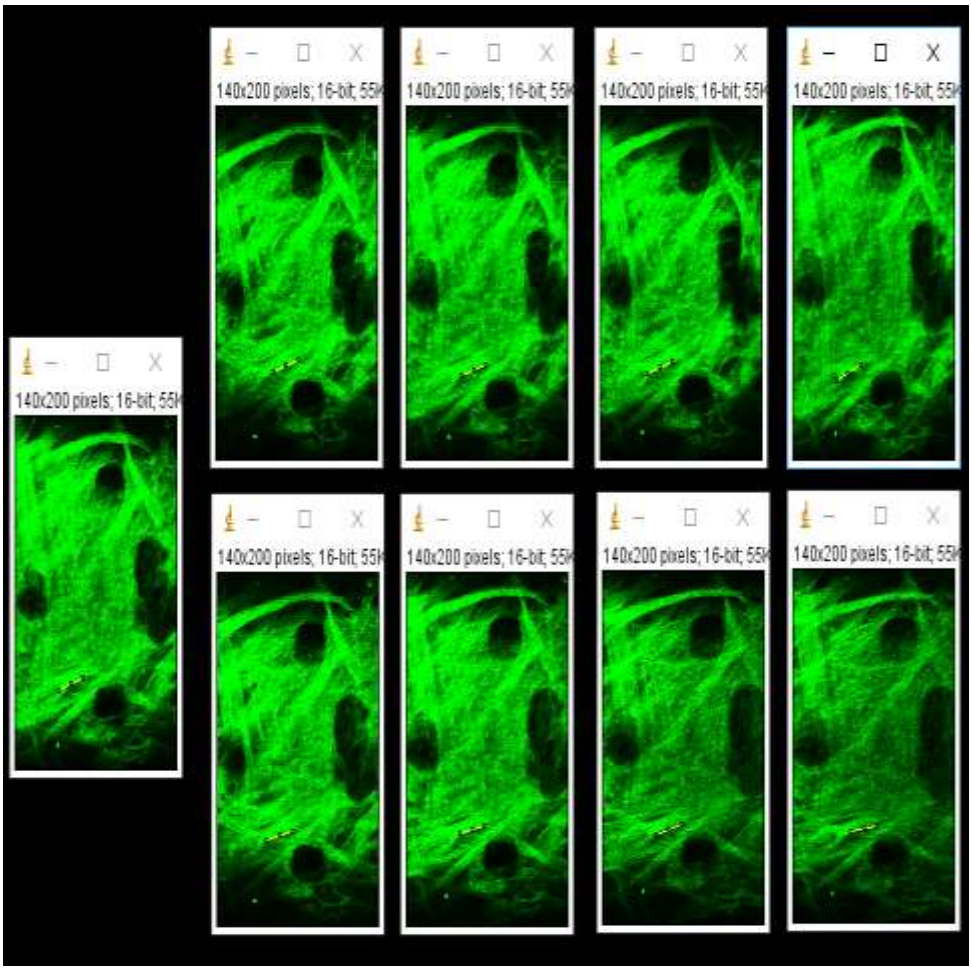

Fig. 5.9 Single fiber analysis for fiber-3 picked up from adventitial images from experiment-1- in-vivo configuration (single image on the left); in-vivo post-overstretch-1 (top row; first from left); in-vivo post-overstretch-2 (top row; second from left); in-vivo post-overstretch-3 (top row; third from left); in-vivo post-overstretch-4 (top row; forth from left); overstretch-1 (bottom row; first from left); overstretch-2 (bottom row; second from left); overstretch-3 (bottom row; third from left); overstretch-4 (bottom row; forth from left) [Scale: 1.62 um/pixel; size: 512 x 512].

Table 5.5 Single fiber analysis results for fiber-3 for all 3 observers picked up from adventitial images for in-vivo and overstretched configurations for experiment-1.

	Fiber angle (1)	Percentage difference with respect to in-vivo	Fiber angle (2)	Percentage difference with respect to in-vivo	Fiber angle (3)	Percentage difference with respect to in-vivo
in-vivo	14.036	-	18.886	-	18.435	-
Overstretch-1	21.541	53.46	22.068	16.86	12.265	-33.46
Overstretch-2	17.103	21.85	16.144	-14.52	10.784	-41.50
Overstretch-3	15.751	12.21	13.325	-29.45	9.866	-46.48
Overstretch-4	14.381	2.45	11.31	-40.11	7.765	-57.88

suggest a deviation from the observed trend. It can thus be reported from the observed trend that the collagen orientation decreased when the vessel sample was overstretched and its severity increased with increase in the amount of overstretch. Table 5.6 shows the orientation of fiber-3 for experiment-1 quantified by all three observers. The calculated percentage difference for the orientation of fiber-3 for all the in-vivo post-overstretch configurations with respect to the in-vivo configuration shows that there is a significant difference in fiber orientation between the in-vivo and in-vivo post-overstretch-1 configurations. As stated earlier, a loss of preconditioning can again be responsible for this difference. Fiber orientation does not show a lot of variation for the in-vivo post-overstretch-2 configuration onwards. A personal judgement when marking the fiber is again responsible for those few values reported for the orientation suggesting a deviation from the observed trend. It can thus be reported from the observed trend that that there was no change in the collagen orientation post-overstretch. In order to better observe the trend, we plotted the graphs with the orientation values represented on the y-axis against corresponding configurations for which they were reported on the x-axis.

Fig. 5.10 shows a graph of orientations for fiber-3 for all three observers corresponding to the in-vivo and overstretched configurations. The line joining points on the graph has a negative slope. This indicates reorganization of the fibers towards the axial direction and that the fibers became more organized and inclined towards the axial direction as overstretch became severe.

Fig. 5.11 shows a graph of orientations for fiber-2 for all three observers corresponding to the in-vivo and in-vivo post-overstretch configurations. A line joining points on the graph remains almost parallel to the x-axis. The x-axis represents the

Table 5.6 Single fiber analysis results for fiber-3 for all 3 observers picked up from adventitial images for in-vivo and in-vivo post-overstretch configurations for experiment-1.

	Fiber angle (1)	Percentage difference with respect to in-vivo	Fiber angle (2)	Percentage difference with respect to in-vivo	Fiber angle (3)	Percentage difference with respect to in-vivo
in-vivo	14.036	-	18.886	-	18.435	-
in-vivo post-overstretch-1	20.225	44.09	20.726	9.74	17.65	-4.26
in-vivo post-overstretch-2	21.541	53.47	21.541	14.05	15.945	-13.51
in-vivo post-overstretch-3	26.565	89.26	19.537	3.44	17.65	-4.26
in-vivo post-overstretch-4	24.677	75.81	-	-	17.65	-4.26

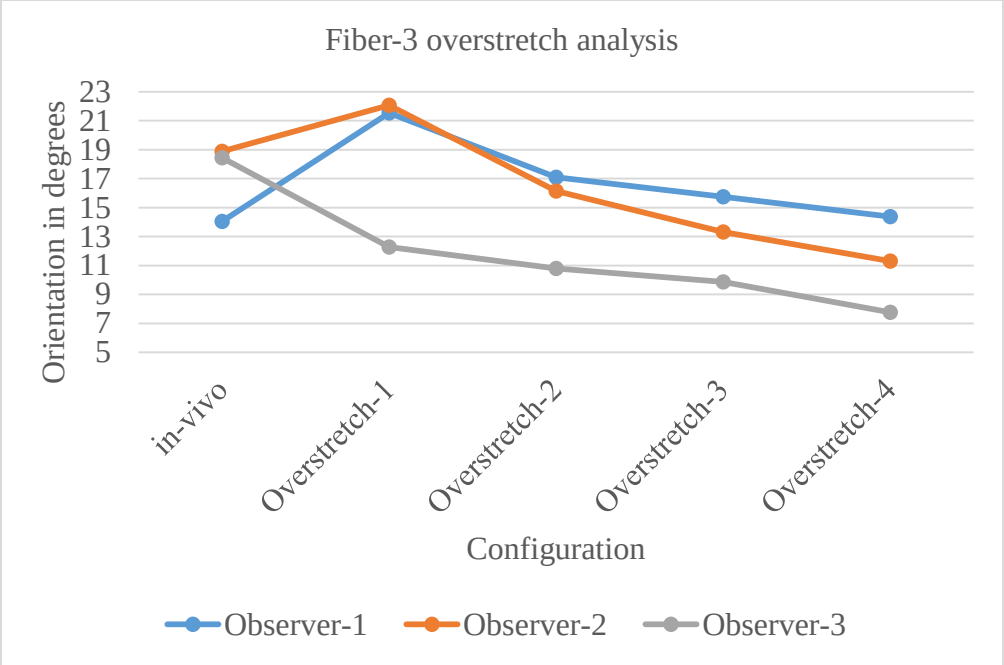

Fig. 5.10 Graph of orientation of fiber-3 for experiment-1 against overstretched configuration for which it is reported.

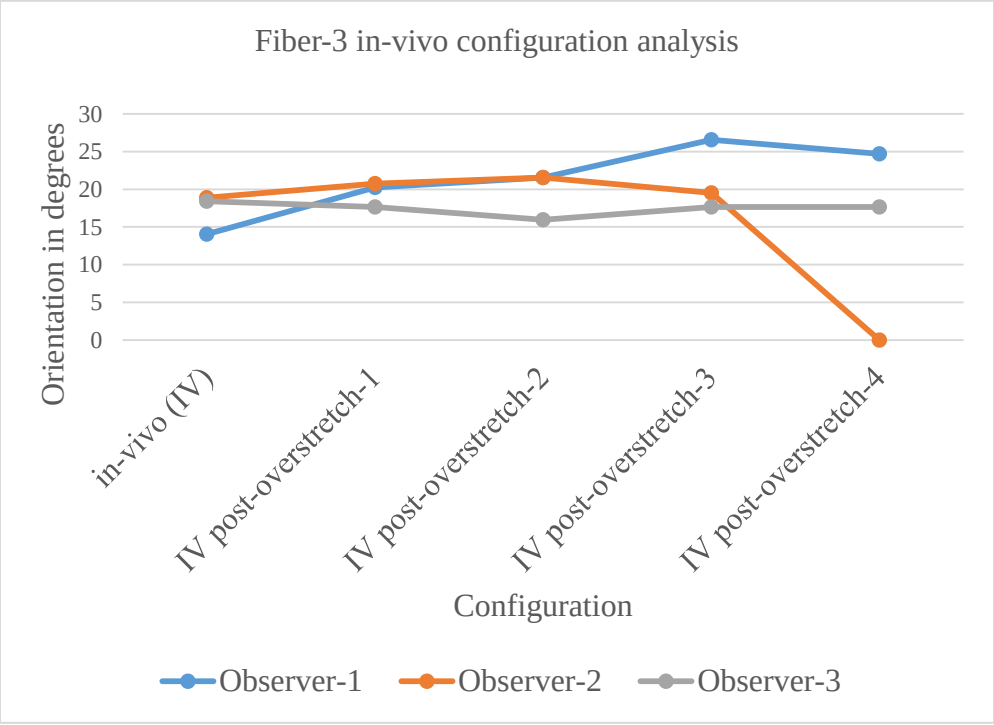

Fig. 5.11 Graph of orientation of fiber-3 for experiment-1 against in-vivo configuration for which it is reported.

configuration whereas the y-axis represents the collagen orientation in degrees. A graph parallel to the x-axis necessarily represents no change in the collagen orientation with change in the amount of overstretch. This indicates that collagen retained its orientation post-overstretch.

5.1.2 Fibril Tool Regional Analysis

As shown in Fig. 5.12, adventitial images for different configurations from experiment-1 were divided into 4 regions of interest and the average orientation was found for each region of interest using Fibril Tool, as mentioned in Table 5.7. To see if the values obtained from Fibril Tool show any trend or not, we plotted the graphs for average orientation for each region of interest (ROI) for all the configurations.

Fig. 5.13 represents a graph of the average orientations for different regions of interest corresponding to the in-vivo and overstretched configurations. As can be observed from the graph, the collagen orientation does not show any trend of the change in orientation for overstretched configurations.

Fig. 5.14 represents a graph of average orientations for different regions of interest corresponding to the in-vivo and in-vivo post-overstretch configurations. As can be observed from this graph, the collagen orientation does not show any trend of change in the orientation for in-vivo post-overstretch configurations. We thus cannot conclude anything based on these graphs. We reported earlier in the Methods Evaluation chapter that for effective working of Fibril Tool, the intensity and brightness of pixels among images must be identical. The images observed here have different intensity and brightness. We can thus associate this with the inconclusive results obtained from the Fibril Tool analysis.

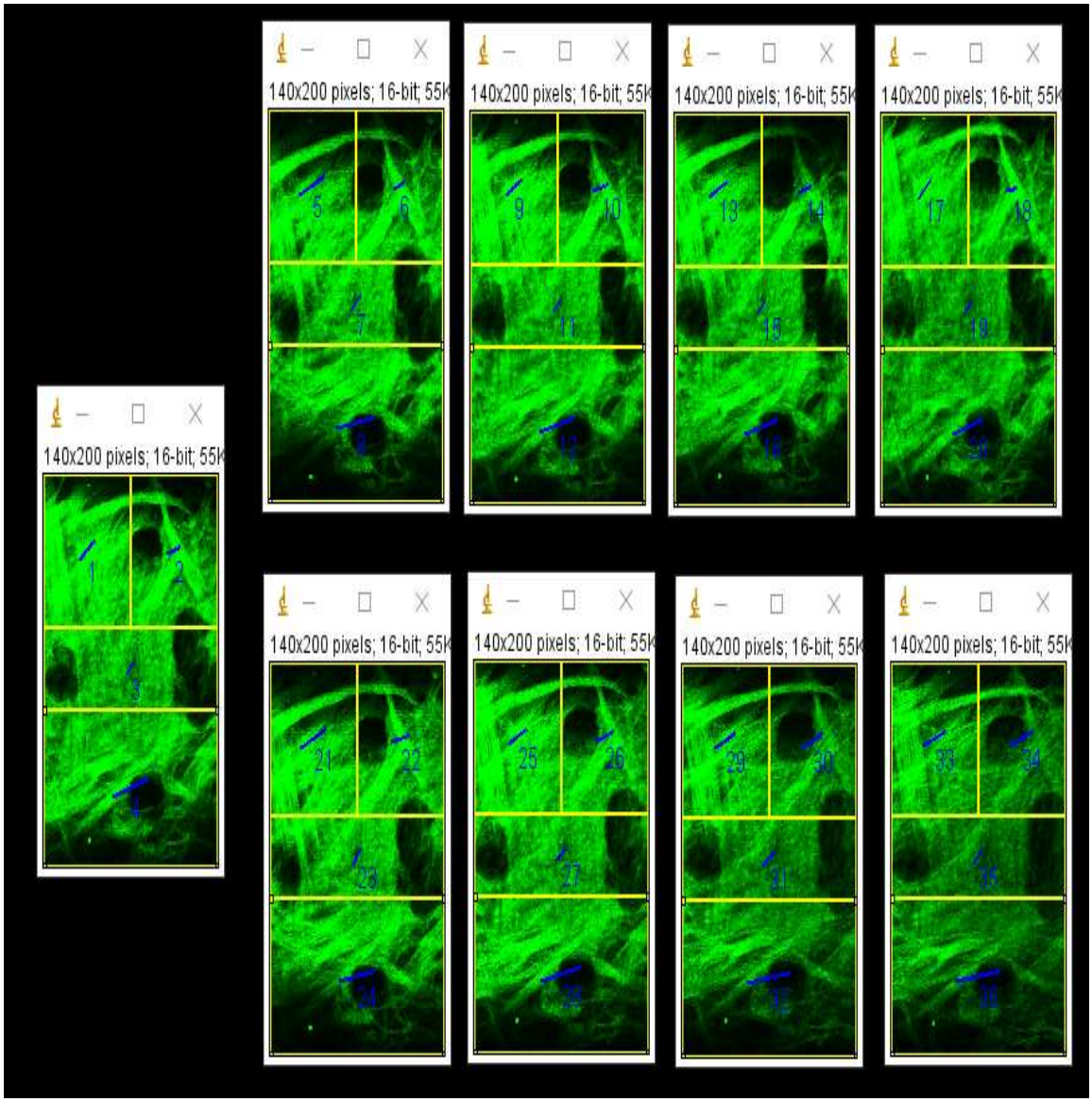

Fig. 5.12 Regional analysis with Fibril Tool where image is divided into four regions of interest as shown above- in-vivo configuration (single image on the left); in-vivo post-overstretch-1 (top row; first from left); in-vivo post-overstretch-2 (top row; second from left); in-vivo post-overstretch-3 (top row; third from left); in-vivo post-overstretch-4 (top row; forth from left); overstretch-1 (bottom row; first from left); overstretch-2 (bottom row; second from left); overstretch-3 (bottom row; third from left); overstretch-4 (bottom row; forth from left)] [Scale: 1.62 um/pixel; size: 512 x 512].

Table 5.7 Results from regional analysis of adventitial images from experiment-1 using Fibril Tool.

ROI	1 (Region on top left)	2 (Region on top right)	3 (Region in the middle)	4 (Region at the bottom)
in-vivo	39.77	14.23	45.93	17.27
Overstretch-1	22.65	11.94	48.13	10.9
in-vivo post-overstretch-1	25.27	19.23	48.41	11.17
Overstretch-2	27.02	19.56	38.08	11.45
in-vivo post-overstretch-2	32.38	17.44	41.06	14.38
Overstretch-3	22.98	22.84	37.27	8.26
in-vivo post-overstretch-3	25.86	17.94	42.37	13.49
Overstretch-4	21.34	22.5	40.65	8.01
in-vivo post-overstretch-4	40.62	15.24	51.46	17.13

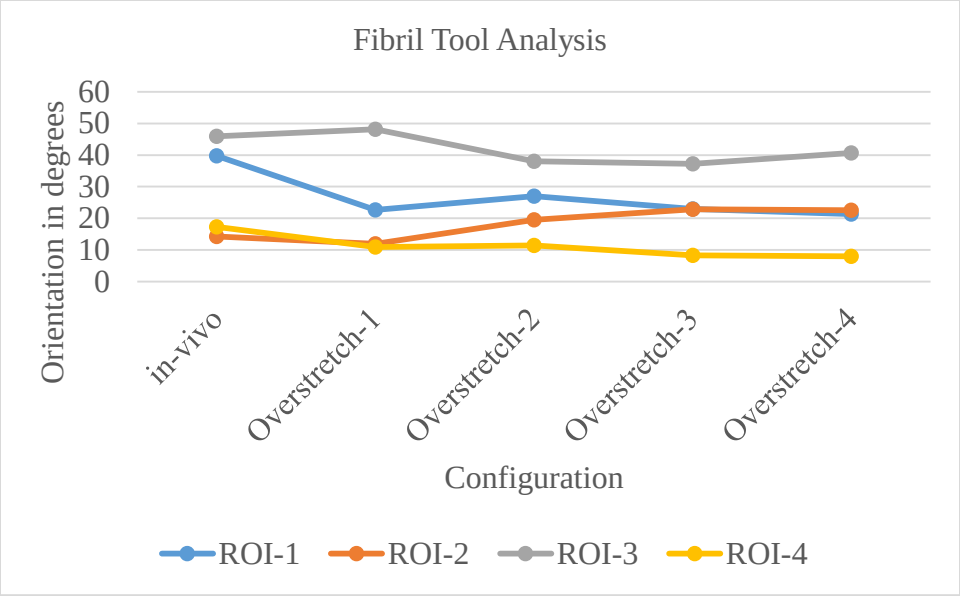

Fig. 5.13 Graph of average orientations for different regions of interest (ROI) obtained using Fibril Tool for experiment-1 against overstretched configuration for which it is reported.

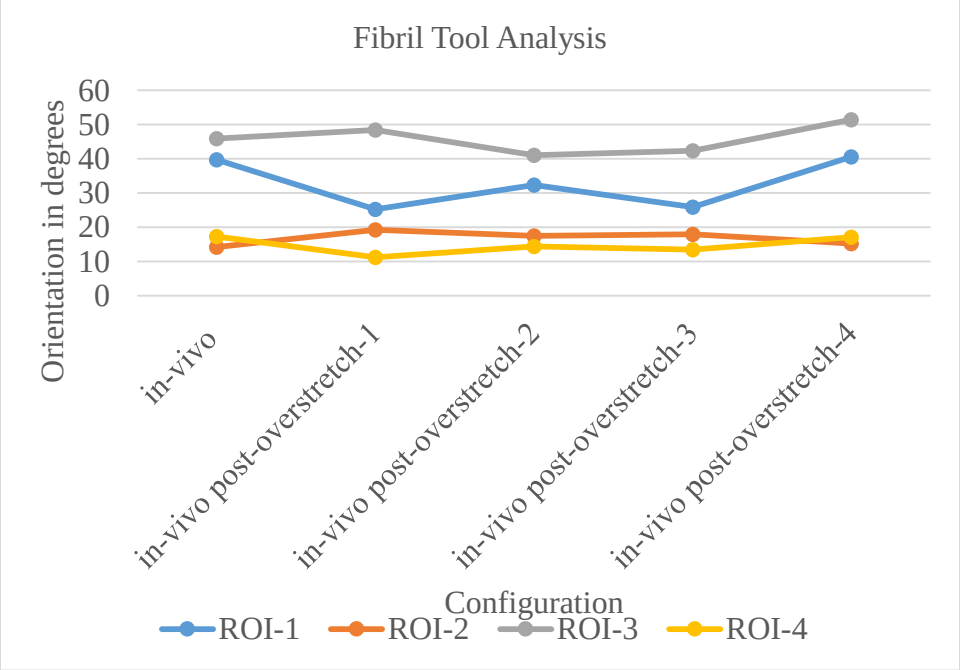

Fig. 5.14 Graph of average orientations for different regions of interest (ROI) obtained using Fibril Tool for experiment-1 against in-vivo configuration for which it is reported.

5.1.3 Orientation J analysis

The orientation graphs for the adventitia for each of the vessel samples were plotted with Orientation J Distribution (Image-J plugin). The adventitial graphs plotted for experiment-1 are shown in Fig. 5.15 (a-i). The graphs show that most of the fibers in the adventitia were oriented around 0˚ for all the configurations. As stated earlier, the collagen fibers forming the adventitia were symmetrically organized. Thus, with every greater overstretch, even if they reoriented themselves and became more disorganized, the mean orientation was not altered. It was also expected that if we plotted a histogram of the orientations, a reduction in a peak value corresponding to the mean and increase in the associated standard deviation would be observed for the in-vivo post-overstretch configurations. As can be observed from these histograms, the mean orientation for all the configurations for experiment-1 is approximately 15-20˚, which matches with our expectation. We further expected to see a decrease in the peak value corresponding to the mean orientation for the in-vivo post-overstretch configurations and an increase in peak value corresponding to the overstretched configurations. As seen from the graphs here, we did not observe any such trend. We reported earlier in the Methods Evaluation chapter that for the effective working of analysis using Orientation J for comparison, the number of fibers and their intensity among different images must be identical. This can be associated with the inconclusive outcomes obtained from these graphs. It was thus necessary to compare the peak value corresponding to the mean orientation and the standard deviation of the histogram numerically to further test the hypothesis. The orientation graphs for the adventitial images for all the configurations corresponding to the experiment-1 are shown in Fig. 5.15.

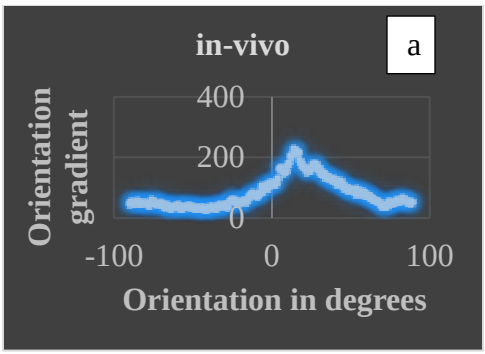

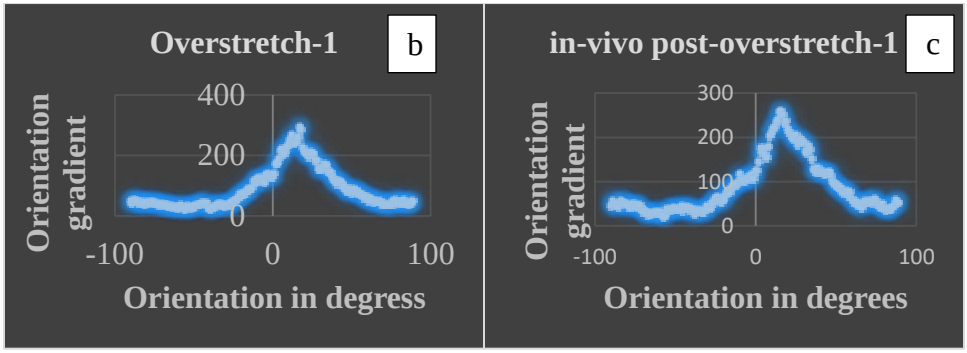

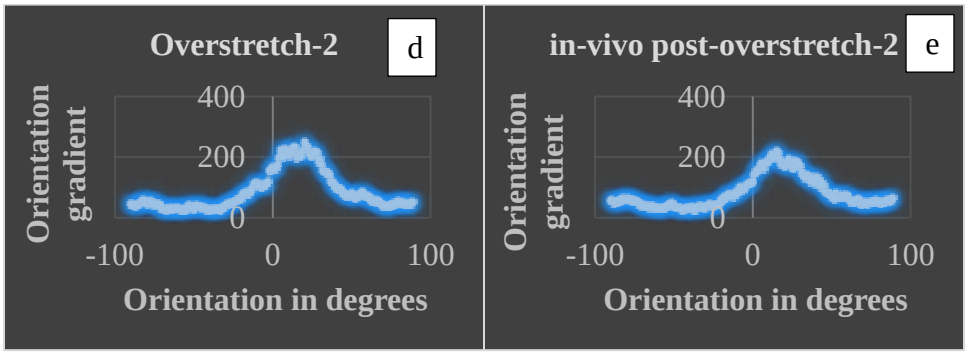

Fig. 5.15 Orientation J Distribution graphs for different configurations for experiment-1 (a) in-vivo; (b) Overstretch-1; (c) in-vivo post-overstretch-1; (d) Overstretch-2; (e) in-vivo post-overstretch-2; (f) Overstretch-3; (g) in-vivo post-overstretch-3; (h) Overstretch-4; (i) in-vivo post-overstretch-4.

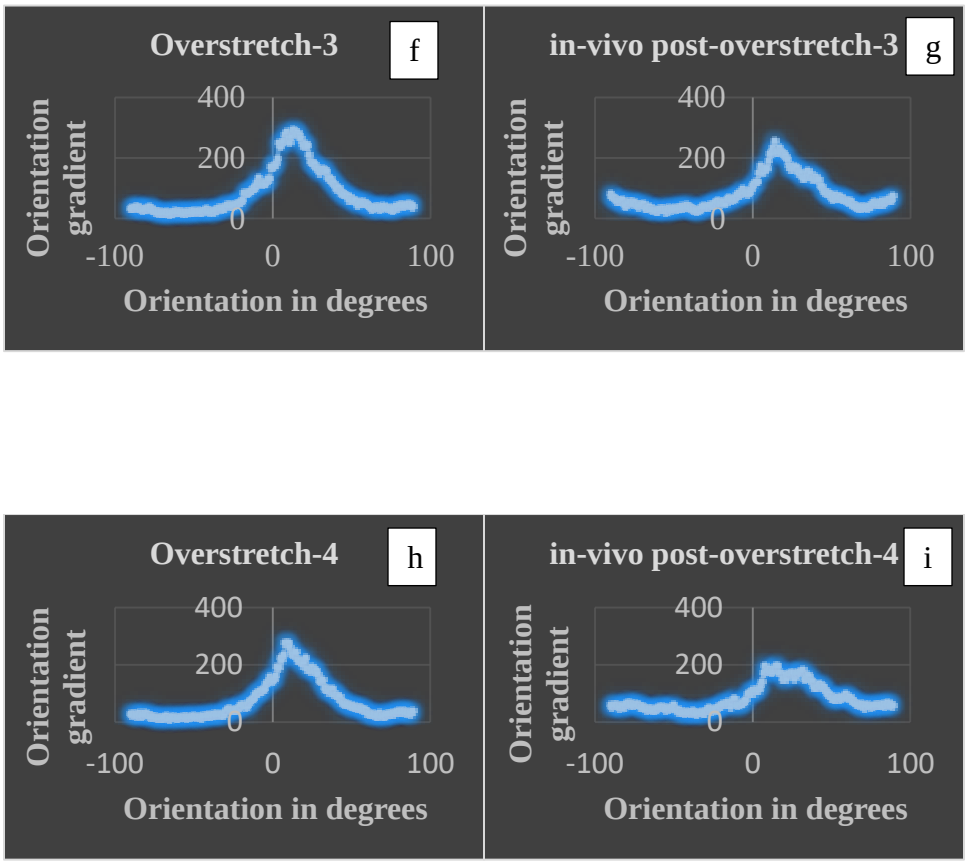

Fig. 5.15 Continued

5.1.3.1 Adventitial binned graph

A direct comparison of the orientation graphs only shows that the mean orientation did not change post-overstretch. The changes, if any, in the peak value corresponding to the mean orientation cannot be used to comment on the hypothesis. We might expect to see a monotonic change in the weights assigned to the orientations surrounding the mean orientation. We thus binned the data and summed up the weights corresponding to the orientations as shown in Table 5.8.

Table 5.8 Values calculated from binning the adventitial data into different ranges.

Orientation Range	0-2 (1)	3-5 (2)	6-8 (3)	9-11 (4)	12-14 (5)	15-17 (6)	18-20 (7)	21-23 (8)
in-vivo	342.53	403.75	476.50	505.12	637.41	652.70	536.08	478.82
Overstretch-1	146.33	577.40	636.04	715.35	749.81	801.90	723.72	609.33
in-vivo post-overstretch 1	392.85	518.75	491.91	632.33	698.24	767.88	687.78	616.34
Overstretch-2	487.55	590.69	631.55	643.68	679.81	614.57	670.93	683.98
in-vivo post-overstretch 2	137.49	488.93	516.33	568.37	608.98	626.84	529.26	553.26
Overstretch-3	173.50	682.31	781.59	796.36	854.92	832.94	739.01	692.06
in-vivo post-overstretch-3	342.10	443.21	477.57	567.44	701.58	670.75	646.10	570.02
Overstretch-4	452.25	600.89	729.92	811.67	712.27	676.88	621.20	595.32
in-vivo post-overstretch-4	324.08	350.52	508.04	542.04	538.72	564.48	475.00	483.16

We plotted these sums against the corresponding bin ranges for the adventitia, as shown in Fig. 5.16 and Fig. 5.17. In the case of an adventitia, we expected to see an increase in summed-up weights as overstretch became severe for the ranges surrounding the mean (mean not included) and a decrease for the range including the mean. It can be observed from the figures that the graphs had no consistent behavior. This method thus could not contribute to support or disprove the hypothesis.

5.1.3.2 Mean and standard deviation values calculated from Orientation J Distribution

The orientation graphs plotted for the adventitia were not very helpful for testing the hypothesis. Although the mean orientation in the graphs was observed at around 0˚ for the adventitia, the area under the curve on either side of the mean was not equal in all of the experiments. It was thus predicted that a numerical data analysis involving a dataset generation from the orientation graphs, followed by a comparison of the calculated mean

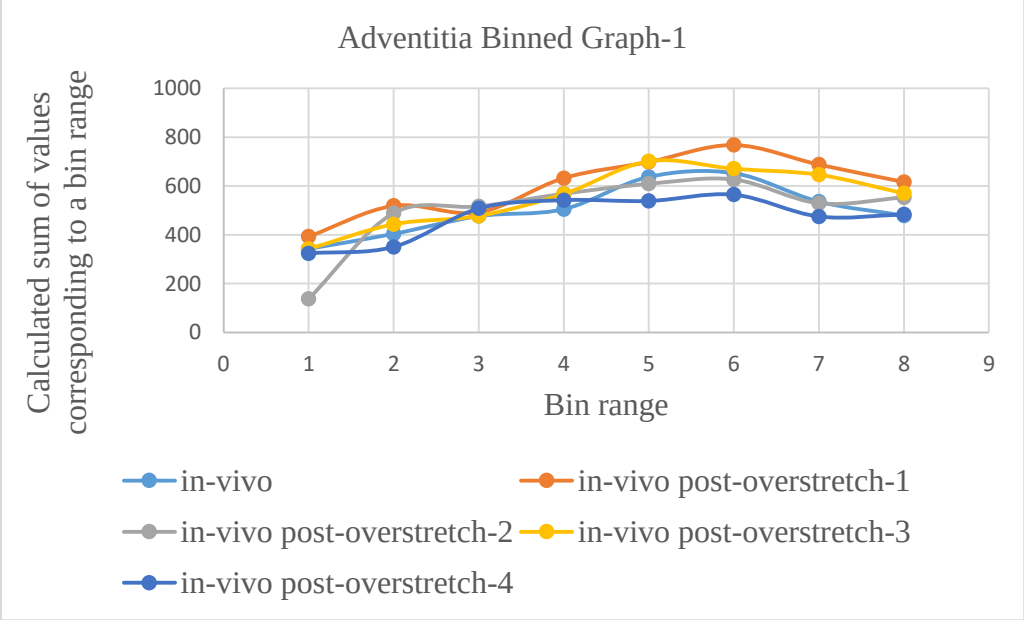

Fig. 5.16 Adventitial binned graph-1 for experiment-1.

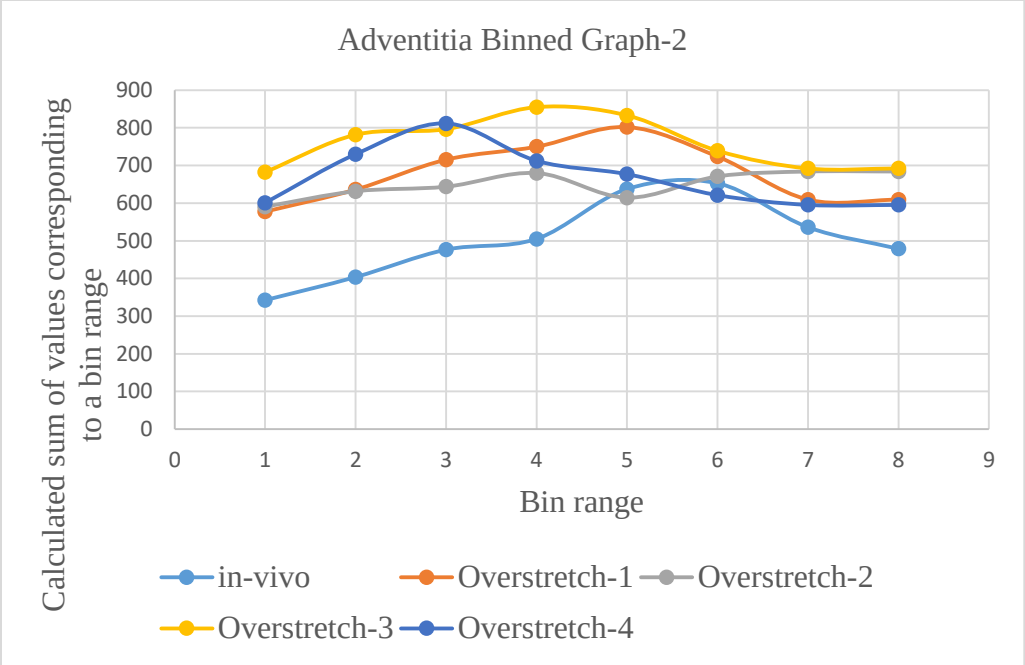

Fig. 5.17 Adventitial binned graph-2 for experiment-1.

and standard deviation for these datasets, would help to gain more understanding of the organization of the fibers and thus help us to identify the orientation changes, if any, among different configurations. If the mean calculated with the generated dataset remains the same for all the configurations, the standard deviation could be compared to gain some insight about any fiber disorganization that happened with increase in the severity of the overstretch. We generated the datasets based on the weights assigned to a particular orientation, as elaborated in the Methods chapter. The mean orientations calculated for different datasets for the same experiment showed a little variation in their values. We considered this low variation to be acceptable and compared the standard deviation for these datasets. According to the hypothesis, increase in the standard deviation was expected as overstretch became severe due to more disorganized fibers. This increase

should also have been monotonic. As shown in Table 5.9, though we have mean values approximately the same for all the configurations, we do not always observe any monotonic increase in the standard deviation as overstretch became severe. This method of numerical data analysis does not support the hypothesis. We thus need different numerical analysis of these datasets to prove or disprove the hypothesis since the hypothesis cannot be either proved or disproved with this method of numerical analysis. We decided to use a numerical analysis technique that takes into consideration the entire dataset instead of part of it. The numerical technique is explained in the following text.

Table 5.9 Mean and standard deviation values calculated from data obtained through Orientation J Distribution.

	Mean	Standard Deviation
in-vivo	11	42
Overstretch-1	10	39
in-vivo post-overstretch 1	11	40
Overstretch-2	10	39
in-vivo post-overstretch 2	10	42
Overstretch-3	12	35
in-vivo post-overstretch-3	10	42
Overstretch-4	12	33
in-vivo post-overstretch-4	11	44

5.1.3.3 p-value table

We wanted to use all the data to see if the datasets were statistically different and see if it gave us different results. In order to statistically compare the datasets, t-tests were performed for a statistical comparison. A p-value of 0.05 was used to determine if two datasets were statistically different. This value was decided based on the experiments performed in the lab earlier by senior lab members. The results of the t-tests, as shown in Table 5.10, were not consistent and thus cannot be used to draw any conclusion.

Table 5.10 p - values calculated from data obtained through Orientation J Distribution.

	p-value	Statistically different or not?
in-vivo and overstretch-1	0.047	Yes
in-vivo and overstretch-2	0.165	No
in-vivo and overstretch-3	0.127	No
in-vivo and overstretch-4	0.037	Yes
in-vivo and in-vivo post-overstretch-1	0.807	No
in-vivo and in-vivo post-overstretch-2	0.0133	Yes
in-vivo and in-vivo post-overstretch-3	0.0111	Yes
in-vivo and in-vivo post-overstretch-4	0.267	No

5.2 Experiment-2 results

5.2.1 Single fiber analysis

5.2.1.1 Fiber-1 analysis

To test our hypothesis, we did a preliminary analysis of the images involving a manual quantification of the orientation. Fig. 5.18 shows the first fiber (marked with a yellow line) from experiment-1 whose orientation was quantified manually using Line Tool in Image J. The figure shows that the orientation of this fiber in all the in-vivo post-overstretch configurations was similar to that of its orientation in in-vivo configuration. It can also be observed that the orientation of this fiber for overstretched configurations decreased with increase in the severity of overstretch. Table 5.11 shows the orientation of fiber-1 for the in-vivo and overstretched configurations quantified by all three observers. We observed a certain trend in the collagen orientation with overstretching. For a better understanding of this observed trend, we represented the variation in the fiber orientation for different configurations using a percentage difference calculated with reference to the in-vivo configuration. The calculated percentage difference clearly showed that the fiber orientation decreased with increase in the severity of overstretch, indicated by the increase in negative percentage value or the decrease in positive percentage value. We expected that the trend would give us a correct idea of the mechanism behind this. The trend observed here seems to have few exceptions where the fiber orientation has been reported to increase with the severity of overstretch. This might be because of the fact that a line drawn on the fiber for manual quantification of fiber is based on a personal judgment, and not done with the help of any software program. The trend can still be trusted based on the consistency observed despite few exceptions.

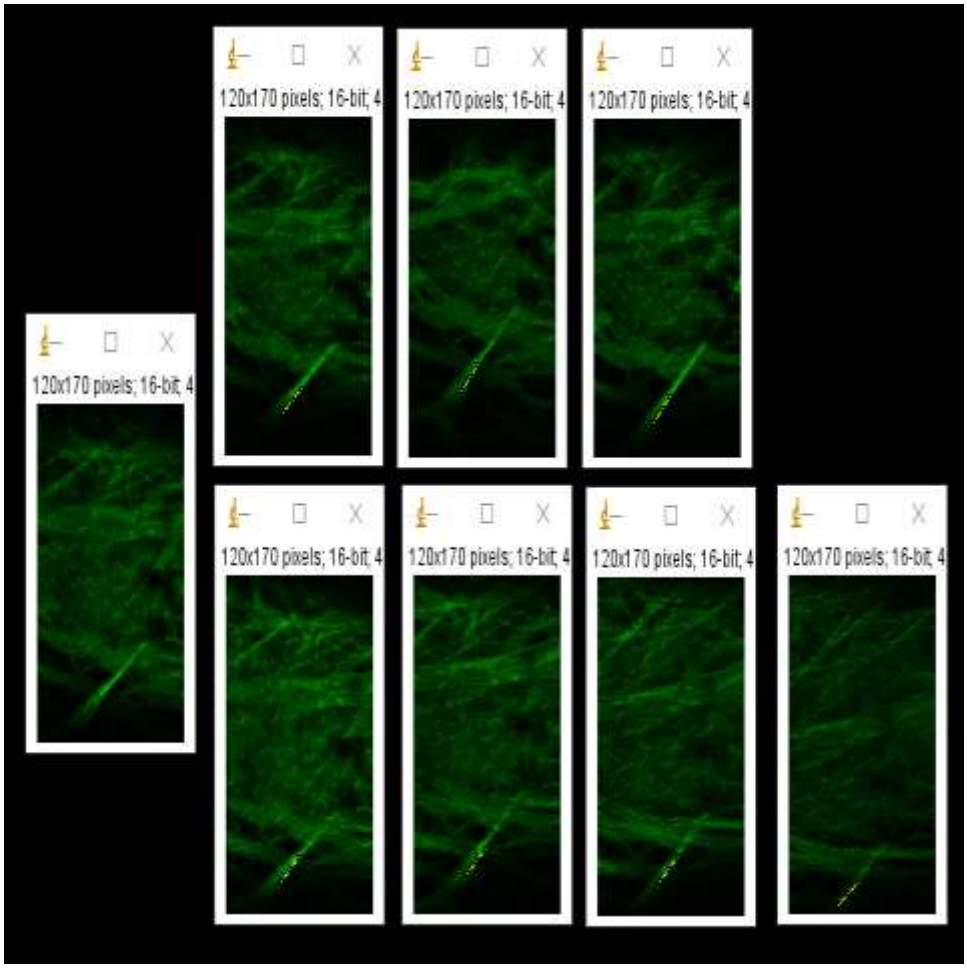

Fig. 5.18 Single fiber analysis for fiber-1 picked up from adventitial images from experiment-2- in-vivo configuration (single image on the left); in-vivo post-overstretch-1 (top row; first from left); in-vivo post-overstretch-2 (top row; second from left); in-vivo post-overstretch-3 (top row; third from left); overstretch-1 (bottom row; first from left); overstretch-2 (bottom row; second from left); overstretch-3 (bottom row; third from left); overstretch-4 (bottom row; forth from left) [Scale: 1.62 um/pixel; size: 512 x 512].

Table 5.11 Single fiber analysis results for fiber-1 picked up from adventitial images for in-vivo and all overstretched configurations from experiment-2.

	Fiber angle (1)	Percentage difference with respect to in-vivo configuration	Fiber angle (2)	Percentage difference with respect to in-vivo configuration	Fiber angle (3)	Percentage difference with respect to in-vivo configuration
in-vivo	36.027	-	38.157	-	42.709	-
Overstretch-1	42.955	19.23	34.592	-9.34	40.601	-4.94
Overstretch-2	41.987	16.54	34.592	-9.34	40.601	-4.94
Overstretch-3	37.999	5.54	33.68	-11.73	40.601	-4.94
Overstretch-4	34.875	-3.19	32.5	-14.83	34.509	-19.19

We thus decided to observe the trend instead of independent values. We note here that the collagen orientation decreased when the vessel sample was overstretched and its severity increased with an increase in the amount of overstretch.

Table 5.12 shows the orientation of fiber-1 for the in-vivo and in-vivo post-overstretch configurations quantified by all three observers. We did not really observe a significant change in the collagen orientation for these configurations for the in-vivo post-overstretch-2 configuration onwards. For a better understanding of this fact, we have represented a variation in the fiber orientation for different in-vivo post-overstretch configurations using a percentage difference calculated with reference to the in-vivo configuration. There was a significant difference in the fiber orientation corresponding to the in-vivo and in-vivo post-overstretch-1 configurations. We reported earlier in the Methods Evaluation chapter that some amount of preconditioning was lost during the transport. This fact can be associated with the observation stated here. Preconditioning restructures the fiber organization. This reorganization of the fibers, which takes place during the preconditioning, was lost during the transport, which is indicated by a loss of preconditioning. When the vessel sample is overstretched for the first time after being transported to the microscopy core, fibers must be reorganized as if the vessel sample was preconditioned. This must result in significant differences in the collagen orientation in its in-vivo configuration when compared with its orientation in the in-vivo post-overstretch-1 configuration. The fiber orientation does not show much variation for in-vivo post-overstretch-2 configuration onwards, which is easier to understand from the calculated percentage difference for fiber-1. The fact that the collagen orientation did not change again shows that there are few exceptions where the fiber orientation has been reported to

Table 5.12 Single fiber analysis results for fiber-1 picked up from adventitial images for in-vivo and all in-vivo post-overstretch configurations from experiment-2.

	Fiber angle (1)	Percentage difference with respect to in-vivo	Fiber angle (2)	Percentage difference with respect to in-vivo	Fiber angle (3)	Percentage difference with respect to in-vivo
in-vivo	36.027	-	38.157	-	42.709	-
in-vivo post-overstretch-1	36.027	0	38.92	1.99	38.66	-9.48
in-vivo post-overstretch-2	41.987	16.54	40	4.83	45	5.36
in-vivo post-overstretch-3	41.987	16.54	40.23	5.43	45	5.36
in-vivo post-overstretch-4	-	16.54	-	-	-	-

increase or decrease inconsistently post-overstretch. This again might be because of the fact that a line drawn on the fiber for a manual quantification is drawn based on a personal judgment and not with the help of any software program. We thus decided to consider the observed trend over independent values. We thus report that there was no change in the collagen orientation post-overstretch. In order to better represent the data, we plotted graphs, with the orientation values represented on the y-axis and corresponding configurations for which they were reported on the x-axis.

Fig. 5.19 shows a graph of orientations for fiber-1 for all three observers corresponding to the in-vivo and overstretched configurations. A line joining points on the graph has a negative slope. This indicates reorganization of the fibers towards the axial direction and that the fibers became more organized and inclined towards the axial direction as overstretch became severe.

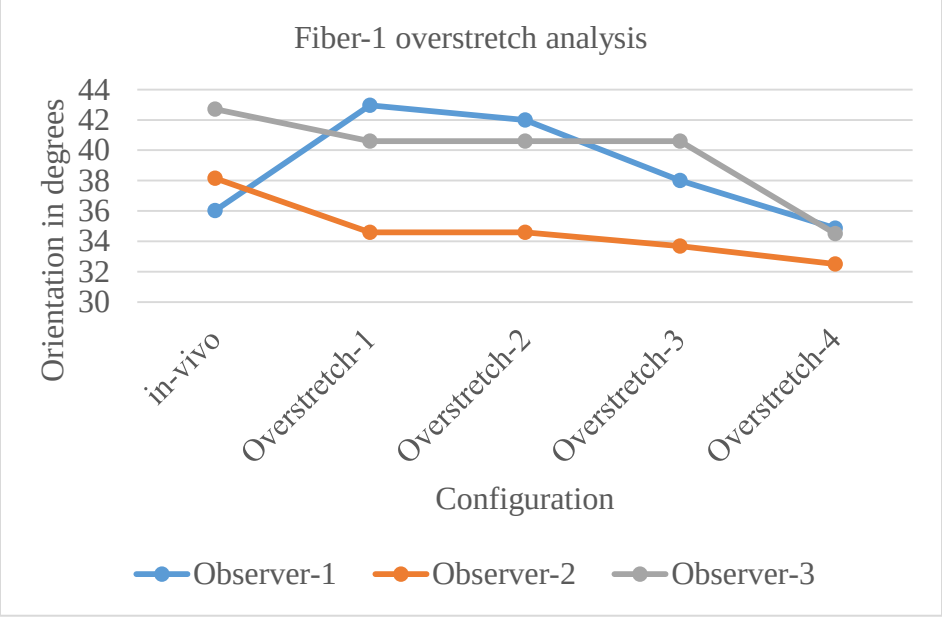

Fig. 5.19 Graph of the orientation of fiber-1 for experiment-2 against overstretched configuration for which it is reported.

Fig. 5.20 shows a graph of orientations for fiber-1 for all three observers corresponding to the in-vivo and in-vivo post-overstretch configurations. A line joining points on the graph remains almost parallel to the x-axis. The x-axis represents the configuration whereas the y-axis represents the collagen orientation in degrees. A graph parallel to the x-axis necessarily represents no change in the collagen orientation with a change in the amount of overstretch. This indicates that collagen retained its orientation post-overstretch.

5.2.1.2 Fiber-2 analysis

Fig. 5.21 shows the second fiber (marked with a yellow line) from experiment-1 whose orientation was quantified manually using Line Tool in Image J. We have done the same analysis for fiber-2 and fiber-3 as that for fiber-1. A similar trend in collagen

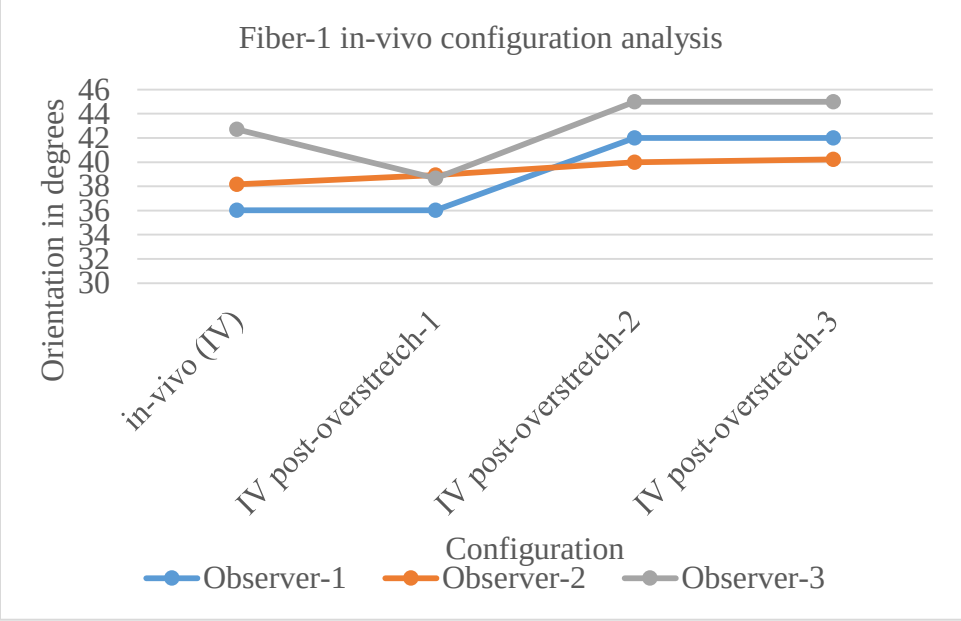

Fig. 5.20 Graph of the orientation of fiber-1 for experiment-2 against in-vivo configuration for which it is reported.

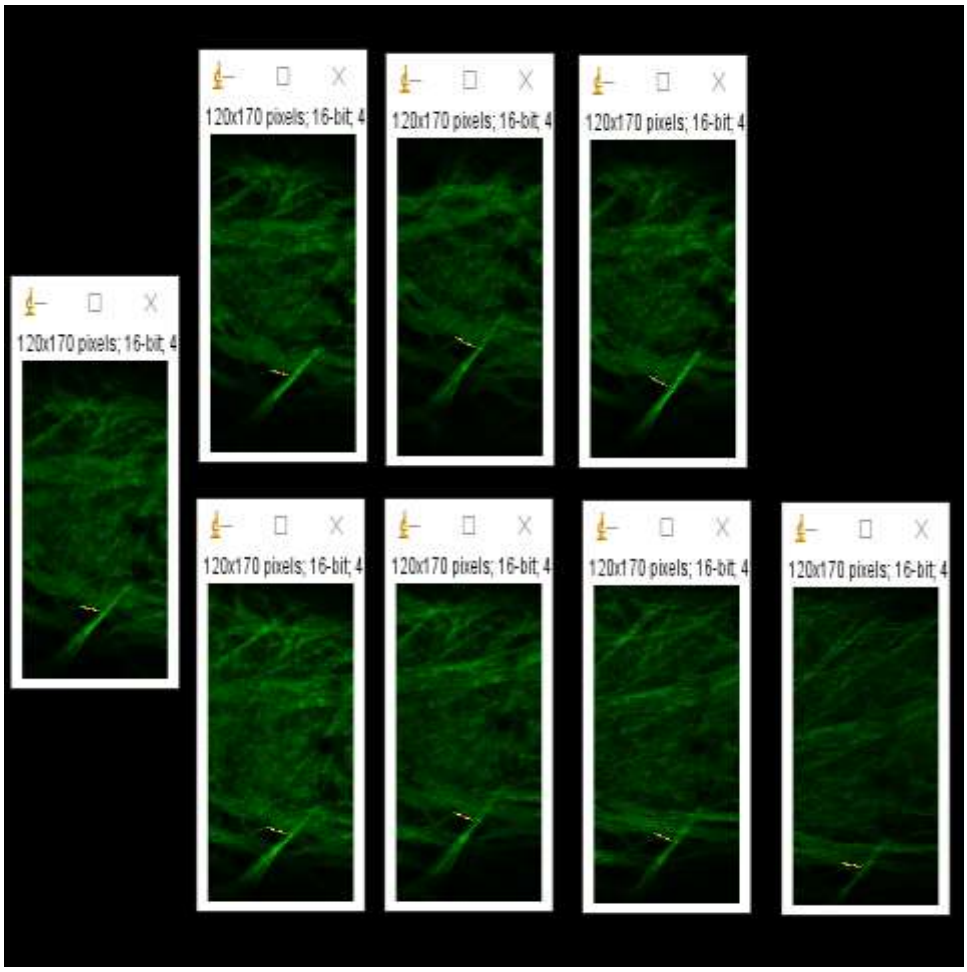

Fig. 5.21 Single fiber analysis for fiber-2 picked up from adventitial images from experiment-2- in-vivo configuration (single image on the left); in-vivo post-overstretch-1 (top row; first from left); in-vivo post-overstretch-2 (top row; second from left); in-vivo post-overstretch-3 (top row; third from left); overstretch-1 (bottom row; first from left); overstretch-2 (bottom row; second from left); overstretch-3 (bottom row; third from left); overstretch-4 (bottom row; forth from left) [Scale: 1.62 um/pixel; size: 512 x 512].

orientation change can be observed for fiber-2 for different overstretched and in-vivo post-overstretch configurations as that of fiber-1, with the increase in the severity of overstretch. Table 5.13 shows the orientation of fiber-2 for the in-vivo and overstretched configurations quantified by all three observers. It can be understood from the calculated percentage difference for the orientation of fiber-2 for all the configurations with respect to the in-vivo configuration that the fiber orientation decreased with increase in the severity of overstretch, as indicated by the increase in negative percentage value or decrease in positive percentage value. A personal judgment when marking the fiber is again responsible for the few values reported for the orientation that suggest a deviation from the observed trend. It can thus be reported from the observed trend that the collagen orientation decreased when the vessel sample was overstretched and its severity increased with the increase in the amount of overstretch. Table 5.14 shows the orientation of fiber-2 for experiment-1 quantified by all three observers. The calculated percentage difference for the orientation of fiber-2 for all the in-vivo post-overstretch configurations with respect to the in-vivo configuration shows that there is a significant difference in the fiber orientation between the in-vivo and in-vivo post-overstretch-1 configurations. As stated earlier, a loss of preconditioning can again be responsible for this difference. The fiber orientation does not show a lot of variation for the in-vivo post-overstretch-2 configuration onwards. A personal judgment when marking the fiber is again responsible for those few values reported for the orientation suggesting a deviation from the observed trend. It can thus be reported from the observed trend that there was no change in the collagen orientation post-overstretch. In order to better observe the trend, we plotted graphs with the orientation values represented on the y-axis against corresponding configurations for which

Table 5.13 Single fiber analysis results for fiber-2 for all 3 observers picked up from adventitial images for in-vivo and overstretched configurations for experiment-2.

	Fiber angle (1)	Percentage difference with respect to in-vivo configuration	Fiber angle (2)	Percentage difference with respect to in-vivo configuration	Fiber angle (3)	Percentage difference with respect to in-vivo configuration
in-vivo	19.026	-	22.62	-	8.13	-
Overstretch-1	19.26	1.23	12.265	-7.81	12.095	48.77
Overstretch-2	9.162	-51.84	11.689	-23.78	15.945	96.13
Overstretch-3	5.711	-69.98	5.356	-13.11	17.103	110.37
Overstretch-4	1.848	-90.29	4.086	-	7.595	-6.58

Table 5.14 Single fiber analysis results for fiber-2 for all 3 observers picked up from adventitial images for in-vivo and in-vivo post-overstretch configurations for experiment-2.

	Fiber angle (1)	Percentage difference with respect to in-vivo	Fiber angle (2)	Percentage difference with respect to in-vivo	Fiber angle (3)	Percentage difference with respect to in-vivo
in-vivo	19.026	-	22.62	-	8.13	-
in-vivo post-overstretch-1	19.654	3.3	20.854	-7.81	8.746	7.58
in-vivo post-overstretch-2	19.654	3.3	17.241	-23.78	19.654	141.75
in-vivo post-overstretch-3	14.36	-24.52	19.654	-13.11	21.038	158.77
in-vivo post-overstretch-4	-	-	-	-	-	-

they were reported on the x-axis. Fig. 5.22 shows a graph of orientations for fiber-2 for all three observers corresponding to the in-vivo and overstretched configurations. A line joining points on the graph has a negative slope. This indicates reorganization of the fibers towards axial direction and that the fibers became more organized and inclined towards the axial direction as overstretch became severe. Fig. 5.23 shows a graph of orientations for fiber-2 for all 3 observers corresponding to the in-vivo and in-vivo post-overstretch configurations. A line joining points on the graph remains almost parallel to the x-axis. A graph parallel to the x-axis necessarily represents no change in the collagen orientation with a change in the amount of overstretch. This indicates that collagen retained its orientation post-overstretch.

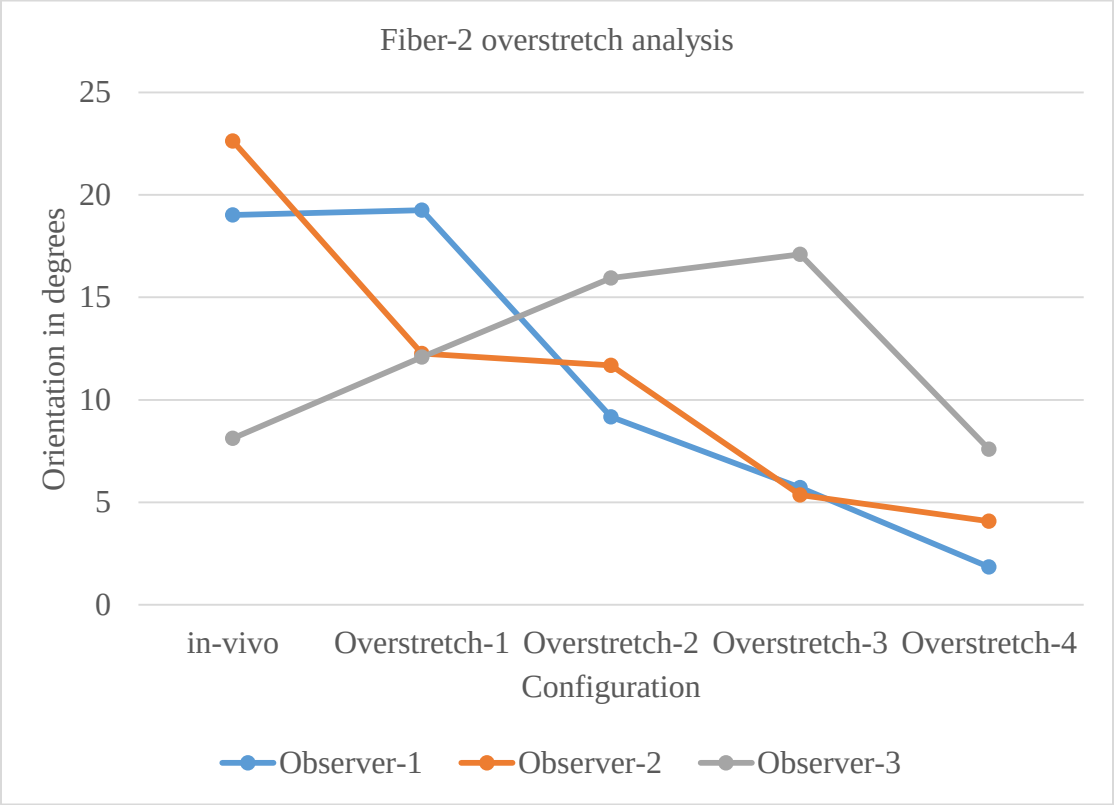

Fig. 5.22 Graph of orientation of fiber-2 for experiment-2 against overstretched configuration for which it is reported.

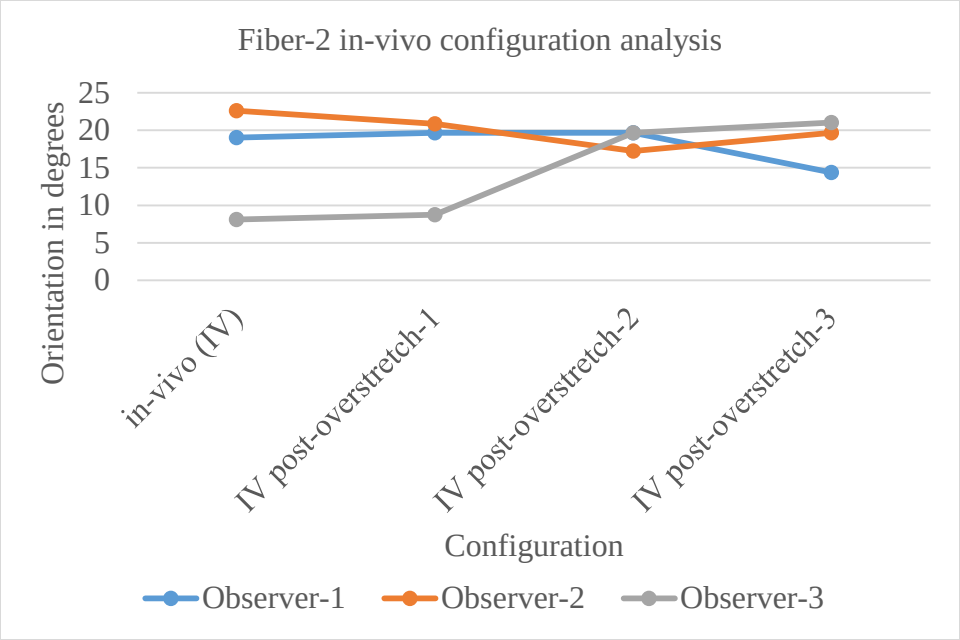

Fig. 5.23 Graph of orientation of fiber-2 for experiment-2 against in-vivo configuration for which it is reported.

5.2.1.3 Fiber-3 analysis

Fig. 5.24 shows the third fiber (marked with a yellow line) from experiment-1 whose orientation was quantified manually using Line Tool in Image J. A similar trend in the collagen orientation change can be observed for fiber-3 for different overstretched and in-vivo post-overstretch configurations as that of fiber-1, with the increase in the severity of overstretch. Table 5.15 shows the orientation of fiber-3 for the in-vivo and overstretched configurations quantified by all three observers. It can be understood from the calculated percentage difference for the orientation of fiber-3 for all the configurations with respect to the in-vivo configuration that the fiber orientation decreased with increase in the severity of overstretch, as indicated by the increase in negative percentage value or the decrease in positive percentage value. A personal judgment when marking the fiber is again responsible for the few values reported for orientation that

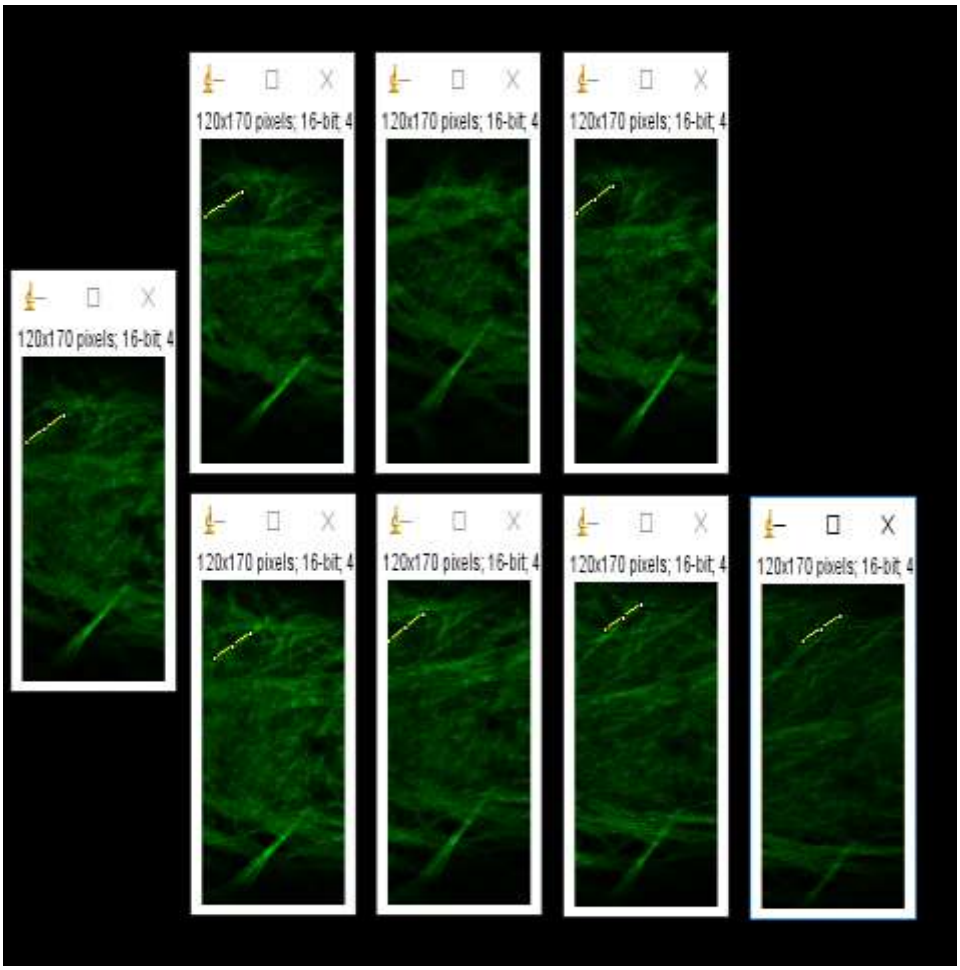

Fig. 5.24 Single fiber analysis for fiber-3 picked up from adventitial images from experiment-2- in-vivo configuration (single image on the left); in-vivo post-overstretch-1 (top row; first from left); in-vivo post-overstretch-2 (top row; second from left); in-vivo post-overstretch-3 (top row; third from left); overstretch-1 (bottom row; first from left); overstretch-2 (bottom row; second from left); overstretch-3 (bottom row; third from left); overstretch-4 (bottom row; forth from left) [Scale: 1.62 um/pixel; size: 512 x 512].

Table 5.15 Single fiber analysis results for fiber-3 for all 3 observers picked up from adventitial images for in-vivo and overstretched configurations for experiment-2.

	Fiber angle (1)	Percentage difference with respect to in-vivo	Fiber angle (2)	Percentage difference with respect to in-vivo	Fiber angle (3)	Percentage difference with respect to in-vivo
in-vivo	24.444	-	33.68	-	24.305	-
Overstretch-1	26.565	8.68	35.09	4.18	23.429	-3.60
Overstretch-2	33.232	35.95	33.69	0.03	24.146	-0.65
Overstretch-3	32.347	32.33	30.651	-8.99	23.429	-3.60
Overstretch-4	30.964	26.67	27.255	-19.08	22.751	-6.39

suggest a deviation from the observed trend. It can thus be reported from the observed trend that the collagen orientation decreased when the vessel sample was overstretched and its severity increased with increase in the amount of overstretch. Table 5.16 shows the orientation of fiber-3 for experiment-1 quantified by all three observers. The calculated percentage difference for the orientation of fiber-3 for all the in-vivo post-overstretch configurations with respect to the in-vivo configuration shows that there is a significant difference in the fiber orientation between the in-vivo and in-vivo post-overstretch-1 configurations. As stated earlier, a loss of preconditioning can again be responsible for this difference. The fiber orientation does not show a lot of variation for the in-vivo post-overstretch-2 configuration onwards. A personal judgment when marking the fiber is again responsible for those few values reported for the orientation suggesting a deviation from the observed trend. It can thus be reported from the observed trend that there was no change in the collagen orientation post-overstretch. In order to better observe the trend, we plotted graphs with the orientation values represented on the y-axis against corresponding configurations for which they were reported on the x-axis.

Fig. 5.25 shows a graph of orientations for fiber-3 for all three observers corresponding to the in-vivo and overstretched configurations. The line joining points on the graph has a negative slope. This indicates reorganization of the fibers towards the axial direction and that the fibers became more organized and inclined towards the axial direction as overstretch became severe.

Fig. 5.26 shows a graph of orientations for fiber-2 for all 3 observers corresponding to the in-vivo and in-vivo post-overstretch configurations. A line joining points on the graph remains almost parallel to the x-axis. The x-axis represents the configuration whereas

Table 5.16 Single fiber analysis results for fiber-3 for all 3 observers picked up from adventitial images for in-vivo and in-vivo post-overstretch configurations for experiment-2.

	Fiber angle (1)	Percentage difference with respect to in-vivo	Fiber angle (2)	Percentage difference with respect to in-vivo	Fiber angle (3)	Percentage difference with respect to in-vivo
in-vivo	24.444	-	33.68	-	24.305	-
in-vivo post-overstretch-1	23.629	-3.33	27.408	-18.62	22.751	-6.39
in-vivo post-overstretch-2	-	-	-	-	-	-
in-vivo post-overstretch-3	23.629	-3.33	33.111	-1.69	25.017	2.93
in-vivo post-overstretch-4	-	-	-	-	-	-

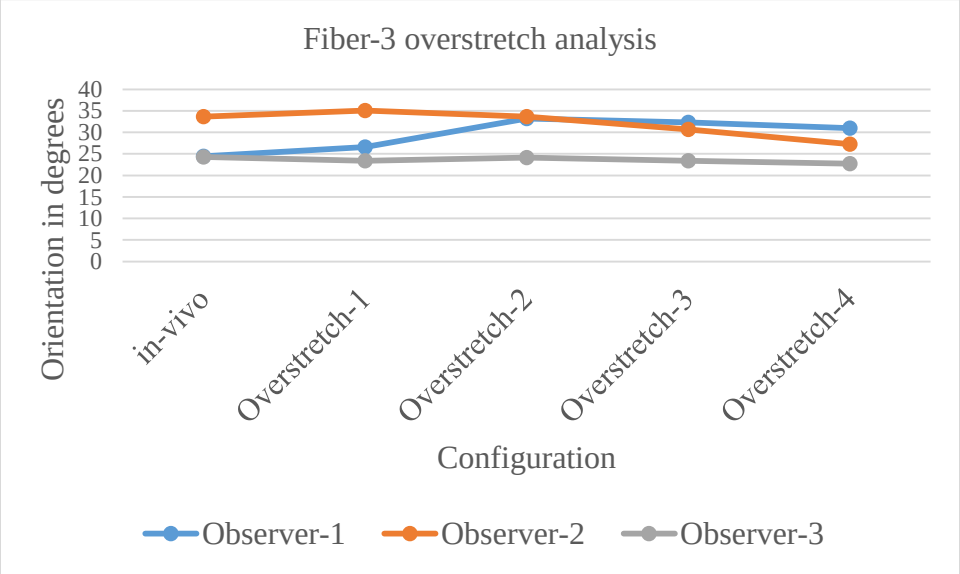

Fig. 5.25 Graph of the orientation of fiber-3 for experiment-2 against overstretched configuration for which it is reported.

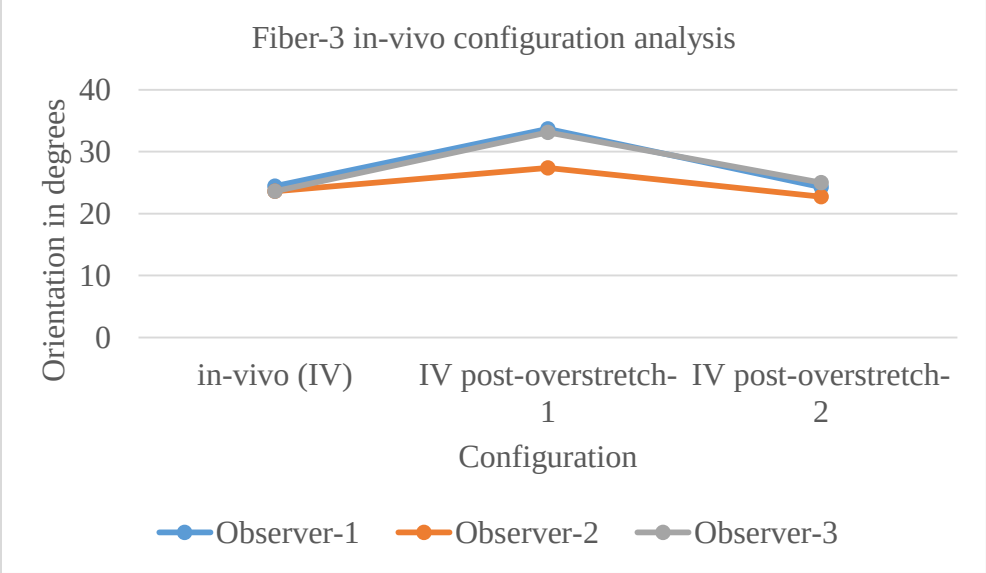

Fig. 5.26 Graph of the orientation of fiber-3 for experiment-2 against in-vivo configuration for which it is reported.

the y-axis represents the collagen orientation in degrees. A graph parallel to the x-axis necessarily represents no change in the collagen orientation with a change in the amount of overstretch. This indicates that collagen retained its orientation post-overstretch.

5.2.2 Fibril Tool Regional Analysis

As shown in Fig. 5.27, the adventitial images for different configurations from experiment-1 were divided into 4 regions of interest and the average orientation was found for each region of interest using Fibril Tool, as mentioned in Table 5.17. To see if the values obtained from Fibril Tool show any trend or not, we plotted graphs for the average orientation for each region of interest (ROI) for all the configurations.

Fig. 5.28 represents a graph of the average orientations for different regions of interest corresponding to the in-vivo and overstretched configurations. As can be observed from the graph, the collagen orientation does not show any trend of the change in orientation for the overstretched configurations.

Fig. 5.29 represents a graph of the average orientations for different regions of interest corresponding to the in-vivo and in-vivo post-overstretch configurations. As can be observed from this graph, the collagen orientation does not show any trend of change in the orientation for in-vivo post-overstretch configurations. We thus cannot conclude anything based on these graphs. We reported earlier in the Methods Evaluation chapter that for effective working of Fibril Tool, the intensity and brightness of pixels among images must be identical. We can thus associate limitation of Fibril Tool with the inconclusive results obtained from the Fibril Tool analysis. A further analysis is required to study effect of other factors affecting Fibril Tool analysis, which is out of the scope of this study.

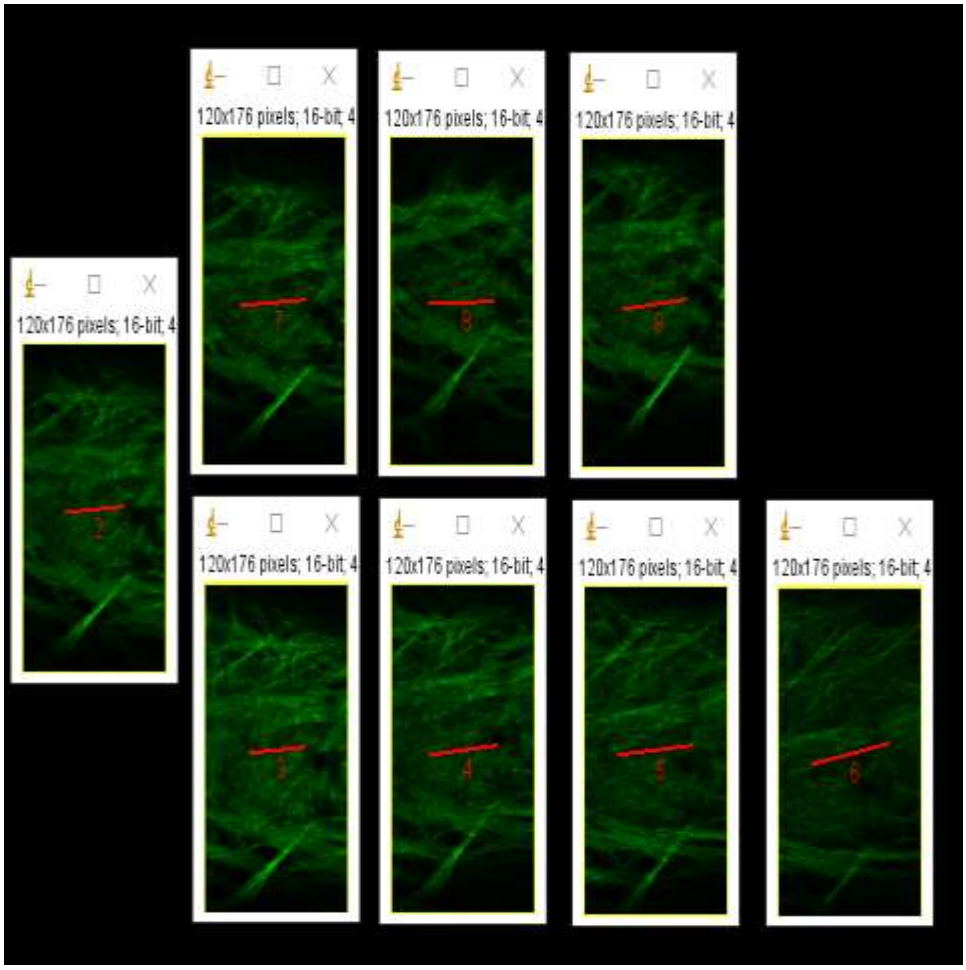

Fig. 5.27 Regional analysis with Fibril Tool as shown above- in-vivo configuration (single image on the left); in-vivo post-overstretch-1 (top row; first from left); in-vivo post-overstretch-2 (top row; second from left); in-vivo post-overstretch-3 (top row; third from left); overstretch-1 (bottom row; first from left); overstretch-2 (bottom row; second from left); overstretch-3 (bottom row; third from left); overstretch-4 (bottom row; forth from left)] [Scale: 1.62 um/pixel; size: 512 x 512].

Table 5.17 Results from regional analysis of adventitial images from experiment-2 using Fibril Tool.

ROI	Orientation
in-vivo	3.43
Overstretch-1	3.08
in-vivo post-overstretch-1	2.18
Overstretch-2	4.94
in-vivo post-overstretch-2	0.67
Overstretch-3	4.69
in-vivo post-overstretch-3	4.68
Overstretch-4	9.24
in-vivo post-overstretch-4	-

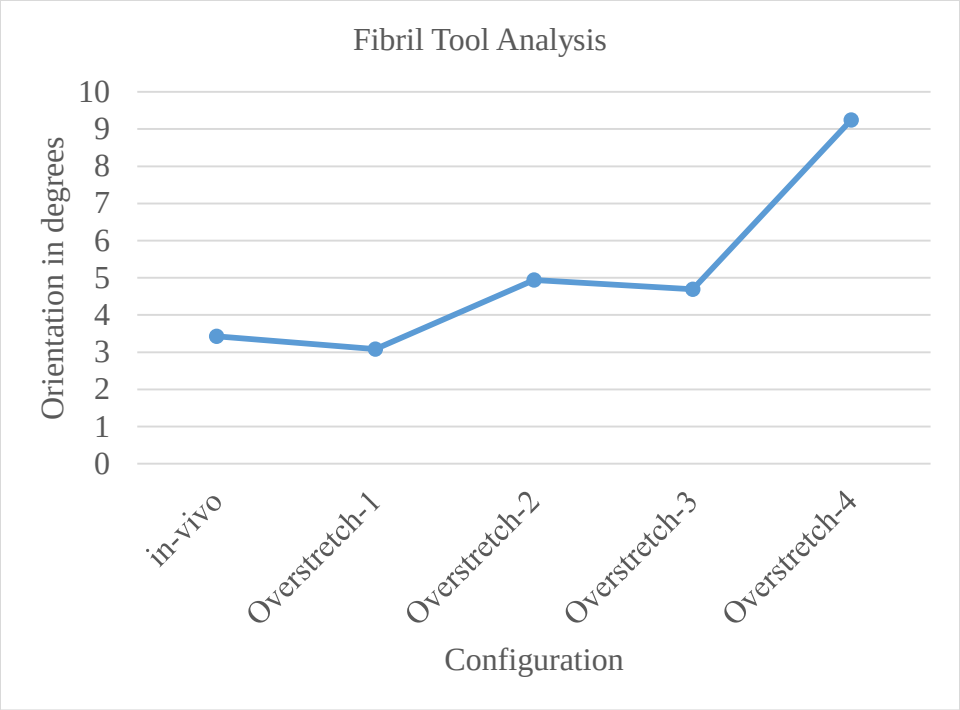

Fig. 5.28 Graph of average orientations for different regions of interest (ROI) obtained using Fibril Tool for experiment-2 against overstretched configuration for which it is reported.

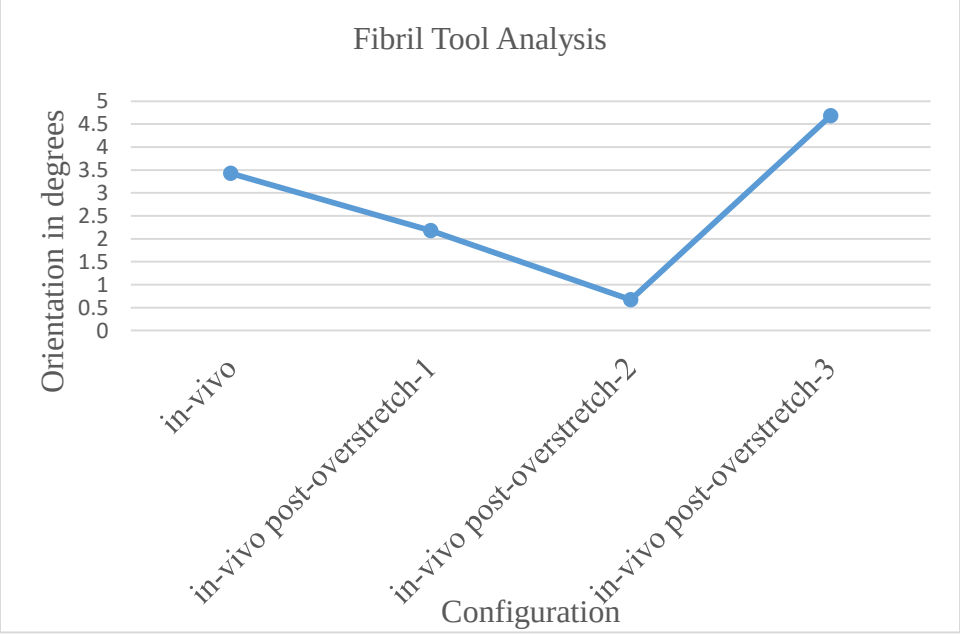

Fig. 5.29 Graph of average orientations for different regions of interest (ROI) obtained using Fibril Tool for experiment-2 against in-vivo configuration for which it is reported.

5.2.3 Orientation J analysis

The orientation graphs for the adventitia for each of the vessel samples were plotted with Orientation J Distribution (Image-J plugin). The adventitial graphs plotted for experiment-1 are shown in Fig. 5.30. The graphs show that most of the fibers in the adventitia were oriented around 0˚ for all the configurations. As stated earlier, the collagen fibers forming the adventitia were symmetrically organized. Thus, with every greater overstretch, even if they reoriented themselves and became more disorganized, the mean orientation was not altered. It was also expected that if we plotted a histogram of the orientations, a reduction in the peak value corresponding to the mean and increase in the associated standard deviation would be observed for the in-vivo post-overstretch configurations. As can be observed from these histograms, the mean orientation for all the configurations for experiment-2 is approximately 15-20˚, which matches our expectation. We further expected to see a decrease in the peak value corresponding to the mean orientation for the in-vivo post-overstretch configurations and an increase in the peak value corresponding to the overstretched configurations. As can be seen from the graphs represented here, we did not observe any such trend. We reported earlier in the Methods Evaluation chapter that for effective working of analysis using Orientation J for comparison, the number of fibers and their intensity among different images must be identical. This can be associated with the inconclusive outcomes obtained from simple visual inspection of these graphs. It was thus necessary to compare the peak value corresponding to the mean orientation and the standard deviation of the histogram numerically to further test the hypothesis. The orientation graphs for the adventitial images corresponding to various configurations for experiment-2 are as shown in Fig. 5.30.

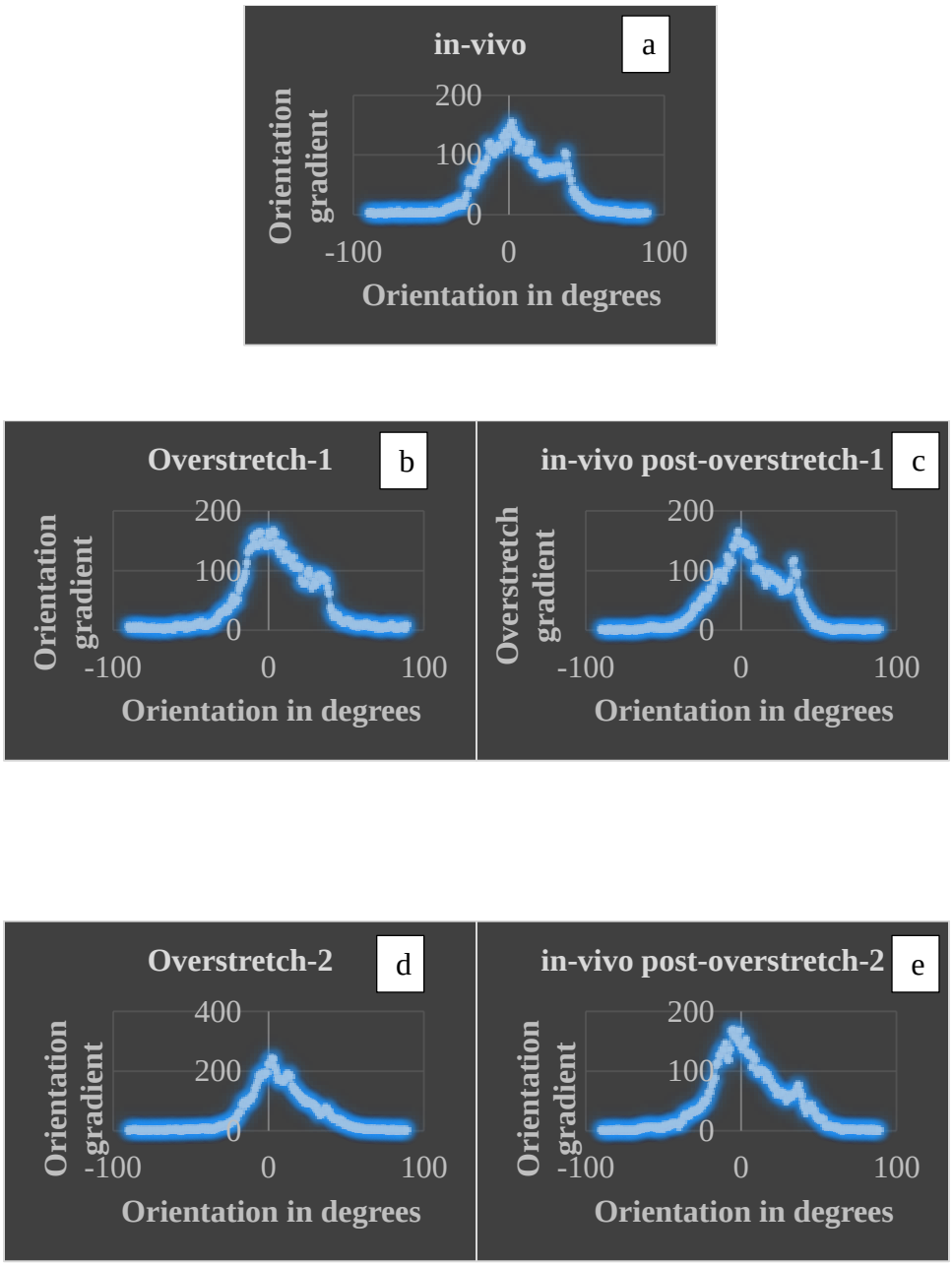

Fig. 5.30 Orientation J Distribution graphs for different configurations for experiment-2 (a) In-vivo; (b) Overstretch-1; (c) In-vivo post-overstretch-1; (d) Overstretch-2; (e) In-vivo post-overstretch-2; (f) Overstretch-3; (g) In-vivo post-overstretch-3; (h) Overstretch-4

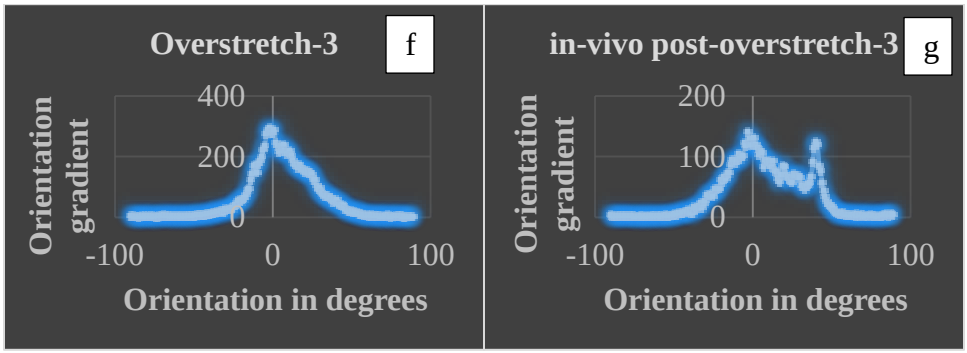

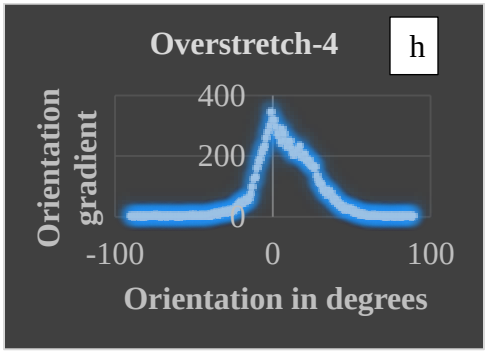

Fig. 5.30 Continued

5.2.3.1 Adventitial binned graph

A direct comparison of the orientation graphs only shows that the mean orientation did not change post-overstretch. The changes, if any, in the peak value corresponding to the mean orientation cannot be used to comment on the hypothesis. We might still expect to see a monotonic change in the weights assigned to the orientations surrounding the mean orientation. We thus binned the data in different ranges. We then summed up the weights corresponding to orientations in each bin, as shown in Table 5.18.

Table 5.18 Values calculated from binning the adventitial data into different ranges.

	0-2 (1)	3-5 (2)	6-8 (3)	9-11 (4)	12-14 (5)	15-17 (6)	18-20 (7)	21-23 (8)
in-vivo	432.29	411.34	344.91	336.97	332.66	260.41	255.41	222.76
Overstretch-1	463.93	475.29	411.74	390.92	364.42	338.60	318.02	242.37
in-vivo post-overstretch 1	439.57	405.14	383.33	305.84	293.52	249.36	272.08	256.49
Overstretch-2	692.88	648.42	522.74	508.92	561.01	429.58	372.15	315.26
in-vivo post-overstretch 2	427.87	412.14	360.93	316.88	302.98	281.25	245.09	207.26
Overstretch-3	808.35	666.49	692.85	640.66	558.56	507.21	468.30	452.71
in-vivo post-overstretch-3	369.54	326.90	282.11	270.27	252.31	194.65	236.99	199.71
Overstretch-4	311.78	792.59	814.09	724.18	635.35	667.05	604.25	560.82
in-vivo post-overstretch-4	324.08	350.52	508.04	542.04	538.72	564.48	475.00	483.16

We plotted these sums against the corresponding bin ranges for the adventitia, as shown in Fig. 5.31 and Fig. 5.32. In the case of an adventitia, we expected to see an increase in summed-up weights as overstretch became severe for the ranges surrounding the mean (mean not included) and a decrease for the range including the mean. It can be observed from the figures that the graphs had no consistent behavior. This method could not thus contribute to support or disprove the hypothesis.

5.2.3.2 Mean and standard deviation values calculated from Orientation J Distribution

The orientation graphs plotted for the adventitia were not very helpful for testing the hypothesis. Although the mean orientation in the graphs was observed at around 0˚ for the adventitia, the area under the curve on either side of the mean was not equal in all of the experiments. It was thus predicted that a numerical data analysis involving the dataset

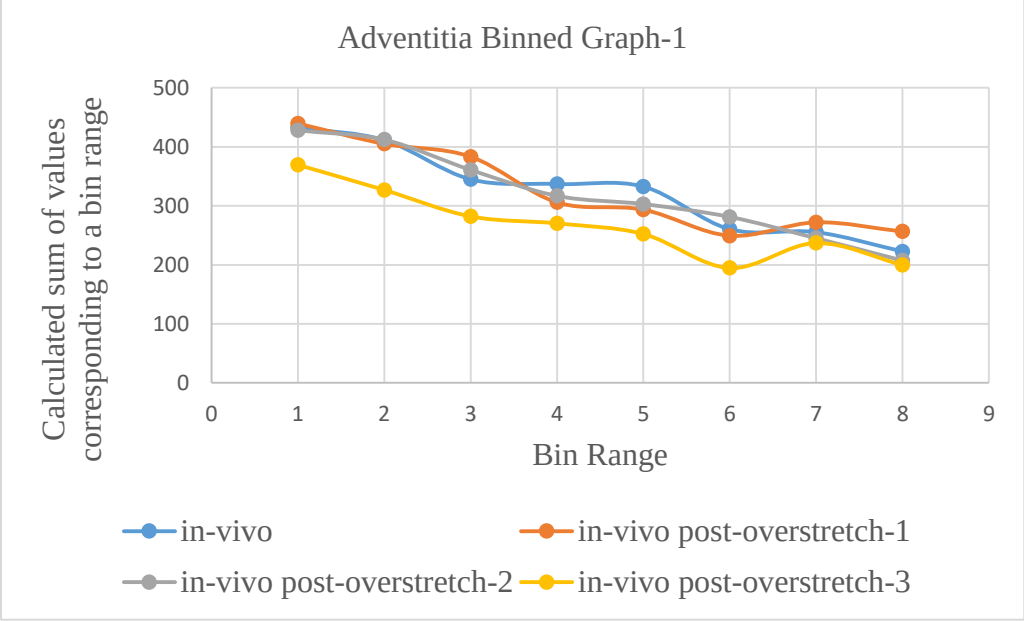

Fig. 5.31 Adventitial binned graph-1 for experiment-2.

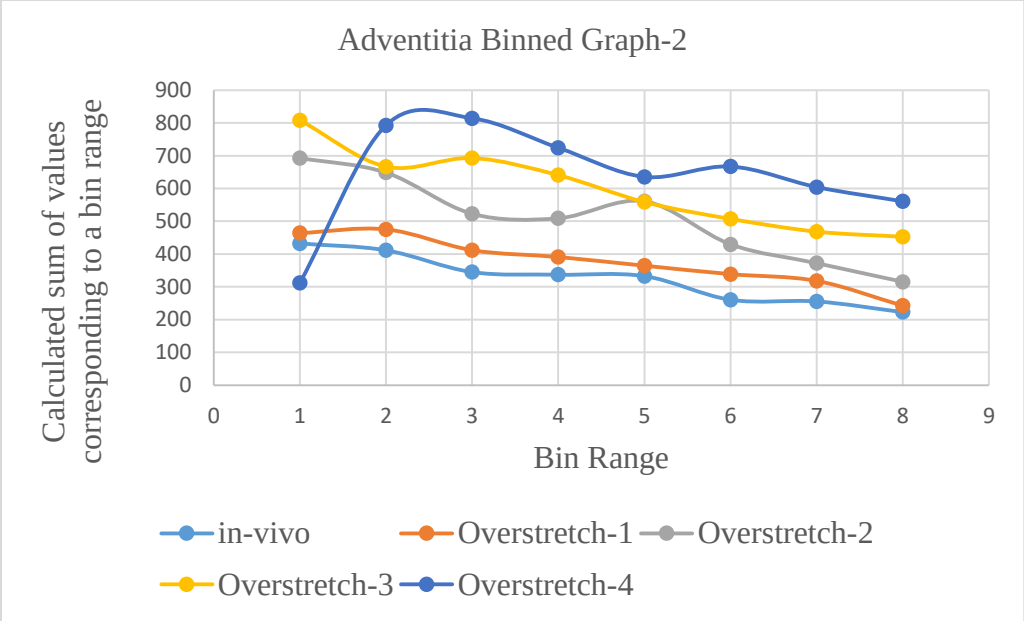

Fig. 5.32 Adventitial binned graph-2 for experiment-2.

generation from the orientation graphs, followed by a comparison of the calculated mean and the standard deviation for these datasets, would help to gain more understanding of the organization of the fibers and thus help us to identify the orientation changes, if any, among different configurations. If the mean calculated with the generated dataset remains the same for all the configurations, the standard deviation could be compared to gain some insight about any fiber disorganization that happened with increase in the severity of the overstretch. We generated datasets based on the weights assigned to a particular orientation, as elaborated in the Methods chapter. The mean orientations calculated for different datasets for the same experiment showed little variation in their values. We considered this low variation to be acceptable and compared the standard deviation for these datasets. According to the hypothesis, increase in the standard deviation was expected as overstretch became severe due to more disorganized fibers. This increase

should also have been monotonic. As shown in Table 5.19, though we have mean values approximately the same for all the configurations, we do not always observe any monotonic increase in the standard deviation as overstretch became severe. This method of numerical data analysis does not support the hypothesis. We thus need different numerical analysis of these datasets to prove or disprove the hypothesis since the hypothesis cannot be either proved or disproved with this method of numerical analysis. We decided to use a numerical analysis technique that takes into consideration the entire dataset instead of part of it. The numerical technique is explained in the following text.

Table 5.19 Mean and standard deviation values calculated from data obtained through Orientation J Distribution.

	Mean	Standard Deviation
in-vivo	7	24
Overstretch-1	6	25
in-vivo post-overstretch 1	5	22
Overstretch-2	8	21
in-vivo post-overstretch 2	4	23
Overstretch-3	6	20
in-vivo post-overstretch-3	8	25
Overstretch-4	8	20
in-vivo post-overstretch-4	-	-

5.2.3.3 p-value table

We wanted to use all the data to see if the datasets were statistically different and see if it gave us different results. In order to statistically compare the datasets, t-tests were performed for a statistical comparison. A p-value of 0.05 was used to determine if two datasets were statistically different. This value was decided based on the experiments performed in the lab earlier by senior lab members. The results of the t-tests, as shown in Table 5.20, were not consistent and thus cannot be used to draw any conclusion.

Table 5.20 p - values calculated from data obtained through Orientation J Distribution.

	p-value	Statistically different or not?
in-vivo and overstretch-1	0.3837	No
in-vivo and overstretch-2	0.1754	No
in-vivo and overstretch-3	0.2048	No
in-vivo and overstretch-4	1.49288E-15	Yes
in-vivo and in-vivo post-overstretch-1	3.4196E-175	Yes
in-vivo and in-vivo post-overstretch-2	2.3253E-210	Yes
in-vivo and in-vivo post-overstretch-3	8.68843E-39	Yes
in-vivo and in-vivo post-overstretch-4	-	-

5.3 Experiment-3 results

5.3.1 Single fiber analysis

5.3.1.1 Fiber-1 analysis

To test our hypothesis, we did a preliminary analysis of the images involving a manual quantification of the orientation. Fig. 5.33 shows the first fiber (marked with a yellow line) from experiment-3 whose orientation was quantified manually using Line Tool in Image J. The figure shows that the orientation of this fiber in all in-vivo post-overstretch configurations was similar to that of its orientation in in-vivo configuration. Table 5.21 shows the orientation of fiber-1 for the in-vivo and in-vivo post-overstretch configurations quantified by all three observers. We did not really observe a significant change in the collagen orientation for these configurations for the in-vivo post-overstretch-2 configuration onwards. For a better understanding of this fact, we have represented variation in the fiber orientation for different in-vivo post-overstretch configurations using a percentage difference calculated with reference to the in-vivo configuration. There was a significant difference in the fiber orientation corresponding to the in-vivo and in-vivo post-overstretch-1 configurations. We reported earlier in the methods evaluation chapter that some amount of preconditioning was lost during transport. This fact can be associated with the observation stated here. Preconditioning restructures the fiber organization. This reorganization of fibers, which takes place during preconditioning, was lost during transport, which is indicated by a loss of preconditioning. When the vessel sample is overstretched for the first time after it is carried to the microscopy core, fibers must be reorganized as if the vessel sample was preconditioned. This must result in significant differences in the collagen orientation in its in-vivo configuration when

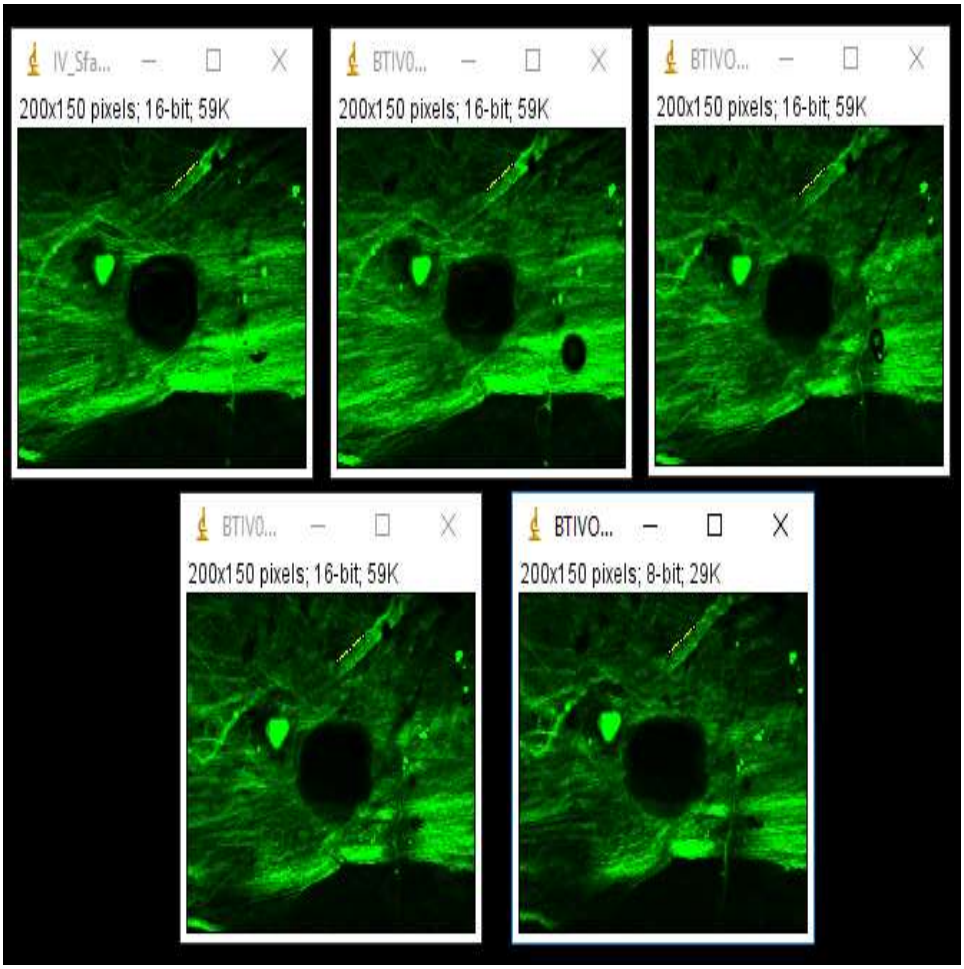

Fig. 5.33 Single fiber analysis for fiber-1 picked up from adventitial images from experiment-3- in-vivo configuration (top row; first from left); in-vivo post-overstretch-1 (top row; second from left); in-vivo post-overstretch-2 (top row; third from left); in-vivo post-overstretch-3 (bottom row; first from left); in-vivo post-overstretch-4 (bottom row; second from left) [Scale: 1.62 um/pixel; size: 512 x 512].

Table 5.21 Single fiber analysis results for fiber-1 picked up from adventitial images for in-vivo and all in-vivo post-overstretch configurations from experiment-3.

	Fiber angle (1)	Percentage difference with respect to in-vivo	Fiber angle (2)	Percentage difference with respect to in-vivo	Fiber angle (3)	Percentage difference with respect to in-vivo
in-vivo	32.905	-	30.141	-	32.905	-
in-vivo post-overstretch-1	31.701	-3.65	30.141	0	32.905	0
in-vivo post-overstretch-2	32.471	-1.32	31.681	5.10932	32.905	0
in-vivo post-overstretch-3	31.701	-3.66	31.109	3.21	31.43	-4.48
in-vivo post-overstretch-4	33.275	1.12	32.735	8.61	32.905	0

compared with its orientation in the in-vivo post-overstretch-1 configuration. The fiber orientation does not show much variation for in-vivo post-overstretch-2 configuration onwards, which is easier to understand from the calculated percentage difference for fiber-1. The fact that the collagen orientation did not change again shows that there are few exceptions where the fiber orientation has been reported to increase or decrease inconsistently post-overstretch. This again might be because of the fact that a line drawn on the fiber for manual quantification is based on personal judgment and not done with any software program. We thus decided to consider the observed trend over independent values. We thus report that there was no change in the collagen orientation post-overstretch. In order to better represent the data, we plotted graphs, with orientation values represented on the y-axis and corresponding configurations for which they were reported on the x-axis.

Fig. 5.34 shows a graph of orientations for fiber-1 for all three observers corresponding to the in-vivo and in-vivo post-overstretch configurations. A line joining points on the graph remains almost parallel to the x-axis. The x-axis represents the configuration whereas y-axis represents the collagen orientation in degrees. A graph parallel to the x-axis necessarily represents no change in the collagen orientation with a change in the amount of overstretch. This indicates that collagen retained its orientation post-overstretch.

5.3.1.2 Fiber-2 analysis

To test our hypothesis, we did a preliminary analysis of the images involving the manual quantification of the orientation. Fig. 5.35 shows the second fiber (marked with a yellow line) from experiment-3 whose orientation was quantified manually using Line

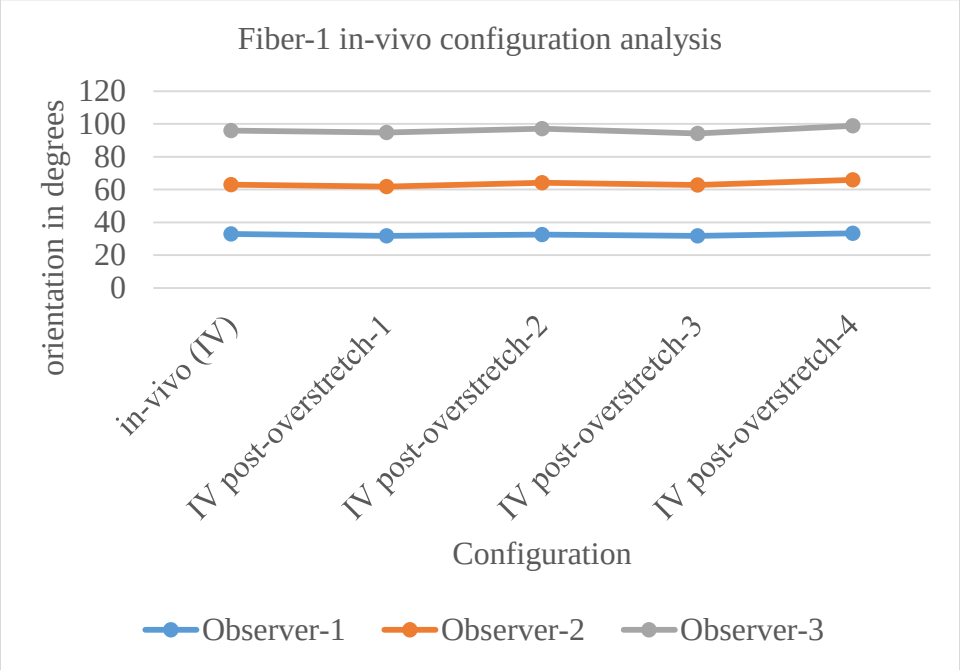

Fig. 5.34 Graph of the orientation of fiber-1 for experiment-3 against overstretched configuration for which it is reported.

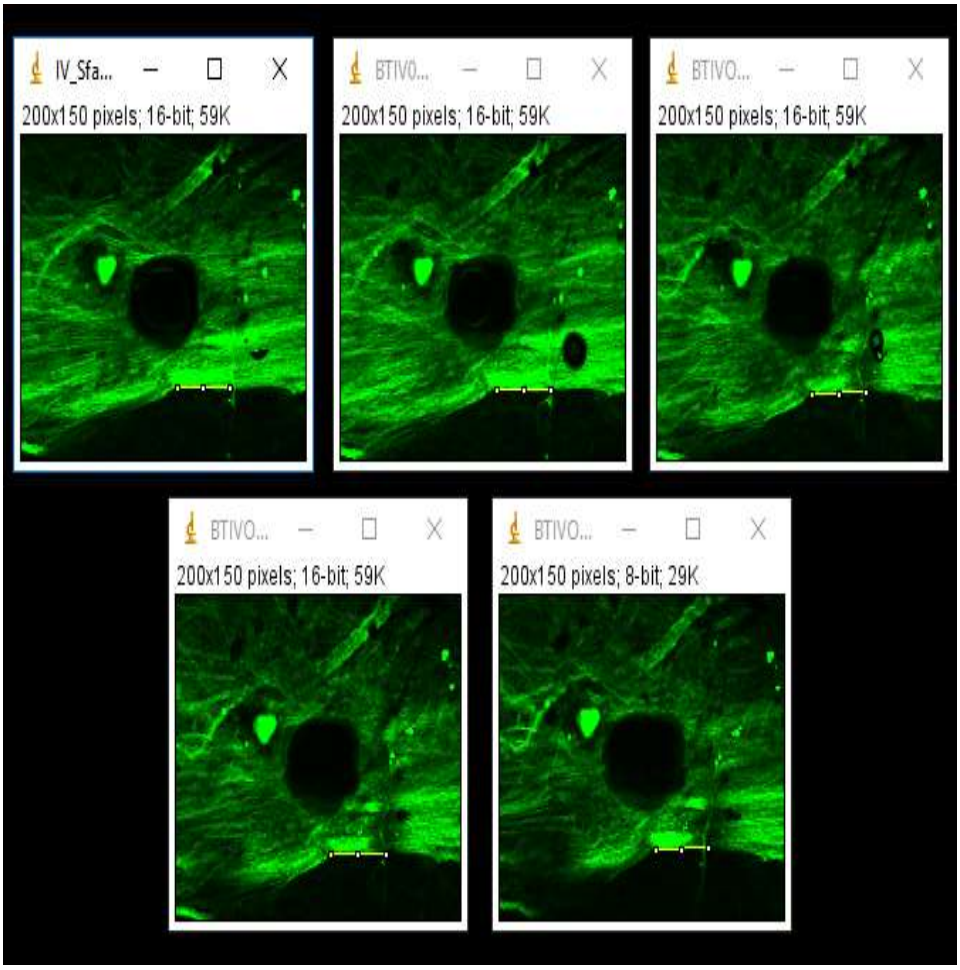

Fig. 5.35 Single fiber analysis for fiber-2 picked up from adventitial images from experiment-3- in-vivo configuration (top row; first from left); in-vivo post-overstretch-1 (top row; second from left); in-vivo post-overstretch-2 (top row; third from left); in-vivo post-overstretch-3 (bottom row; first from left); in-vivo post-overstretch-4 (bottom row; second from left) [Scale: 1.62 um/pixel; size: 512 x 512].

Tool in Image J. The figure shows that the orientation of this fiber in all the in-vivo post-overstretch configurations was similar to that of its orientation in in-vivo configuration. Table 5.22 shows the orientation of fiber-2 for the in-vivo and in-vivo post-overstretch configurations quantified by all three observers. We did not really observe a significant change in the collagen orientation for these configurations for the in-vivo post-overstretch-2 configuration onwards. For a better understanding of this fact, we have represented variation in the fiber orientation for different in-vivo post-overstretch configurations using a percentage difference calculated with reference to the in-vivo configuration. There was a significant difference in fiber orientation corresponding to the in-vivo and in-vivo post-overstretch-1 configurations. We reported earlier in the methods evaluation chapter that some amount of preconditioning, was lost during transport. This fact can be associated with the observation stated here. Preconditioning restructures the fiber organization. This reorganization of the fibers, which takes place during the preconditioning was lost during transport, which is indicated by a loss of preconditioning. When a vessel sample is overstretched for the first time after it is carried to the microscopy core, fibers must be reorganized as if the vessel sample was preconditioned. This must result in significant differences in the collagen orientation in its in-vivo configuration when compared with its orientation in the in-vivo post-overstretch-1 configuration. The fiber orientation does not show much variation for in-vivo post-overstretch-2 configuration onwards, which is easier to understand from the calculated percentage difference for fiber-1. The fact that the collagen orientation did not change again shows that there are few exceptions where the fiber orientation has been reported to increase or decrease inconsistently post-overstretch. This again might be because of the fact that a line drawn

Table 5.22 Single fiber analysis results for fiber-2 picked up from adventitial images for in-vivo and all in-vivo post-overstretch configurations from experiment-3.

	Fiber angle (1)	Percentage difference with respect to in-vivo	Fiber angle (2)	Percentage difference with respect to in-vivo	Fiber angle (3)	Percentage difference with respect to in-vivo
in-vivo	0	-	0	-	0	-
in-vivo post-overstretch-1	0	0	0	0	0	0
in-vivo post-overstretch-2	0.754	37.7	1.685	84.25	1.507	75.35
in-vivo post-overstretch-3	0	0	0	0	1.548	77.4
in-vivo post-overstretch-4	45	-15.30	45	0	47.603	-5.16

on the fiber for manual quantification is based on personal judgment and not done with the help of any software program. We thus decided to consider the observed trend over independent values. We thus report that there was no change in the collagen orientation post-overstretch. In order to better represent the data, we plotted the graphs, with orientation values represented on the y-axis and corresponding configurations for which they were reported on the x-axis. Fig. 5.36 shows a graph of orientations for fiber-2 for all three observers corresponding to the in-vivo and in-vivo post-overstretch configurations.

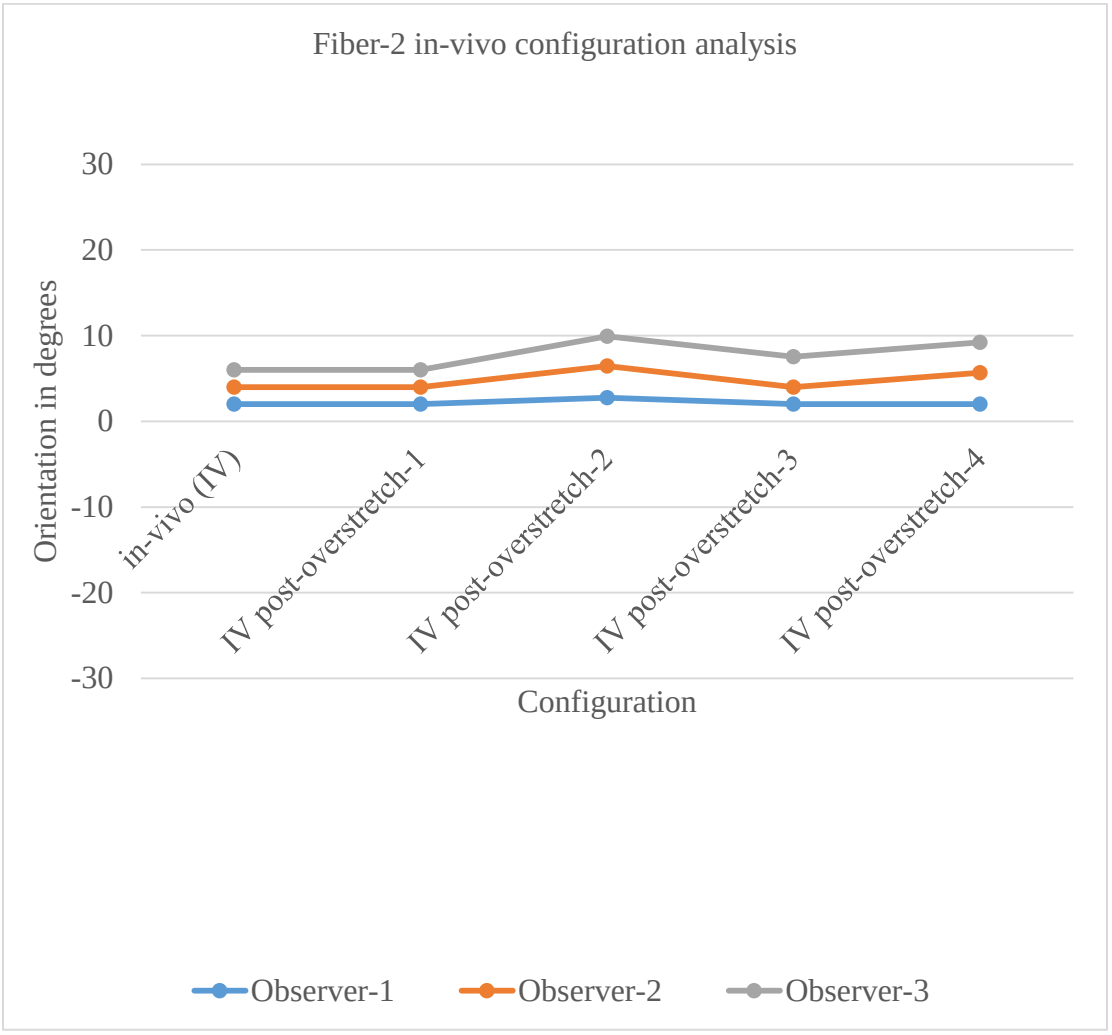

Fig. 5.36 Graph of the orientation of fiber-2 for experiment-3 against in-vivo configuration for which it is reported.

A line joining points on the graph remains almost parallel to the x-axis. The x-axis represents the configuration whereas y-axis represents the collagen orientation in degrees. A graph parallel to the x-axis necessarily represents no change in the collagen orientation with a change in the amount of overstretch. This indicates that collagen retained its orientation post-overstretch.

5.3.2 Fibril Tool regional analysis

As shown in Fig. 5.37, the adventitial images for different configurations from experiment-3 were divided into 3 regions of interest and the average orientation was found

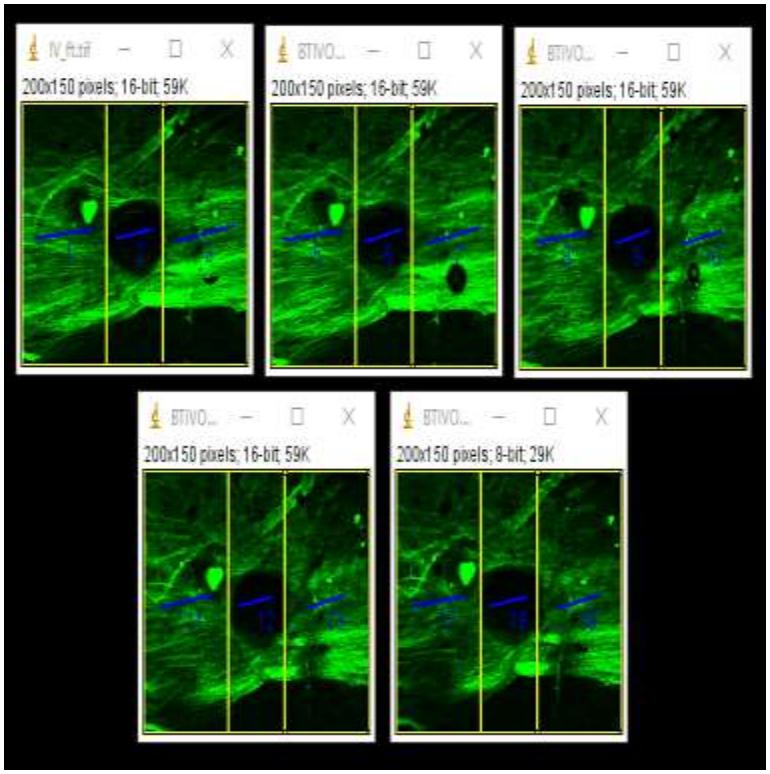

Fig. 5.37 Regional analysis with Fibril tool where image is divided into three regions of interest as shown above- in-vivo configuration (top row; first from left); in-vivo post-overstretch-1 (top row; second from left); in-vivo post-overstretch-2 (top row; third from left); in-vivo post-overstretch-3 (bottom row; first from left); in-vivo post-overstretch-4 (bottom row; second from left) [Scale: 1.62 um/pixel; size: 512 x 512].

for each region of interest using Fibril Tool, as mentioned in Table 5.23. To see if the values obtained from Fibril Tool show any trend or not, we plotted the graphs for average orientation for each region of interest (ROI) for all the configurations.

Fig. 5.38 represents a graph of average orientations for different regions of interest corresponding to the in-vivo and in-vivo post-overstretch configurations. As can be observed from this graph, the collagen orientation does not show any trend of the change in orientation for in-vivo post-overstretch configurations. We thus cannot conclude anything based on these graphs.

Table 5.23 Results from regional analysis of adventitial images from experiment-3 using Fibril Tool.

ROI	1	2	3
in-vivo	6.08	7.62	9.89
in-vivo post-overstretch-1	6.15	11.12	9.98
in-vivo post-overstretch-2	5.53	13.1	13.46
in-vivo post-overstretch-3	7.71	9.6	14.97
in-vivo post-overstretch-4	5.59	8.59	10.58

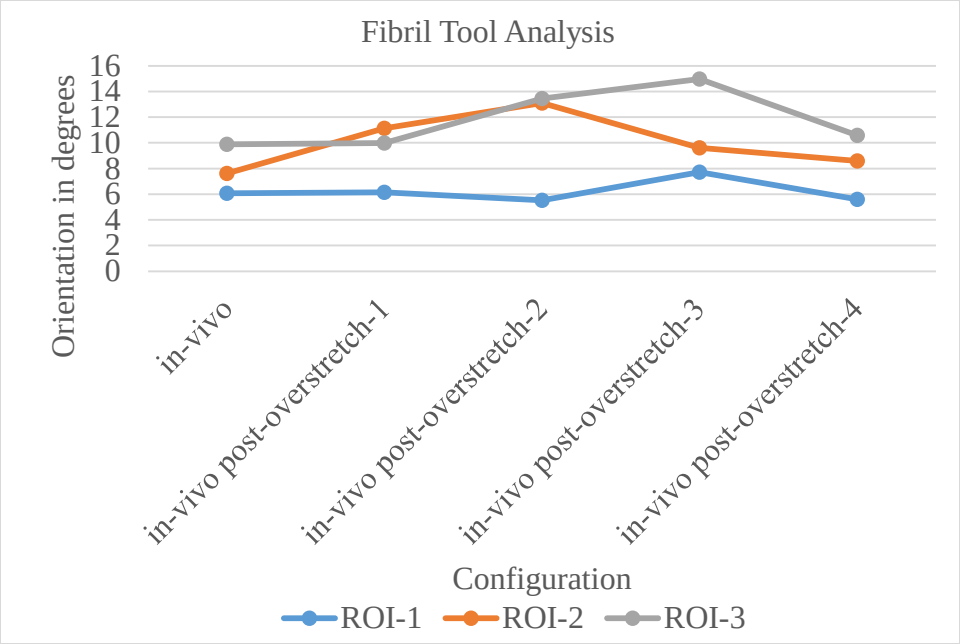

Fig. 5.38 Graph of average orientations for different regions of interest (ROI) obtained using Fibril Tool for experiment-3 against in-vivo configuration for which it is reported.

5.3.3 Orientation J analysis

The orientation graphs for the adventitia for each of the vessel samples were plotted with Orientation J Distribution (Image-J plugin). The adventitial graphs plotted for experiment-3 are shown in Fig. 5.39. The graphs show that most of the fibers in the adventitia were oriented around 0˚ for all the configurations. As stated earlier, the collagen fibers forming the adventitia were symmetrically organized. Thus, with every greater overstretch, even if they reoriented themselves and became more disorganized, the mean orientation was not altered. It was also expected that if we plotted a histogram of the orientations, reduction in a peak value corresponding to the mean and increase in the associated standard deviation would be observed for the in-vivo post-overstretch configurations. As can be observed from these histograms, the mean orientation for all the configurations for experiment-3 is approximately 15-20˚, which matches our expectation.

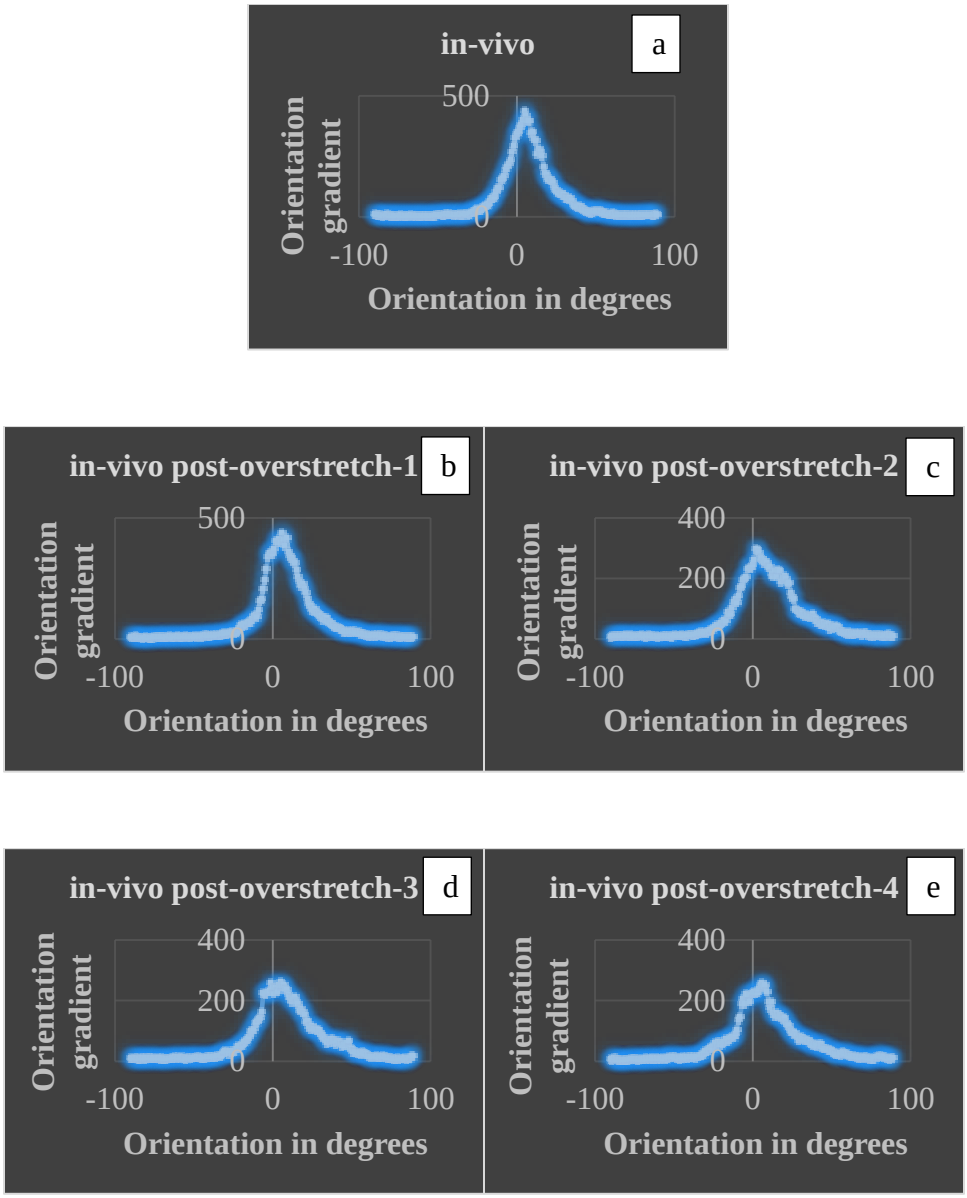

Fig. 5.39 Orientation J Distribution graphs for different configurations for experiment-3 (a) In-vivo; (b) In-vivo post-overstretch-1; (c) In-vivo post-overstretch-2; (d) In-vivo post-overstretch-3; (e) In-vivo post-overstretch-4.

We further expected to see a decrease in peak value corresponding to the mean orientation for the in-vivo post-overstretch configurations and an increase in a peak value corresponding to the overstretched configurations. As can be seen from the graphs represented here, we did not observe any such trend. We reported earlier in the Methods Evaluation chapter that for effective working of analysis using Orientation J for comparison, the number of fibers and their intensity among different images must be identical. This can be associated with the inconclusive outcomes obtained from simple visual inspection of these graphs. It was thus necessary to compare the peak value corresponding to the mean orientation and the standard deviation of the histogram numerically to further test the hypothesis. Orientation graphs for adventitial images corresponding to various configurations for experiment-3 are as shown in Fig. 5.39. The graphs fail to give any idea about the mechanism responsible for the vessel behavior.

5.3.3.1 Adventitial binned graph

The orientation graphs plotted for the adventitia were not helpful for testing the hypothesis. A direct comparison of these graphs only shows that the mean orientation did not change post-overstretch for the adventitial collagen fibers. The changes, if any, in the peak value corresponding to the mean orientation cannot be used to comment on the hypothesis. We might still expect to see a monotonic change in the weights assigned to the orientations surrounding the mean orientation. We thus binned the data in different ranges. We then summed up the weights corresponding to all the orientations in each bin, as shown in Table 5.24, and plotted these sums against the corresponding bin ranges for the adventitia, as shown in Fig. 5.40. In the case of an adventitia, we expected to see an increase

Table 5.24 Values calculated from binning the adventitial data into different ranges.

	0-2 (1)	3-5 (2)	6-8 (3)	9-11 (4)	12-14 (5)
in-vivo	1058.954	1217.478	1206.606	1017.147	853.3568
in-vivo post-overstretch 1	1128.463	1207.389	1229.493	1119.007	967.3909
in-vivo post-overstretch 2	802.4032	845.997	770.3486	722.8757	644.7107
in-vivo post-overstretch-3	707.1063	739.7097	734.779	660.7553	610.5926
in-vivo post-overstretch-4	677.7629	717.6477	754.128	599.9838	502.487

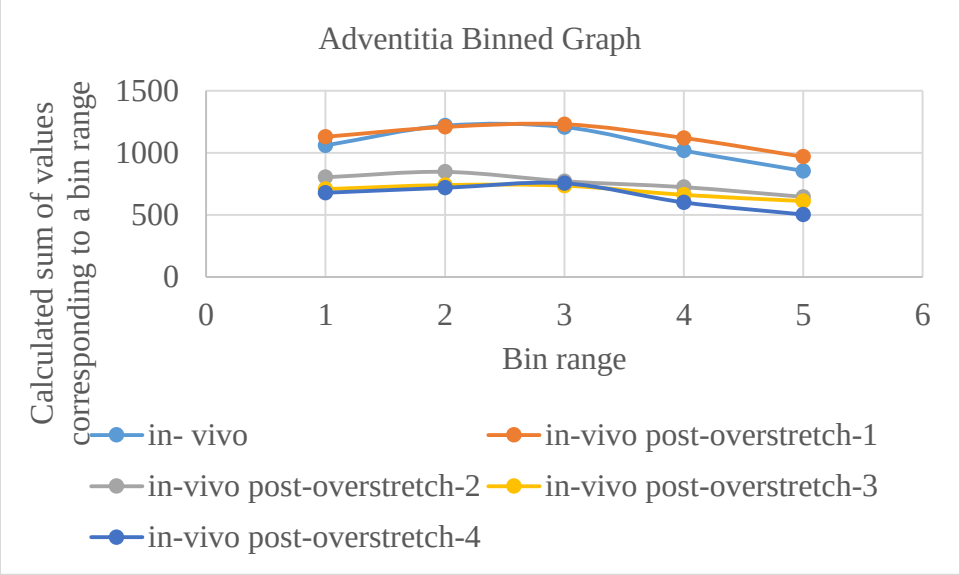

Fig. 5.40 Adventitial binned graph for experiment-3.

in summed-up weights as overstretch became severe for the ranges surrounding the mean (mean not included) and a decrease for the range including the mean. It can be observed from the figures that the graphs had no consistent behavior. This method thus could not contribute to support or disprove the hypothesis.

5.3.3.2 Mean and standard deviation values calculated from Orientation J Distribution

The orientation graphs plotted for the adventitia were not very helpful for testing the hypothesis. Although the mean orientation in the graphs was observed at around 0˚ for the adventitia, the area under the curve on either side of the mean was not equal in all of the experiments. It was thus predicted that a numerical data analysis involving the dataset generation from the orientation graphs, followed by a comparison of the calculated mean and standard deviation for these datasets, would help to gain more understanding of the organization of the fibers and thus help us to identify the orientation changes, if any, among different configurations. If the mean calculated with the generated dataset remains the same for all the configurations, the standard deviation could be compared to gain some insight about any fiber disorganization that happened with increase in the severity of overstretch. We generated the datasets based on the weights assigned to a particular orientation, as elaborated in the Methods chapter. The mean orientations calculated for different datasets for the same experiment showed a little variation in their values. We considered this low variation to be acceptable and compared the standard deviation for these datasets.

According to the hypothesis, increase in the standard deviation were expected post-overstretch due to more disorganized fibers. This increase should also have been monotonic. As shown in Table 5.25, though we have mean values approximately the same

Table 5.25 Mean and standard deviation values calculated from data obtained through Orientation J Distribution.

	Mean	Standard Deviation
in-vivo	7	21
in-vivo post-overstretch 1	8	23
in-vivo post-overstretch 2	9	26
in-vivo post-overstretch-3	8	27
in-vivo post-overstretch-4	8	26

for all the configurations, we do not always observe any monotonic increase in the standard deviation as overstretch became severe. This method of numerical data analysis does not support the hypothesis. We thus need different numerical analysis of these datasets to prove or disprove the hypothesis. We decided to use a numerical analysis technique that takes into consideration the entire dataset instead of part of it.

5.3.3.3 p-value table

We wanted to use all data to see if the datasets were statistically different and see if it gave us different results. In order to statistically compare the datasets, t-tests were performed for statistical comparison. A p-value of 0.05 was used to determine if two datasets were statistically different. The results of the t-tests, as shown in Table 5.26, were not consistent and thus cannot be used to draw any conclusion.

Table 5.26 p – values calculated from data obtained through Orientation J Distribution.

	p-value	Statistically different or not?
in-vivo and in-vivo post-overstretch-1	0.001014	Yes
in-vivo and in-vivo post-overstretch-2	1.93192E-07	Yes
in-vivo and in-vivo post-overstretch-3	0.004287	Yes
in-vivo and in-vivo post-overstretch-4	0.047831412	Yes

CHAPTER 5

DISCUSSION

In earlier experiments [10], we have observed softening of the blood vessel starting from an axial overstretch value of approximately 1.2. Researchers reported earlier that collagen and elastin are the main constituents of the blood vessel microstructure that govern its mechanical properties [11]. Literature reports that elastin is not responsible for softening [12], leaving collagen as the only constituent to be investigated for its effects on change in the mechanical properties. Collagen orientation change has been reported during an axial overstretch in other biological tissues [15], [22]. We thus hypothesized that adventitial collagen fibers that are axially oriented would become less uniform in their orientation following an axial overstretch. This increase in disorganization is expected to be monotonic with the amount of overstretch because the softening is reported to increase with overstretch. The medial circumferential fibers are not expected to show any significant change in their orientation post-overstretch. We also know from unpublished literature from the lab that fibers tend to align themselves in an axial direction when overstretched axially. To confirm this fact and to test our hypothesis, we developed an experimental technique. To the best of our knowledge, this is the first experiment to study the change in collagen orientation of cerebral arteries during and after axial overstretch. Collagen orientation change cannot be studied using light microscopy, which we have used in earlier

experiments. Developing a new method involved finding an appropriate microscopy technique, image processing tools, and statistical techniques to quantify the collagen orientation, and validating or verifying the effectiveness of these tools and techniques to give accurate results.

We found a 2P microscopy to be the most effective method of imaging collagen for quantification of its orientation among the methods we studied. We compared 2P collagen images obtained from the literature with our experimental data, with a focus on imaging and quantification of collagen orientation. We also referred to the orientation graphs for the adventitial collagen from the literature and found them comparable with those obtained from our experimental data. We thus concluded that a 2P microscopy is an effective tool for imaging collagen for quantification of its orientation.

Preconditioning is a process of finding the in-vivo length of the blood vessel sample, and it is also a method of bringing the vessel sample back to a state similar to its physiological state. Earlier experiments in the lab carried out preconditioning of the vessel sample immediately followed by a mechanical testing. For the current experiment, a tester had to be detached from the lab equipment and carried out to the microscopy core, which resulted in a time gap between preconditioning and mechanical testing of the vessel sample. We reported earlier that this leads to loss of preconditioning. Preconditioning reorganizes a network of fibers. This means that loss of preconditioning makes the fibers lose their organization achieved during the preconditioned state. The mechanical testing for this experiment included overstretching the vessel sample and bringing it back to its in-vivo configuration. The same procedure was repeated for multiple stretch levels. We have also reported a decrease in the collagen orientation when the vessel sample is overstretched,

which essentially indicates that fiber organization gets altered during the entire experiment, and we still did not see change in collagen orientation for in-vivo post-overstretch configurations. We can thus say that loss of preconditioning does not affect our conclusion about the collagen orientation change during and after overstretch. This conclusion has been drawn based on the trend that we observed with manual quantification of individual fibers using Line Tool. We tried automating the process with different image processing tools, such as Fibril Tool and Orientation J, which are plugins for Image J. We realized that since we moved the vessel sample during the entire course of the experiment, we could not image the vessel sample under identical microscopic conditions for each and every configuration, which gave us images with different brightness, contrast, and number of fibers for different in-vivo configurations. We showed earlier that these tools do not work effectively in comparing images of different brightness, contrast, and number of fibers, and so these tools are not helpful in determining the collagen orientation change for our experiment. We relied on the conclusion from our preliminary analysis—i.e., single fiber analysis. In this analysis, a line was drawn on the fiber according to a personal judgment, so few values reported for collagen orientation indicate deviation from the observed trend. To understand the accuracy of the trends we obtained through this method, we repeated this process of manual quantification with the help of two other observers. All the observers reported approximately the same values of fiber angles. The trend observed for overstretch as well as post-overstretch configurations was also the same for all observers. We decided to draw a conclusion based on the trends we observed from single fiber analysis.

We reported a decrease in the collagen orientation (angle measured with respect to the positive x-axis) for axially oriented collagen fibers in the middle cerebral arteries of

sheep during axial overstretch, and also that the orientation decreased further as overstretch increased. Earlier investigation showed an increase in collagen orientation for adventitial fibers in pig coronary arteries when overstretched circumferentially [4]. We feel our conclusion is logical because elastin and collagen are the main microstructural elements governing the mechanical behavior of the vessel sample. We did not observe change in the collagen orientation post-overstretch. As mentioned earlier, collagen seems to be the main factor affecting softening of the blood vessel. If the collagen orientation does not change, it indicates that there must be another parameter associated with collagen that is responsible for this change. Collagen crimp change might also be happening, similarly to what has been reported in the literature for other biological tissues [14], but further testing of the cerebral blood vessels is required.

We have thus developed a method of mechanically testing the biological tissue outside the lab space. We managed to replicate certain lab conditions, such as maintaining luminal pressure equal to the in-vivo pressure and applying the required precise motion to the vessel sample. We successfully imaged collagen for different configurations of the vessel sample. The quality of the captured data is suitable for quantification of the collagen orientation. We drew our conclusion based on the trend that we observed with manual quantification of the collagen orientation using Line Tool. The results cannot be quantified for different overstretch levels due to manual error that might have been caused by drawing a line on the fiber for quantification of the fiber orientation. This limitation can be overcome by developing a dedicated digital correlation technique for comparison of collagen orientation among different configurations. A digital correlation technique must be developed that can accommodate slight changes in brightness and contrast of the images

under comparison. The data acquisition could also be improved to achieve comparable brightness and contrast among images of different configurations in the same experiment. An attempt should be made to reduce the time gap between preconditioning and mechanical testing. This would help us eliminate a small difference observed in collagen orientation for in-vivo and in-vivo post-overstretch-1 configurations. We have used a photobleaching technique to produce black spots on the surface of the vessel sample, which helps us identify whether or not we are imaging the same portion of the vessel sample before and after overstretch. We reported that photobleaching does not affect mechanical properties of the vessel sample [36], so it can be used in future experiments. This technique can be used for quantifying overstretch of the vessel sample instead of quantifying it using needles on which the vessel sample is mounted. We observed in earlier experiments that the vessel strain quantification is a more appropriate method of overstretch quantification than the needle strain quantification because of the end effects arising from tying ends of the vessel sample to the needles with sutures.

We could not quantify medial fibers since the image processing tools we used for quantification required images to have distinct features so they could be identified in all the configurations and thus used to compare the collagen orientation among different configurations. Medial fibers, which are circumferential in orientation, are not expected to be affected by axial overstretch. If we still have to compare medial signal from the vessel sample, we might have to computationally flatten the data obtained from the vessel sample. This way, we will have a set of images representing different configurations of the media, which can be compared to draw a conclusion.

CHAPTER 7

CONCLUSION

We hypothesized that the axially oriented adventitial collagen fibers would become less uniform in their orientation following overstretch. This increase in disorganization is expected to be monotonic with the amount of overstretch as the softening becomes more severe. The medial, circumferential fibers are not expected to show any significant change in their orientation post-overstretch.

To test our hypothesis, we developed a new experimental method of testing the blood vessel sample outside of the lab space. This new experimental method offered many different challenges. We had to verify all the steps involved in this method, which included checking the quality of the data for quantification, knowing if the photobleaching influences the results, if the tools used for quantification are sensitive enough to identify the orientation changes, and if the vessel sample remained preconditioned during the travel from lab to the microscopy core etc. We verified the steps listed above and reported problems associated with them.

We found that a single fiber analysis using a manually drawn line over the fiber to be the most reliable tool for quantification of the fiber orientation for this preliminary study. The results obtained through Fibril Tool and Orientation J Distribution seem to get affected significantly by brightness and contrast of the images. If we have to compare the collagen

orientation among different configurations using these tools, we have to make sure that all of them possess similar brightness and contrast.

The results obtained through single fiber analysis indicate that the fibers tend to get more organized when the vessel sample is overstretched. It also shows that the fibers reorient themselves when they are overstretched so as to become more axially inclined. The method did not show any specific trend for the collagen orientation when the vessel sample was brought back to its in-vivo configuration post-overstretch. The collagen orientation was reported to be nearly the same post-overstretch as it was before overstretched in some of the cases where images had enough clarity and brightness. It is thus reasonable to assume that the collagen retains its orientation after mild axial overstretch.

We also found some limitations with the study and the possible measures that could be taken to overcome them if we have to perform these experiments again in future. If these measures could be implemented successfully, we would have more reliable and repeatable results.

APPENDIX

COMPUTATIONAL FLATTENING MECHANISM PROCEDURE AND VERIFICATION

We developed a computational flattening mechanism in our lab (Lab of Head Injury and Vessel Biomechanics) in order to flatten the data obtained from a cylindrical vessel. The basic assumption for developing this mechanism is that the vessel forms a perfect cylinder.

The procedure for flattening mechanism is as follows:

I. Image- Properties- Pixel Width: 1; Pixel Height: 1; Voxel Depth: 3.086 (Z-Step Size / Pixel Size). This would set properties of the stack of the images for further processing.

II. Image- Stacks- Reslice- Output spacing (pixels): 1; Start at: Left (Resliced stack)

III. Select any 3 points on any one of the images in the resliced stack such that they define a circle. Use 3 point formula to find the center of the circle.

IV. Make line that joins center of the circle to any one point on the circle.

V. Note the outer radius of the circle and measure the angle between any 2 points on the circle (say ‘α’) starting at one of the points.

VI. Calculate the degrees per slice as follows :-

VII. $X= [\pi * \alpha / 180]$

VIII. Degrees per slice = 1/ X.

IX. Plugins- Radial Reslice- Angle (degrees): α; Degrees per slice as calculated; Direction: Anti-clockwise. (If the line starts on the right side of the image.) (Radially resliced stack.)

X. Select a rectangular region where the data are seen in the radially resliced stack.

XI. Image- Stacks- Reslice- Output spacing (pixels): 1; Start at: Left (This would give unrolled stack of the images containing adventitial, transition, and medial images.)

XII. Separate adventitial, transition, and medial images from the data observed.

In order to verify the mechanism, we constructed a solid cylinder having two layers (colored with yellow and green) of equal thickness with hole at the center as shown in Fig. A.1. The dimensions are given in the Table A.1. The purpose of creating this type of geometry was to approximately replicate the blood vessel structure. Usually, media and adventitia have similar thickness, which were represented by two concentric layers of equal thickness. The vessel has a lumen in the center that was represented by a hole. Maximum diameter and length of the vessel were kept constant so as to avoid any later complication with the scaling factor for image processing.

When we capture the data for the vessel sample with 2P microscope, we capture the data from the vessel sample starting from the top portion and progressively moving towards the bottom. In this case, we get the image of a particular layer of the vessel sample, i.e. within focal length of the objective. For obtaining similar data from the constructed 3D cylinder in AutoCAD 2015 3D, the bottom half portion of the cylinder was erased (the data is collected only from the top portion of the vessel sample) and the remaining half was divided into 80 layers so that each layer has a unit thickness (1 mm). After the cylinder was divided into layers, the cylinder was viewed using ‘top view’. In order to obtain the data similar to 2P microscopy, all the layers except the one whose image is required were hidden temporarily. Images of all 80 layers were obtained in a similar way. Stack was then formed As a result, we obtained 28 images that were completely yellow in color and 28 images that were completely green with 4 images having interference of yellow and green where transition was occurring from yellow to green. The thickness of each layer was 1 mm and hence 30 images correspond to a thickness of 30 mm. This matches with the thickness of

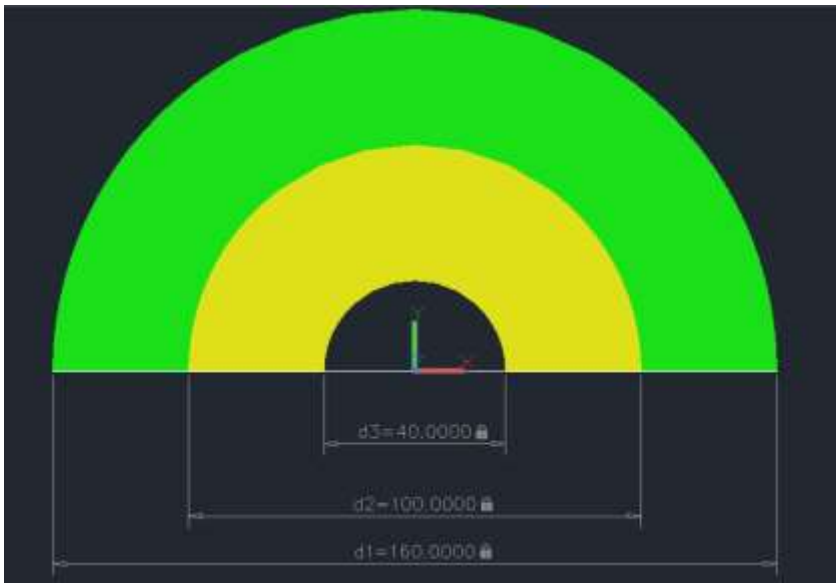

Fig. A.1 Front view of the cylinder constructed in an AutoCAD 3D to represent a blood vessel.

Table A.1 Table representing dimensions of the cylinder created to represent the vessel sample.

Dimension name	Value
Hole diameter	40 mm
Outer diameter of inner layer (yellow) of the cylinder	100 mm
Outer diameter of the cylinder	160 mm

yellow and green layers of the cylinder. The interference that we observed can be attributed to the fact that the resolution of the images obtained from AutoCAD is not upto the mark and is much lesser compared to the resolution we get in actual image data collected from 2P microscope. We did not see any distortion of pixels in any of the images and hence, we concluded that the flattening mechanism developed in our lab can efficiently flatten the data captured from a perfect cylinder. The assumption in developing this mechanism was that blood vessel is a perfect cylinder. It is not pragmatic to expect a blood vessel to be a perfect cylinder. When blood vessel is mounted on the needles and is stretched beyond its in-vivo length, it is expected to get elliptical in shape. We thus decided to construct 3D ellipse similar to a cylinder. We constructed 3D ellipse as shown in Fig. A.2 and Fig. A.3. The dimensions used for construction are given in Table A.2. We again erased the bottom half portion of the ellipse and captured data from the ellipse in similar way as that of the cylinder.

For all of the blood vessel samples, we chose data from top circumferential portion which made approximately an angle of 30˚ at the center. We thus processed data from the

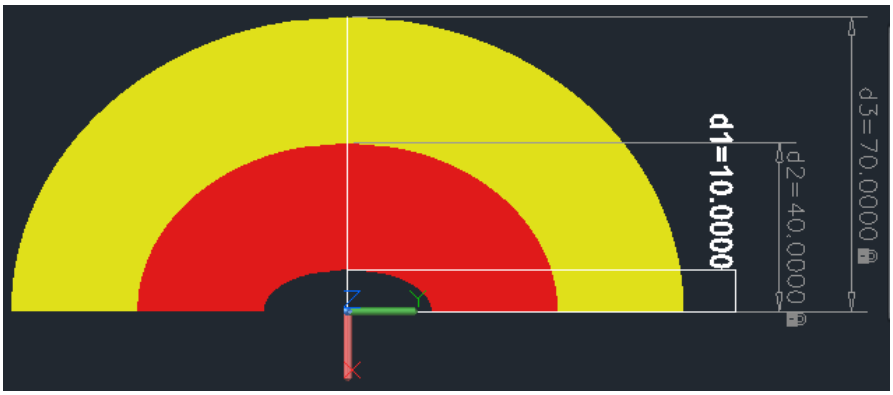

Fig. A.2 Front view of the ellipse constructed in an AutoCAD 3D to represent a blood vessel (shows inner diameters).

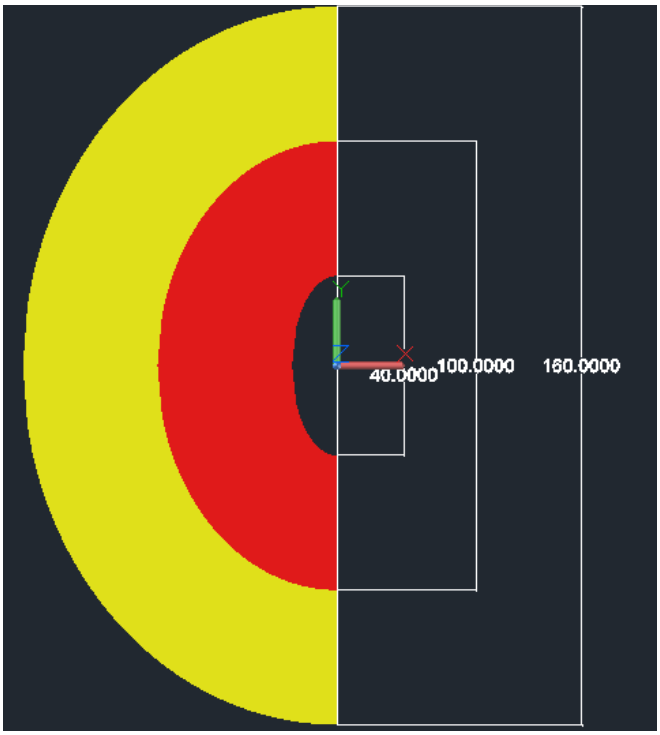

Fig. A.3 Front view of the cylinder constructed in an AutoCAD 3D to represent a blood vessel (shows outer diameters).

Table A.2 Table representing dimensions of the ellipse created to represent the vessel sample.

Dimension	Value
Smaller diameter of the hole	10 mm
Larger diameter of the hole	40 mm
Smaller outer diameter of the inner layer (red) of the ellipse	40 mm
Larger outer diameter of the inner layer (red) of the ellipse	100 mm
Smaller outer diameter of the outer layer (yellow) of the ellipse	70 mm
Larger outer diameter of the outer layer (yellow) of the ellipse	160 mm

obtained similar results as that of the circular cylinder (with interference in only couple of images).

We expected similar results from the elliptical data since the portion corresponding to this small angle would be circular. This way we verified the flattening mechanism and found it suitable for the vessel sample with circular and elliptical shapes.

We skipped using this mechanism since some of the data obtained from our experiments could not be flattened. The vessel sample might have become irregular in shape during the experiment and hence it could not be flattened.

REFERENCES

[1] D. W. Wright, A. Kellermann, L.C. McGuire, B. Chen, T. Popovic, "CDC grand rounds: reducing severe traumatic brain injury in the United States," *Morbidity and Mortality Weekly Report (MMWR)*, vol. 62, pp. 549–552, 2013.

[2] V. G. Coronado, L. Xu, S. V. Basavaraju, L. C. Mcguire, M. M. Wald, and M. D. Faul, "Surveillance for traumatic brain injury-related deaths – United States, 1997–2007 ," *Morbidity and mortality weekly report (MMWR)* , vol. 60, pp. 1–32, 2011.

[3] A. S. Go, D. Mozaffarian, V. L. Roger, E. J. Benjamin, J. D. Berry, and M. J. Blaha, "Heart disease and stroke statistics--2014 update: a report from the American Heart Association," *Circulation*, vol. 129, no. 3, pp. 28-292, 2013.

[4] Y.-H. Chen, J.-H. Kang, and H.-C. Lin, "Patients with traumatic brain injury: population-based study suggests increased risk of stroke," *Stroke*, vol. 42, no. 10, pp. 2733–2739, 2011.

[5] N. K. Hills, S. C. Johnston, S. Sidney, B. A. Zielinski, and H. J. Fullerton, "Recent trauma and acute infection as risk factors for childhood arterial ischemic stroke," *Annals of Neurology*, vol. 72, no. 6, pp. 850–858, 2012.

[6] J. F. Burke, J. L. Stulc, L. E. Skolarus, E. D. Sears, D. B. Zahuranec, and L. B. Morgenstern, "Traumatic brain injury may be an independent risk factor for stroke," *Neurology*, vol. 81, no. 1, pp. 33–39, 2013.

[7] A. Jullienne, A. Obenaus, A. Ichkova, C. Savona-Baron, W. J. Pearce, and J. Badaut, "Chronic cerebrovascular dysfunction after traumatic brain injury," *Journal of Neuroscience Research*, vol. 94, no. 7, pp. 609–622, 2016.

[8] G. Holzapfel and P. Fratzl, "Collagen in arterial walls: biomechanical aspects," *Collagen: Structure and Mechanics*, 1 ed., pp. 285–324, 2008.

[9] J. Diamant, A. Keller, E. Baer, M. Litt, and R. G. C. Arridge, "Collagen; ultrastructure and its relation to mechanical properties as a function of ageing," *Proceedings of the Royal Society B: Biological Sciences*, vol. 180, no. 1060, pp. 293–315, 1972.

[10] E.D. Bell, J. W. Sullivan, and K.L. Monson, "Subfailure overstretch induces persistant changes in the passive mechanical response of cerebral

arteries," *Frontiers in Bioengineering and Biotechnology*, vol. 3, no. 2, pp. 1-10, 2015.

[11] M. R. Roach and A. C. Burton, "The reason for the shape of the distensibility curves of arteries," *Canadian Journal of Biochemistry and Physiology*, vol. 35,

no. 1, pp. 681–690, 1957.

[12] H. Weisbecker, C. Viertler, D. M. Pierce, and G. A. Holzapfel, "The role of elastin and collagen in the softening behavior of the human thoracic aortic media," *Journal of Biomechanical Engineering*, vol. 46, pp. 1859–1865, Apr. 2013.

[13] K. P. Quinn, J. A. Bauman, N. D. Crosby, and B. A. Winkelstein, "Anomalous fiber realignment during tensile loading of the rat facet capsular ligament identifies mechanically induced damage and physiological dysfunction," *Journal of Biomechanical Engineering*, vol. 43, no. 10, pp. 1870–1875, 2010.

[14] K. S. Miller, L. Edelstein, B. K. Connizzo, and L. J. Soslowsky, "Examining differences in local collagen fiber crimp frequency throughout mechanical testing in a developmental mouse supraspinatus tendon model," *Journal of Biomechanical Engineering*, vol. 134, no. 4, pp. 2061-2065, 2012.

[15] K. S. Miller, L. Edelstein, B. K. Connizzo, and L. J. Soslowsky, "Effect of preconditioning and stress relaxation on local collagen fiber realignment: inhomogeneous properties of rat supraspinatus tendon," *Journal of Biomechanical Engineering*, vol. 134, no. 4, pp. 1-7, 2012.

[16] K. P. Quinn and B. A. Winkelstein, "Preconditioning is correlated with altered collagen fiber alignment in ligament," *Journal of Biomechanical Engineering*, vol. 133, no. 6, pp. 1-4, 2011.

[17] W. C. Li, H. M. Zhang, P. J. Wang, G. M. Xi, H. Q. Wang, and Y. Chen, "Quantitative analysis of the microstructure of human umbilical vein for assessing feasibility as vessel substitute," *Annals of Vascular Surgery*, vol. 22, no. 3, pp. 417-424, 2008.

[18] P. B. Canham, H. M. Finlay, J. G. Dixon, D. R. Boughner, and A. Chen, "Measurements from light and polarised light microscopy of human coronary arteries fixed at distending pressure," *Cardiovascular Research*, vol. 23, no. 11, pp. 973–982, Jan. 1989.

[19] H. M. Finlay, L. Mccullough, and P. B. Canham, "Three-dimensional collagen organization of human brain arteries at different transmural pressures," *Journal of Vascular Research*, vol. 32, no. 5, pp. 301–312, 1995.

[20] J. W. Orberg, L. Klein, and A. Hiltner, "Scanning electron microscopy of

collagen fibers in intestine," *Connective Tissue Research*, vol. 9, no. 3, pp. 187–193, 1982.

[21] J. C. Geer, "Fine structure of human aortic intimal thickening and fatty streaks," *Laboratory Investigaton; a journal of technical methods and pathology*, vol. 14, pp. 1764–1783, 1965.

[22] R. Rezakhaniha, A. Agianniotis, J. T. C. Schrauwen, A. Griffa, D. Sage, C. V. C. Bouten, F. N. V. D. Vosse, M. Unser, and N. Stergiopulos, "Experimental investigation of collagen waviness and orientation in the arterial adventitia using confocal laser scanning microscopy," *Biomechanics and Modeling in Mechanobiology*, vol. 11, no. 3-4, pp. 461–473, Oct. 2011.

[23] B. Wicker, H. Hutchens, Q. Wu, A. Yeh, and J. Humphrey, "Normal basilar artery structure and biaxial mechanical behaviour," *Computer Methods in Biomechanics and Biomedical Engineering*, vol. 11, no. 5, pp. 539–551, 2008.

[24] https://en.wikipedia.org/wiki/Immunohistochemistry.

[25] https://en.wikipedia.org/wiki/Primary_and_secondary_antibodies

[26] http://Abcam.com

[27] A. Zoumi, X. Lu, G. S. Kassab, and B. J. Tromberg, "Imaging coronary artery microstructure using second-harmonic and two-photon fluorescence microscopy," *Biophysical Journal*, vol. 87, no. 4, pp. 2778–2786, 2004.

[28] S. R. Watson, P. Liu, E. A. Peña, M. A. Sutton, J. F. Eberth, and S. M. Lessner, "Comparison of aortic collagen fiber angle distribution in mouse models of atherosclerosis using second-harmonic generation (SHG) microscopy," *Microscopy and Microanalysis*, vol. 22, no. 01, pp. 55–62, Jul. 2016.

[29] G. Cox and E. Kable, "Second-harmonic imaging of collagen," *Cell Imaging Techniques Methods in Molecular Biology*™, vol. 319, pp. 15–35, 2006.

[30] https://en.wikipedia.org/wiki/Second-harmonic_imaging_microscopy

[31] J. D. Humphrey, "Mechanics of the arterial wall: review and directions," *Critical Reviews in Biomedical Engineering*, vol. 23, no. 5-6, pp. 1–162, 1995.

[32] B. D. Stemper, N. Yoganandan, M. R. Stineman, T. A. Gennarelli, J. L. Baisden, and F. A. Pintar, "Mechanics of fresh, refrigerated, and frozen arterial tissue," *Journal of Surgical Research*, vol. 139, no. 2, pp. 236–242, 2007.

[33] A. G. Kunkel, "Effect of storage duration on the mechanical behavior of mouse

carotid artery," *Journal of Biomechanical Engineering*, vol. 133, no. 7, pp. 1-6, 2011.

[34] E. D. Bell, A. J. Donato, and K. L. Monson, "Cerebrovascular dysfunction following subfailure axial stretch," *Journal of the Mechanical Behavior of Biomedical Materials*, vol. 65, pp. 627–633, 2017.

[35] P. Van Loon, W. Klip, and E. L. Bradley, "Length-force and volume-pressure relationships of arteries," *Biorheology*, vol. 14, pp. 181–201, 1977

[36] C. Jayyosi, G. Fargier, M. Coret, and K. Bruyère-Garnier, "Photobleaching as a tool to measure the local strain field in fibrous membranes of connective tissues," *Acta Biomaterialia*, vol. 10, no. 6, pp. 2591–2601, 2014.

[37] S. Ghazanfari, A. Driessen-Mol, G. Strijkers, F. Kanters, F. Baaijens, and C. Bouten, "A comparative analysis of the collagen architecture in the carotid artery: Second harmonic generation versus diffusion tensor imaging," *Biochemical and Biophysical Research Communications*, vol. 426, no. 1, pp. 54–58, 2012.